An aerial photograph of a rugged, mountainous landscape. The terrain is characterized by steep, rocky slopes and a prominent river valley that winds through the center. The colors are muted, with shades of brown, tan, and grey, suggesting a high-altitude or arctic environment. The overall scene is one of natural grandeur and geological complexity.

**Impact of magmatism on hydrocarbon systems of the Sverdrup Basin,
Canadian Arctic Islands, Nunavut; a numerical modeling experiment.**

by

Samantha F. Jones

**Submitted in partial fulfillment of the requirements
for the degree of Bachelor of Science**

at

**Dalhousie University
Halifax, Nova Scotia
Canada**

April 2006



Department of Earth Sciences
Halifax, Nova Scotia
Canada B3H 3I5
(902) 494-2358
FAX (902) 494-6889

DATE: April 18, 2006

AUTHOR: Samantha F. Jones

TITLE: Impact of magmatism on hydrocarbon systems of the Sverdrup Basin, Canadian
Arctic Islands, Nunavut; a numerical modeling experiment.

Degree: BSc. Honours Convocation: May 29th Year: 2006

Permission is herewith granted to Dalhousie University to circulate and to have copied for non-commercial purposes, at its discretion, the above title upon the request of individuals or institutions.

THE AUTHOR RESERVES OTHER PUBLICATION RIGHTS, AND NEITHER THE THESIS NOR EXTENSIVE EXTRACTS FROM IT MAY BE PRINTED OR OTHERWISE REPRODUCED WITHOUT THE AUTHOR'S WRITTEN PERMISSION.

THE AUTHOR ATTESTS THAT PERMISSION HAS BEEN OBTAINED FOR THE USE OF ANY COPYRIGHTED MATERIAL APPEARING IN THIS THESIS (OTHER THAN BRIEF EXCERPTS REQUIRING ONLY PROPER ACKNOWLEDGEMENT IN SCHOLARLY WRITING) AND THAT ALL SUCH USE IS CLEARLY ACKNOWLEDGED.

In memory of two loving Grandfathers, Francis Jones and Robert Parker

*Cover Photo: View of the Strand Fiord Formation across the river valley from Junction Diapir, at the 2000' contour. Field expedition to Axel Heiberg Island, July 2004.
Copyright Christopher Hamilton.*

Impact of magmatism on hydrocarbon systems of the Sverdrup Basin, Canadian Arctic Islands, Nunavut; a numerical modeling experiment.

Samantha F. Jones

TABLE OF CONTENTS

Table of Contents	i
Abstract	iii
Acknowledgements	v
List of Figures	vi
List of Tables	x
CHAPTER 1: INTRODUCTION	
1.1 Opening Statement	1
1.2 Study Area and the Strand Fiord Project	1
1.3 Previous Research	4
1.4 Methods for Hydrocarbon Modeling	5
1.5 Objectives	6
1.6 Thesis Organization	7
CHAPTER 2: THE SVERDURP BASIN: REGIONAL GEOLOGY AND MAGMATIC PROVINCE	
2.1 Geological Overview of the Sverdrup Basin	8
2.2 The Magmatic System	15
2.3 The Hydrocarbon System	17
2.4 System Integration	18
2.5 Summary	20
CHAPTER 3: ATTRIBUTES OF VOLCANIC AND INTRUSIVE ROCKS IN THE SVERDRUP BASIN MAGMATIC PROVINCE	
3.1 Distribution of Igneous Rocks on Axel Heiberg Island	22
3.2 Field Setting	23
3.2.1 Volcanic Rocks	23
3.2.2 Intrusive Rocks	27
3.3 Age Determination of Igneous Units in the SBMP	28
3.4 Magma Types in the SBMP	33
3.5 Magma Emplacement	37
3.6 Igneous Rocks Intersected by the Depot Point L-24 Well	37
3.7 Summary	40
CHAPTER 4: MODEL CONSTRUCTION AND INPUT DATA	
4.1 Introduction	41
4.2 Using PetroMod [®] for 1D Modeling	42
4.3 Lithologies	43
4.4 Source Rock Properties	43
4.5 Vitrinite Reflectance	48

4.6 Heat Flow	49
4.7 Erosion Rates and Fission-track Data	52
4.8 Sea Level	53
4.9 Sediment-water interface Temperature	54
4.10 Sill Characteristics	54
4.11 Summary	55
CHAPTER 5: ONE-DIMENSIONAL MODEL RESULTS	
5.1 Introduction	57
5.2 Interpreting Data Displays	57
5.3 Burial History	60
5.4 Thermal Profile	60
5.5 Hydrocarbon Potential	64
5.6 Sensitivity Study	68
5.6.1 Lack of Intrusive Activity and Lack of Rifting	68
5.6.2 Varying the Age of Sill Intrusion	72
5.6.3 Important Variables Not Considered in this Study	77
5.7 Summary	78
CHAPTER 6: DISCUSSION AND CONCLUSION	
6.1 Discussion	79
6.1.1 Solutions to the Four Scientific Questions	79
6.1.2 Future Work	83
6.2 Conclusion	84
REFERENCES	87
APPENDIX A: Hand Sample and Petrological Descriptions of Igneous Rocks	96
APPENDIX B: Geologic Time Scale	107
APPENDIX C: Additional Model Plots	108

Abstract

This study uses numerical modeling to investigate for the first time the interactions between a hydrocarbon system and sill intrusion in the north-eastern Sverdrup Basin, Canadian Arctic. Although exploration was successful in the western Sverdrup Basin, the results in the north-eastern part of the basin were disappointing, despite the presence of suitable Mesozoic source rocks, migration paths and structural/stratigraphic traps, many involving evaporites. These results were explained by invoking (1) the development of structural traps during inversion of the basin in the Eocene followed the main phase of hydrocarbon generation and migration, and (2) the proximity of evaporite diapirs that locally modified the geothermal gradient and led to overmature hydrocarbons. This project investigates the local thermal effects of Cretaceous sills and extrusive volcanism to determine their potential impact on the hydrocarbon system.

The 1-D numerical model explores the effects of rifting and magmatic events on the thermal history of the Depot Point L-24 well near Eureka Sound on eastern Axel Heiberg Island. The thermal history is deduced from vitrinite reflectance data, fission-track data, and the regional geology and when modeled, identifies when hydrocarbon generation is possible. The subsequent introduction of units representing sills or erupted lava flows illustrates the temporal and spatial links between hydrocarbon production and igneous activity. A comparison between classic hydrocarbon systems and magmatic systems is essential in interpreting the Depot Point L-24 model results.

The model results show that rifting and sill intrusion occur after hydrocarbon generation ceased in the Hare Fiord and Van Hauen Formations, thus rifting and sill

emplacement will not affect the generation potential of these formations. The Blaa Mountain Formation, a shallower source rock, underwent its main phase of hydrocarbon generation at 125 Ma, the time of rifting and sill intrusion, and rapidly generated natural gas. A short sensitivity study reveals that the emplacement of sills increases the hydrocarbon generation rates in the Blaa Mountain Formation, and promotes the production of natural gas rather than oil. In addition, a critical examination of the model results allows the user to identify knowledge gaps. This iterative process eventually leads to more robust numerical solutions and a higher quality of model results that form a basis for groundtruthing and future work.

Acknowledgments

I wish to thank my supervisors, Marie-Claude Williamson, Marcos Zentilli, and Hans Wielens, for all of their support and guidance. Thank you Marcos for proposing the initiation of this research project. This project would not have been successful without your expertise and experience.

At the Geological Survey of Canada- Atlantic, I would like to thank Frank Thomas for assistance in the Environmental Scanning Electron Microscope laboratory and Gordon Oakey for his support and enthusiasm. Thank you to Tom Brent and Christopher Harrison at Geological Survey of Canada- Calgary for providing the well data on Depot Point L-24 and synthesis papers. At Dalhousie University I wish to thank Grant Wach whose knowledge expanded the scope of this project and Patrick Ryall for coordinating the Honours thesis sessions. Also, thank you and congratulations to all of the Earth Sciences students in the graduating class.

At Saint Mary's University I would like to thank Andrew MacRae for his photographic contribution and communication about the study area. Thank you to Wolf Rottke and Thomas Leythaeuser of the Integrated Exploration Systems Support Team for their quick feedback and generous technical support. Thank you to Natural Sciences and Engineering Research Council for research funding during the summer of 2005.

Ryan, thank you for all of your encouragement and patience. Sarah-Jean, thank you for your sense of humor, how could I keep sane without you. And thank you to my Mom and Dad for their continued support in my career as a young geoscientist.

List of Figures:	Page
Figure 1.1: Location map of the Sverdrup Basin and Axel Heiberg Island (Modified from Vogt <i>et al.</i> , 2006).	2
Figure 1.2: Location map focused on Axel Heiberg Island which shows Expedition Fiord, Strand Fiord, and L-24 Depot Point.	3
Figure 2.1: Map of the Sverdrup Basin which shows the extent of igneous intrusive and extrusive activity. (Modified from Villeneuve and Williamson, in press)	9
Figure 2.2: A geological map of the study area on Axel Heiberg Island (Modified from Thorsteinsson, 1971a, 1971b, 1971c).	11
Figure 2.3: This simplified cross section provides an overview of the formations present within the study area (From Embry, 1991).	13
Figure 3.1: A map showing the localities of igneous units on Axel Heiberg Island that are discussed throughout Chapter 3.	24
Figure 3.2: This collection of stratigraphic sections shows the thinning of the Strand Fiord Formation towards the east from East Fiord/Agate Fiord to Glacier Fiord (From MacRae <i>et al.</i> , 1996).	25
Figure 3.3: Photograph of the Strand Fiord Formation (From MacRae, 1996).	26
Figure 3.4: Photograph of columnar jointing in the Strand Fiord Formation at East Fiord, western Axel Heiberg Island (Photograph by M-C. Williamson).	26
Figure 3.5: Photograph which shows fan patterned, thin columnar	27

jointing in the Strand Fiord Formation on the south shore of Strand
Fiord (Photograph by M-C. Williamson).

Figure 3.6: Map showing the density of sill spacing on the south shore
of Buchanan Lake, eastern Axel Heiberg Island (Modified from Williamson,
1988). 29

Figure 3.7: Photograph of the Buchanan Lake sills (From Williamson,
1988). 30

Figure 3.8: Photograph of the Buchanan Lake sills (From Williamson,
1988). 30

Figure 3.9: Photograph of sills at Eureka Pass, central Axel Heiberg
Island (Field notes Williamson, 2003). 31

Figure 3.10: Photograph of the sheet-like weathering patterns in the
olivine-bearing sills at Eureka Pass, central Axel Heiberg Island (Field
notes Williamson, 2003). 31

Figure 3.11: Photograph of a typical coarse-grained igneous intrusive
rock from Axel Heiberg Island, plane polarized light (Photograph by
Sheri Lyon). 36

Figure 3.12: Photograph of a typical coarse-grained igneous intrusive
rock from Axel Heiberg Island, crossed nicols (Photograph by Sheri
Lyon). 36

Figure 3.13: Digitized litholog for the Depot Point L-24 well. 39

Figure 4.1: Digitized litholog for the Depot Point L-24 well. 45

Figure 4.2: This enlarged section from the Depot Point L-24 lithology 46

log shows the red basaltic sill and the bordering contact-metamorphic zones.

- Figure 4.3:** Plot of model input data: a) a sea level curve, b) the sediment water interface temperature, and c) the heat flow values. 51
- Figure 5.1:** Simple three-layer model showing sediment deposition. 58
- Figure 5.2:** Simple three-layer model showing erosion of formations. 59
- Figure 5.3:** Simple three-layer model showing sill emplacement. 59
- Figure 5.4:** Burial history plot for the Depot Point L-24 well. 61
- Figure 5.5:** Burial history plot with a temperature overlay for the Depot Point L-24 well. 62
- Figure 5.6:** Temperature profile around sills. 63
- Figure 5.7:** Burial history plot with a source rock temperature overlay for the Depot Point L-24 well. 65
- Figure 5.8:** Burial history plot with a maturity zone overlay for the Depot Point L-24 well. 66
- Figure 5.9:** Depot Point L-24 well temperature overlay without including sill intrusion. 69
- Figure 5.10:** Depot Point L-24 well temperature overlay without rifting. 69
- Figure 5.11 a):** Maturity zones for the Depot Point L-24 well. 71
- Figure 5.11 b):** Maturity zones for the Depot Point L-24 well; the intrusion of sills has been omitted. 71
- Figure 5.12:** Depot Point L-24 well temperature overlay with sill intrusion at 90 Ma. 73
- Figure 5.13:** Depot Point L-24 well temperature overlay with sill 73

intrusion at 110 Ma.

- Figure 5.14 a):** Maturity zones for the Depot Point L-24 well. 75
- Figure 5.14 b):** Maturity zones for the Depot Point L-24 well; the intrusion of sills occurs at 122Ma. 75
- Figure 5.15:** A comparison of the maturity zones in three Depot Point L-24 model variations. 76
- Figure A.1:** Petrography sample location map, Axel Heiberg Island. 100
- Figure B.1:** Geological time scale (After Gradstein and Ogg, 1996) 107
- Figure C.1:** Burial history plot with an oil generation overlay; emphasis on the Blaa Mountain Formation. 108
- Figure C2:** Burial history plot with a gas generation overlay; emphasis on the Blaa Mountain Formation. 109
- Figure C3:** Burial history plot with an oil generation overlay; emphasis on the Hare Fiord and Van Hauen Formations. 110
- Figure C4:** Burial history plot with gas generation overlay; emphasis on the Hare Fiord and Van Hauen Formations. 111

List of Tables:	Page
Table 3.1: Sill data indicated by the Depot Point L-24 well.	38
Table 4.1: Model input: lithologies intersected by the Depot Point L-24 well and inferred formations.	44
Table 4.2: Estimated total organic carbon and hydrogen index values for potential source rocks.	48
Table 4.3: Vitrinite reflectance values (From Arne <i>et al.</i> , 2002) for the Depot Point L-24 well.	49
Table 4.4: Data sets for present day and paleo-heat flow for the Depot Point L-24 well (From Jones <i>et al.</i> , 1989 and Majorowicz and Embry, 1998).	50
Table 4.5: Model input: heat flow values.	50
Table A.1: Alteration Index (Modified from Williamson, 1988 and Williamson, <i>pers comm.</i>)	98
Table A.2: Petrographic Descriptions: Intrusive Rocks from Axel Heiberg Island.	101

CHAPTER ONE: INTRODUCTION

1.1 Opening Statement

It is common practice for exploration geologists to develop numerical models, which when correctly built may help predict and locate valuable resources. When such models are constructed for simulating hydrocarbon generation and migration, sedimentary rock properties including thickness, thermal conductivity, porosity, permeability, total organic carbon, geochemical maturation parameters, vitrinite reflectance, paleo-temperatures, and heat flow are important input values. However, quantitative hydrocarbon systems models rarely include igneous rocks, which as shown through this thesis, can have profound effects on oil and gas generation processes because of the considerable heat they introduce.

The Sverdrup Basin, located in Nunavut in the Canadian Arctic, is a large sedimentary basin with known hydrocarbon resources. In addition to over 10 km of sedimentary strata, the basin contains locally abundant extrusive volcanic rocks and their intrusive equivalents. This thesis demonstrates that hydrocarbon systems modeling in this region should not overlook the thermal influence of the igneous rocks. This study comprises a compilation of field observations, stratigraphy, well data, characteristics of the igneous rocks, and geochronological data, and presents for the first time a numerical model synthesis to determine the effects of sill emplacement on a hydrocarbon system in the Sverdrup Basin.

1.2 Study Area and the Strand Fiord Project

The study area for this thesis is located in the eastern part of the Sverdrup Basin on Axel Heiberg Island in Nunavut, Canada. Figure 1.1 shows the Canadian Arctic

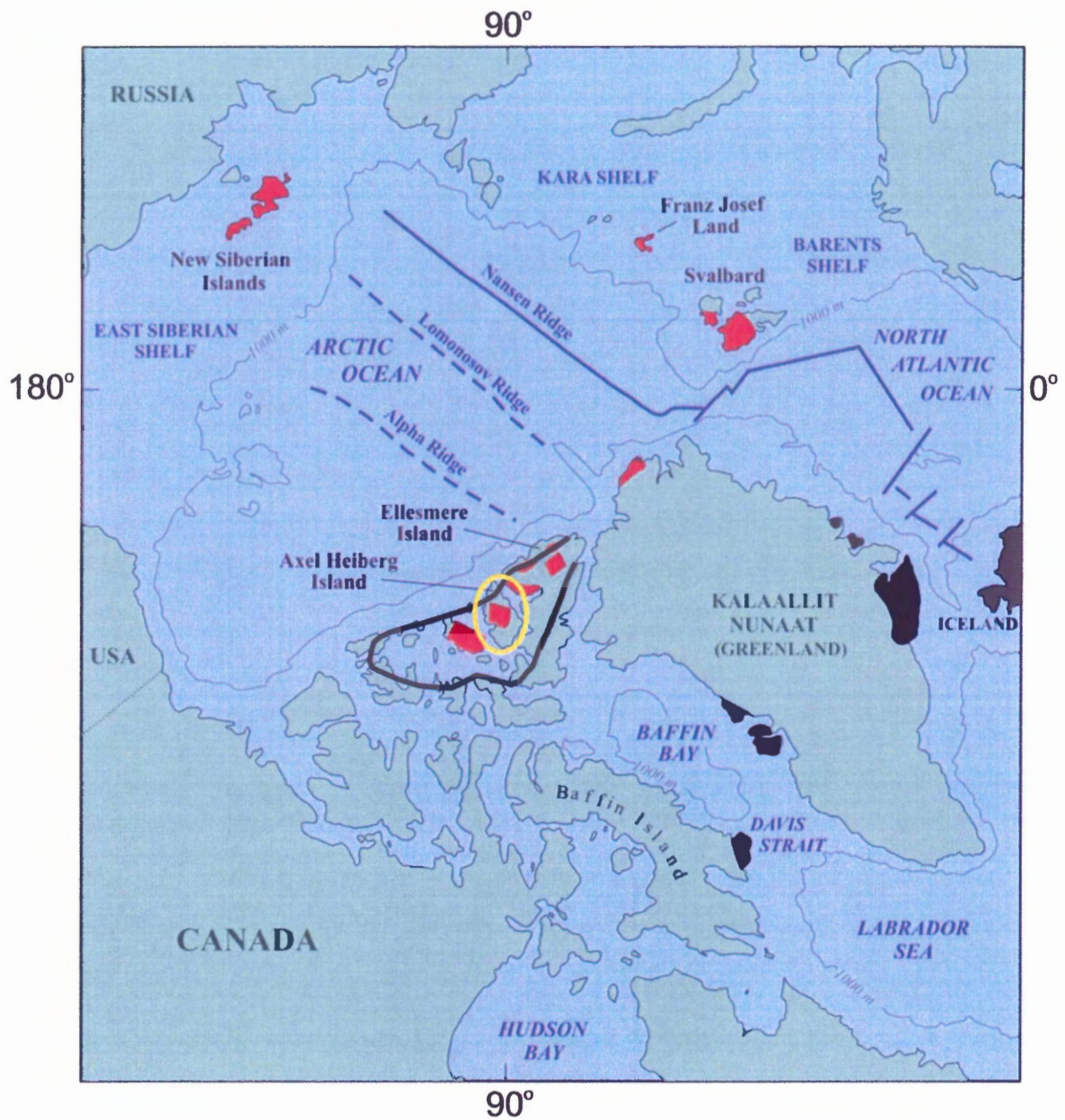


Figure 1.1: Location map showing northern Canada, the Sverdrup Basin (outlined in black), and Axel Heberg Island (circled in yellow). The red areas represent localities in circum Arctic regions where igneous rocks of Mesozoic age have been identified (Modified from Vogt *et al.*, 2006).

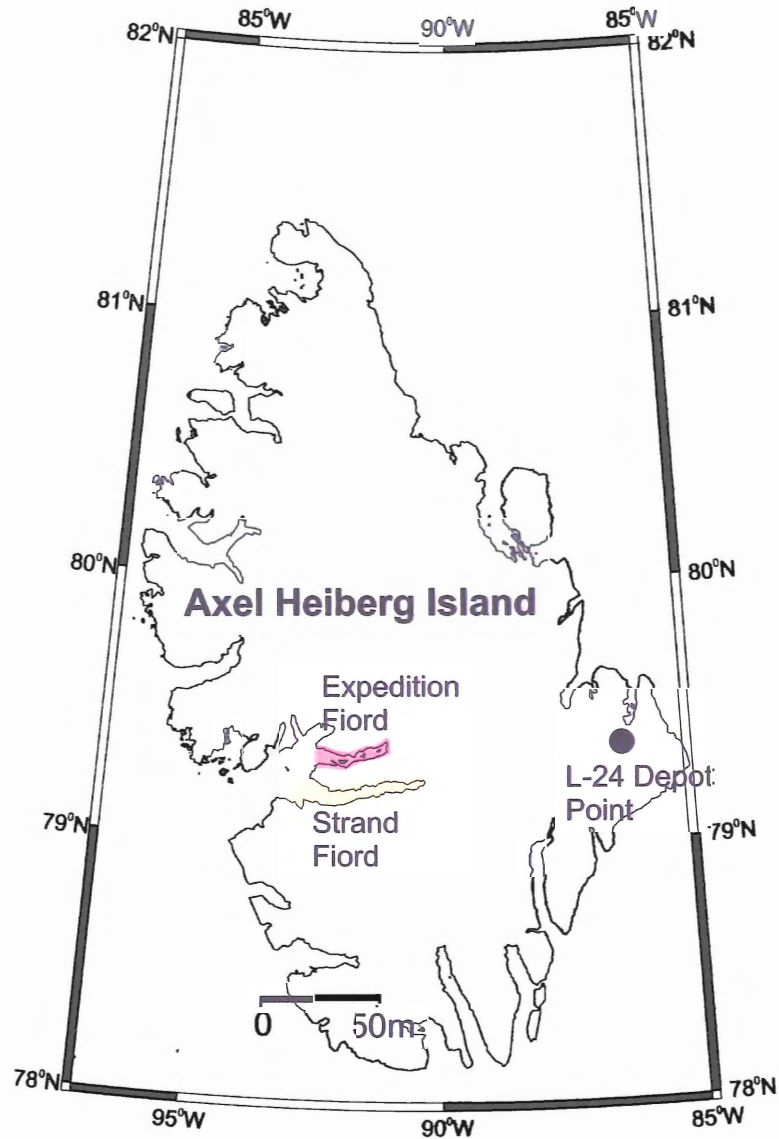


Figure 1.2: This location map focuses on Axel Heiberg Island. Expedition Fiord (shaded in pink), Strand Fiord (shaded in yellow), and the Depot Point L-24 well are shown.

Archipelago, the Sverdrup Basin (outlined in black), and Axel Heiberg Island (circled in yellow). The red areas represent igneous rock localities of Mesozoic age identified in circum Arctic regions (e.g. Vogt *et al.*, 2006; Harrison, 2005). Figure 1.2 focuses on Axel Heiberg Island. Strand and Expedition Fiords and the Depot Point L-24 well, the subject of the numerical modeling experiment, are indicated. Work in this region is part of the Strand Fiord project, which was initiated in 2002 by Dr. Marie-Claude Williamson

of the Geological Survey of Canada (GSC) and Dr. Marcos Zentilli of Dalhousie University. Numerical modeling has not been used previously as part of the Strand Fiord project. The results presented here expand the scope of the project and open a new field of investigation in this region of Nunavut.

1.3 Previous Research

As previously mentioned, this thesis contributes to the Strand Fiord Project, a recent collaboration between the Geological Survey of Canada and Dalhousie University, which emphasizes the interactions between igneous rocks and evaporite diapirs and their combined thermal effects on the surrounding lithologies and resource potential. Williamson (1988) characterized the Cretaceous volcanic system that led to the emplacement of a large igneous province (LIP) in the Sverdrup Basin and produced continental flood basalts, comparable in volume to the Columbia River Basalt of the western United States (Williamson, 1998). The numerical modeling in the basin focuses on the sills, which Williamson and MacRae (2001) suggest are part of a network many times greater in volume than the extruded igneous rock. A GIS map of western and central Axel Heiberg Island that emphasizes salt structures and igneous lithologies prepared by Lyon (2005) is the most recent contribution to the Strand Fiord Project. The geological units, stratigraphy, and structures represented in this detailed GIS are based on 1:250,000 geological maps compiled by the Geological Survey of Canada.

Fission-track studies of the Mesozoic succession are useful in constraining the time period of basin inversion. Fission-track analyses and vitrinite reflectance data from Axel Heiberg and Ellesmere Islands (Figure 1.1) provide information about cooling in the

eastern Sverdrup Basin (Arne *et al.*, 2002) and the timing of thrust fault movement (Arne *et al.*, 1998; Grist and Zentilli, 2005).

The resource potential of the Sverdrup Basin is a topic of interest for academic research as well as industry. There is currently a renewal in hydrocarbon and mineralization research. So far, nineteen hydrocarbon discoveries have been made in the western Sverdrup Basin where one hundred and nineteen wells have been drilled in Mesozoic plays (Chen *et al.*, 2000) giving a success rate of almost 16%. Most of these discoveries are natural gas pools (Chen *et al.*, 2002). However, in the eastern part of the Sverdrup Basin, despite the presence of adequate source rocks and structures, the exploration results were disappointing; the explanation may be a problem of timing in the hydrocarbon system, where traps were formed after the hydrocarbons migrated (Arne *et al.*, 2002), or a detrimental thermal effect from sill intrusions, as explored in this study. In 2001, Williamson and MacRae presented a preliminary report on the potential for basalt-hosted Ni-Cu-PGE deposits.

1.4 Methods for Hydrocarbon Modeling

A classic approach to basin modeling can be merged with data on volcanic systems using various computer software programs. PetroMod[®] is the software chosen for model construction and simulation in this thesis. One-dimensional thermal and sedimentation modeling has been successfully applied in other regions to simulate hydrocarbon generation and maturity levels (e.g. Waples, 1998). Basin analysis provides a breakdown of the evolution of basin systems over time through the compilation of physical properties and processes. High-quality model results require the input of measured physical properties that act as boundary conditions and keep the model as

realistic as possible (Waples, 1998). This study uses log data from the Depot Point L-24 well as a framework. The rest of the model input data is a collection of measured data sets and inferred values that are discussed in detail throughout this thesis.

1.5 Objectives

The scientific goal of this project is to explore the interaction of the volcanic and hydrocarbon systems within the eastern Sverdrup Basin, in particular the thermal impact of sill emplacement on the timing and rates of hydrocarbon generation. The end product consists of a computer model that integrates available data sets and allows the simulation of hydrocarbon generation within a localized section of the study area and provides a temperature profile in the lithologic column. This model allows the thermal effects of sill emplacement within the eastern part of the Sverdrup Basin to be recognized. Oil and gas migration and entrapment are not predicted by the one-dimensional modeling, and a detailed study is beyond the scope of this thesis.

The following scientific questions are addressed by this thesis:

1. Key observations on the hydrocarbon and magmatic systems in the Sverdrup Basin: why should they be integrated?
2. How and where in the evolution of the Sverdrup Basin does sill emplacement affect the hydrocarbon system?
3. How do the results for the modeled Depot Point L-24 well differ from scenarios where sills are not introduced or where the age of sill emplacement is different?
4. Can one-dimensional modeling quantify the effects of igneous activity on the hydrocarbon system within the Sverdrup Basin?

1.6 Thesis Organization

The first section of this thesis provides an overview of the Sverdrup Basin and discusses the geology within the study area with emphasis on characteristics of the magmatic and hydrocarbon systems. Chapter 2 is an overview of the Sverdrup Basin regional geology and the local geology of the study area on Axel Heiberg Island. Field observations, sill characteristics, and age data by M-C. Williamson and colleagues are discussed in Chapter 3. Chapter 4 introduces the modeling software, PetroMod[®] and presents all of the model input including well litholog data produced by the Canadian Stratigraphic Service Limited, heat flow data, vitrinite reflectance data, paleo-sea level, and other parameters. Chapter 5 explains and discusses the model results and concludes with a short sensitivity study limited to the effects of varying the age of sill emplacement and of omitting the sills. Chapter 6 reviews the entire project by discussing answers to the scientific questions posed in the introduction. The conclusion also includes information about the applicability of the methods used in this thesis in other areas and the potential for model refinement and future work.

Appendices include (A) hand sample descriptions and petrographic descriptions for igneous rocks from Axel Heiberg Island, (B) the version of the geologic time scale used in assigning formational ages, and (C) model result images additional to those presented in Chapter 5.

CHAPTER TWO: THE SVERDRUP BASIN: REGIONAL GEOLOGY AND MAGMATIC PROVINCE

2.1 Geological Overview of the Sverdrup Basin

The development of the Sverdrup basin in the Canadian Arctic Islands was the main process occurring in the Arctic Islands from the Namurian (Late Carboniferous) into the Late Cretaceous (Davies and Nassichuk, 1991). The Sverdrup Basin is a northeasterly-trending elongated structural depression (Balkwill *et al.*, 1983), which occupies a 1300 km by 400 km area and contains upper Paleozoic and Mesozoic strata (Trettin, 1989; Figure 2.1). The Arctic Platform is the southern border and the uplifted Sverdrup Rim is the northern border of the Sverdrup Basin (Balkwill *et al.*, 1983). The present day dimensions of the Sverdrup Basin are not consistent with paleo-dimensions because of post-depositional deformation (Trettin, 1989). It is likely that this basin formed through graben development during the Late Mississippian (Balkwill *et al.*, 1983) as result of Carboniferous to Early Permian rifting possibly related to thermal subsidence following previous Ellesmerian orogenic events (Sweeney, 1977).

The deposition of Proterozoic to Early Carboniferous rocks in the Arctic Islands and the Late Devonian to Early Carboniferous Ellesmerian Orogeny - a product of the accretion of volcanic arcs to Laurentia - predate the development of the Sverdrup Basin (Harrison, 2005; Trettin, 1989). The succession of sedimentary rocks deposited within the Sverdrup Basin is latest Paleozoic to Mesozoic (Embry, 1991) with a maximum thickness of 13 kilometers in the basin centre (Chen *et al.*, 2000). These strata were deposited during an estimated thirty transgressive-regressive cycles, which were caused

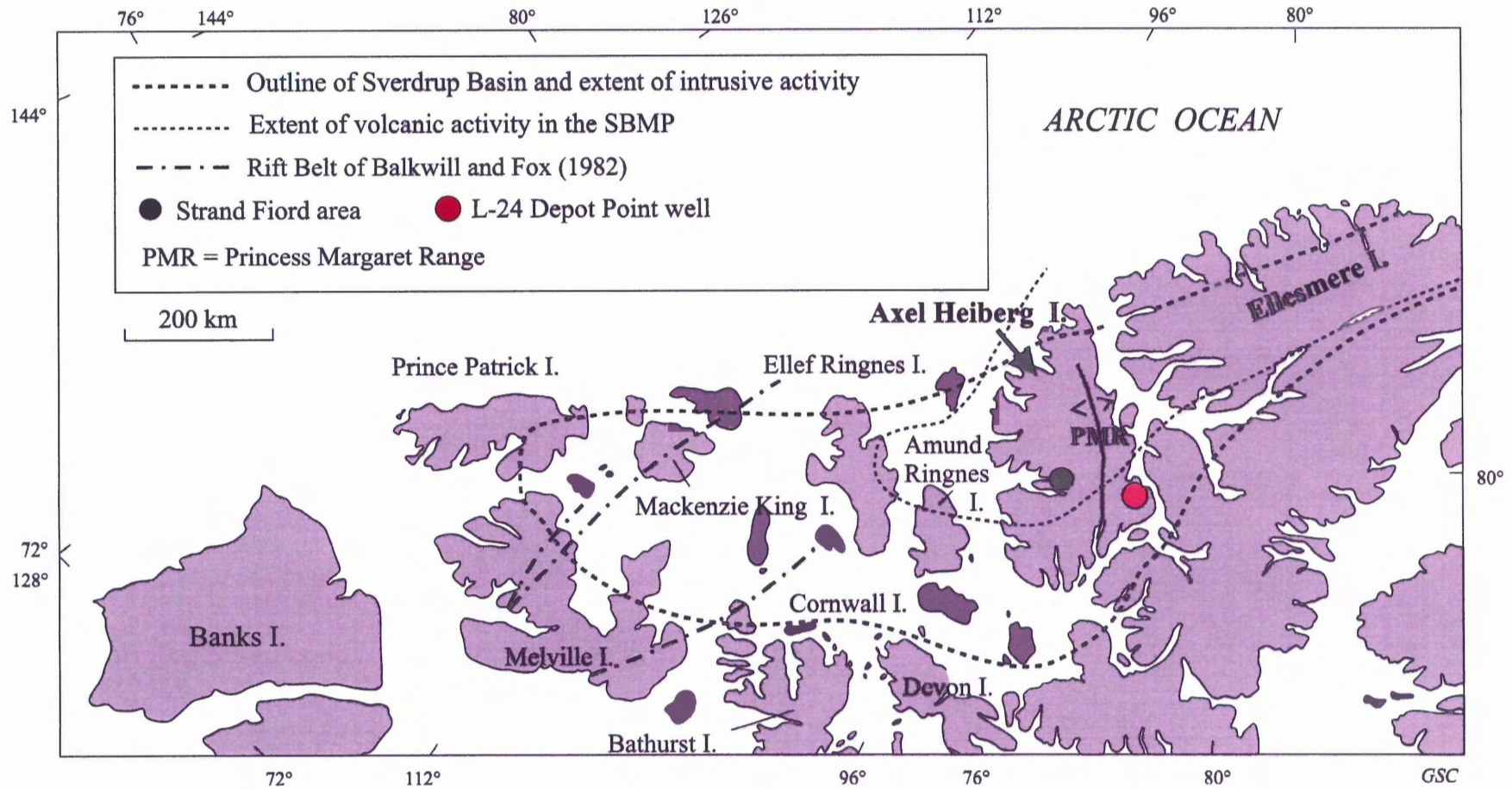


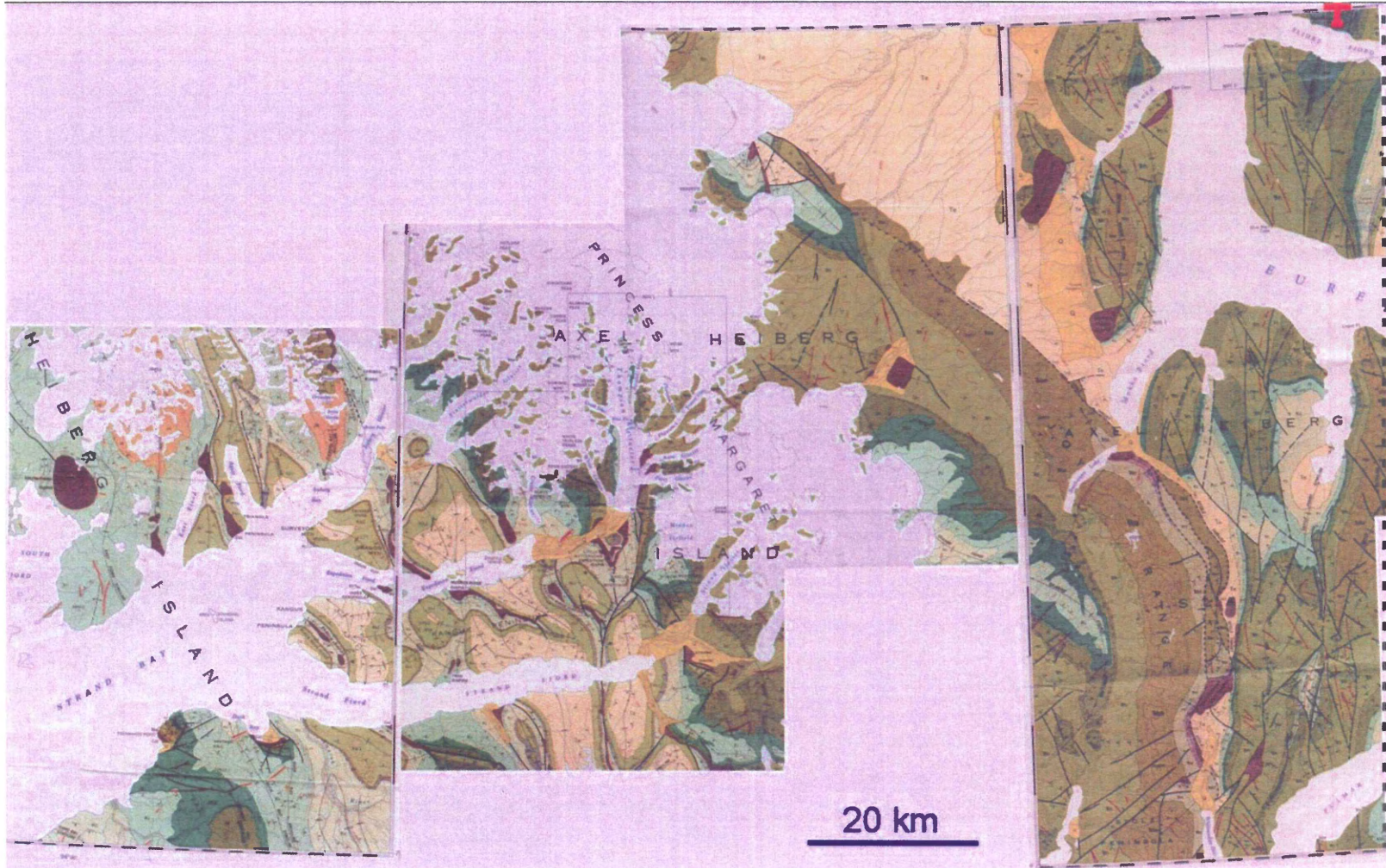
Figure 2.1: The Sverdrup Basin and the Sverdrup Basin Magmatic Province (SBMP) are outlined on this Arctic map. The Strand Fiord region and the Depot Point L-24 well are highlighted with black and red dots, respectively. The extent of igneous intrusive and extrusive activity is indicated by dashed lines. For symbol definitions see the legend (Modified from Villeneuve and Williamson, in press).

by changes in subsidence, eustatic sea level, and sediment supply (Embry, 1991). Most of the lithologies deposited in the basin are clastic; however, during the late Paleozoic, at the start of basin development, evaporite and carbonate rocks were formed (Trettin, 1989). A particularly important unit is the Otto Fiord Formation, which is an Upper Mississippian to Middle Pennsylvanian salt layer (Davies and Nassichuk, 1991). Salt related structures in the basin began to develop when the Otto Fiord Formation started to move and form diapirs (Embry, 1991). Salt diapirism is still occurring and is evident on Axel Heiberg Island (Zentilli *et al.*, 2005). This was initiated by younger clastic deposits which buried the evaporite strata (Harrison, 2005). The formations deposited within the Sverdrup Basin in the study area from oldest to most recent are: Otto Fiord, Hare Fiord, Van Hauen, Blind Fiord, Blaa Mountain, Heiberg, Ringnes, Awingak, Deer Bay, Isachsen, Christopher, Hassel, Strand Fiord, Kanguk, and Expedition (e.g. Balkwill *et al.*, 1983; Embry, 1991). Figure 2.2 is a composite of several geological maps at a scale of 1:250,000 that illustrates the formations relevant to this study. A cross section of the Sverdrup Basin shows which formations were deposited and subsequently eroded away above the Depot Point L-24 well and the formations that exist below the total depth of penetration of the well. The formations in the study area used as model input are discussed in more detail in Chapter 4.

Rifting in the east-central Sverdrup Basin caused by the opening of the adjacent Arctic Ocean in the Jurassic resulted in intrusive and extrusive igneous activity that affected the Paleozoic and Mesozoic strata in the Sverdrup Basin (e.g. Embry, 1991; Harrison, 2005). Lava successions extend from Amund Ringnes Island to the northeastern Sverdrup Basin. The intrusive dykes and sills are more widespread

80°00'N
96°00'W

80°00'N
84°00'W










79°00'N
96°00'W

79°00'N
84°00'W

Figure 2.2: This composite image shows several geological maps (1:250,000 scale) covering the area between 79°00'N and 80°00'N and 96°00'W and 84°00'W. The location of this map relative to the coastline is shown in Figure 3.1. For a legend, see the next page (Modified from Thorsteinsson, 1971a, 1971b, and 1971c.).

Legend

Quaternary		Quaternary sediments	
Tertiary		Eureka Sound Formation (sandstone and siltstone)	
Cretaceous		Kanguk Formation (shale and siltstone)	
		Hassel Formation (sandstone)	
		Christopher Formation (shale and siltstone)	
		Isachsen Formation (sandstone)	
Jurassic		Deer Bay Formation (shale and siltstone)	 Deer Bay Formation, Awingak Formation, and Savik Formation; undivided
		Awingak Formation and Savik Formation (sandstone)	
Triassic		Heiberg Formation (sandstone)	
		Blaa Mountain Formation (shale)	
Carboniferous		Otto Fiord Formation (halite)	

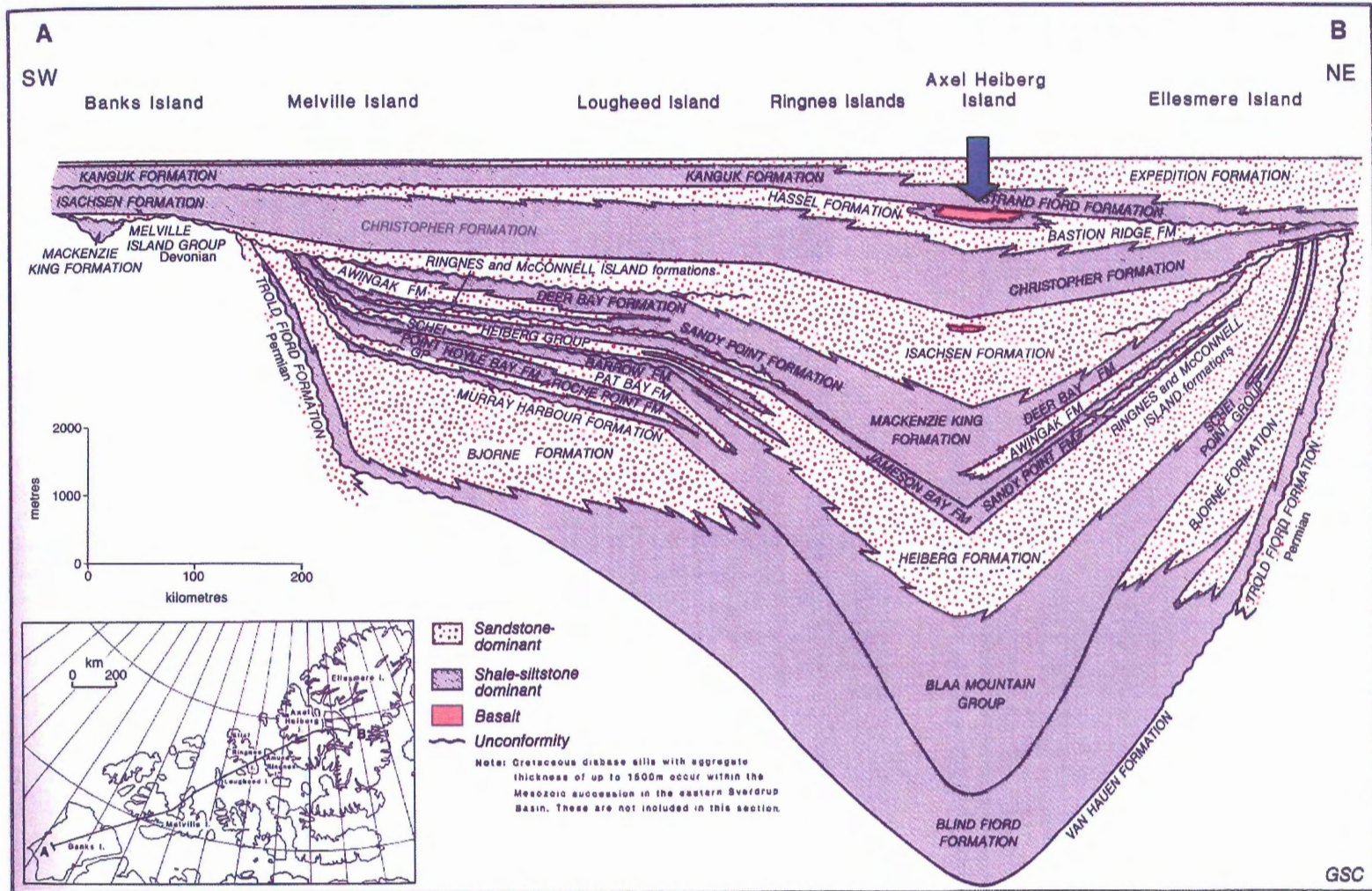


Figure 2.3: This simplified cross section provides an overview of the formation present within the study area. Cross sections including this one are used in determining the original thicknesses of the formations that have not been preserved at the well location, but are required in the completion of burial history. The blue arrow indicates the approximate location of the Depot Point L-24 well (total depth of 4033 m) (Modified from Embry, 1991).

and continue farther south and west to the border of the Sverdrup Basin (Villeneuve and Williamson, in press) as shown in figure 2.1. The igneous component of the Sverdrup Basin is discussed in detail later in this chapter and in Chapter 3.

Balkwill (1978) divided the structural components of the Sverdrup Basin into three categories; halokinetic structures, dykes and sills, and faults and folds developed during the Eurekan Orogeny. Halokinetic structures refer to the evaporite diapirs and related folds and faults which are well defined on Axel Heiberg Island (Balkwill, 1978) within the study area. The depositional phase of the Sverdrup Basin ended in the Late Cretaceous and basin inversion and erosion became the dominant processes in the Tertiary. Rifting terminated with the onset of the Eurekan orogen, which most strongly affected the eastern regions of the Canadian Arctic Islands (Harrison, 2005). The Eurekan orogen can be summarized as Late Cretaceous to Paleocene exhumation followed by compressional folding and faulting in the middle Eocene to early Miocene and subsequent exhumation during the remainder of the Miocene and possibly longer (Balkwill, 1978).

Variations in climate and sea level are important factors in the history of the Sverdrup basin and are required for model construction. Sea level was highly variable as proposed by Embry (1991) to explain episodic sediment deposition patterns during the Mesozoic. Lithological evidence including coal beds, limestone, ice-rafted clasts, and red beds provide clues regarding climate change, all of which have been used in the interpretation of paleo-climate in the Arctic (Embry, 1991). The discovery of warm-climate vertebrate fossil assemblages on western Axel Heiberg Island (Tarduno *et al.*, 1998) and the presence of Eocene fossil forests on eastern Axel Heiberg and Ellesmere

Islands (Kuagai *et al.*, 1995; Greenwood and Basinger, 1994) indicate Late Cretaceous and Tertiary thermal maxima.

2.2 The Magmatic System

The Sverdrup Basin is an intracontinental rift basin that hosts both extrusive and intrusive igneous rocks. The Sverdrup Basin is classified as a volcanic basin because of its significant magmatic component. The Karoo Basin in South Africa is an example of a volcanic basin which hosts a dense network of dykes and sills (Svensen and Planke, 2003) analogous to the Sverdrup Basin. The magmatic system, particularly the sills and their impacts on the hydrocarbon system, in the Karoo Basin has been studied extensively and compared with Arctic Basins; the Møre and Vøring Basins in the Norwegian Sea (Svensen and Planke, 2003). This highlights the potential for comparison between the Sverdrup and Karoo Basins and emphasizes the importance of understanding the igneous rocks within the Sverdrup Basin.

Basaltic magmatism in the Sverdrup Basin occurred during two separate time periods: 1) Late Carboniferous and Permian subaerial basalts and related basic intrusive rocks were emplaced on northern Axel Heiberg Island and northwestern Ellesmere Island as a result of Late Paleozoic rifting (Cameron, 1989). This period of magmatic activity pre-dates the deposition of the rocks modeled in this study; therefore a detailed analysis of the Paleozoic igneous rocks is beyond the scope of this thesis.

2) Renewed rifting in the Cretaceous coincided with another period of basaltic magmatism (Williamson, 1988). Extrusive and intrusive units exist within the Isachsen, Christopher, and Hassel Formations (Balkwill *et al.*, 1983). The Strand Fiord Formation on Axel Heiberg Island is a series of lower Upper Cretaceous basaltic flows (Balkwill,

1978). Some of the intrusive units, sills and dykes, from the Isachsen, Christopher, and Hassel Formations have been dated and have Cretaceous ages (Buchan and Ernst, submitted). The Cretaceous magmatism can be further divided into several pulses (Villeneuve and Williamson, in press) which are discussed further in Chapter 3. Twenty-eight successive flows with defined vesicular flow tops have been identified within the Strand Fiord Formation (Embry and Osadetz, 1988) and the entire unit reaches a thickness of almost 1000 meters in the thickest measured sections (MacRae *et al.*, 1996).

Figure 2.1 indicates the approximate extent of igneous rocks within the Sverdrup basin. The intrusive and extrusive boundaries are based on outcrop locations and well data (Villeneuve and Williamson, in press). This figure also shows the locations of the Depot Point L-24 well and the Strand Fiord region on western Axel Heiberg Island, where igneous rocks outcrop on land. The Cretaceous volcanic and intrusive rocks are collectively referred to as the Sverdrup Basin Magmatic Province, SBMP (Williamson, 1998). The SBMP is illustrated in figure 2.1. There are no documented mafic intrusions that cross-cut the uppermost Cretaceous and Tertiary units within the basin (Balkwill, 1978) which were deposited after the igneous activity ended.

Many of the SBMP dykes are part of a fan pattern that radiates across the Queen Elisabeth Islands. These dykes belong to a large group of associated igneous intrusive rocks which are widespread across the Arctic, known as the High Arctic Large Igneous Province (HALIP). Aside from the Sverdrup Basin, HALIP intrusive rocks are present in northern Greenland, Svalbard, and Franz Josef Land (Buchan and Ernst, submitted; Tarduno, 1998). The HALIP dyke swarms could have originated from a mantle plume located at the southern end of the Alpha Ridge (e.g. Buchan and Ernst, submitted). The

Alpha Ridge (Figure 1.1) may represent a magmatic province of oceanic origin (Vogt *et al.*, 2006) possibly linked to hotspot activity that could have also influenced the style of magmatism in the Sverdrup basin (Embry and Osadetz, 1988).

2.3 The Hydrocarbon System

A hydrocarbon system is comprised of several components and processes; a source, migration, a reservoir, entrapment (seal required), and preservation (Hunt, 1996). The entire hydrocarbon system is not modeled in this thesis. The source rock is the most important hydrocarbon system component in one-dimensional modeling.

Mesozoic rocks on Melville Island, King Christian Island, and western Ellef Ringnes Island in the south-central to southwestern Sverdrup Basin host oil and natural gas. Between 1969 and 1986, 119 exploratory wells were drilled in the Sverdrup Basin. Twenty-five pools with gas and eight pools with oil were discovered (Chen *et al.*, 2002). Many wells investigated targets within the upper Paleozoic and Mesozoic units (Balkwill, 1978) and most of the discoveries are present in the upper Triassic to Lower Jurassic Heiberg sandstone (Chen *et al.*, 2002).

When assessing the hydrocarbon resources of any basin, targets must be identified and ranked in order of potential. Plays and discoveries in the Sverdrup Basin are related to structural traps, mainly salt-cored, low amplitude folds (Chen *et al.*, 2002). Strata within the Blaa Mountain, Ringnes, and Awingak Formations have good source rock potential with total organic carbon (TOC) values of 4.0-6.0 and hydrogen indices (HI) of 100-400. Strata within the Hare Fiord, Van Hauen, Jameson Bay, Deer Bay, and Christopher Formations have lower source rock potential with TOC values of 0.5-2.5 and HI values of 50-300 (Gentzis and Goodarzi, 1993a; Gentzis and Goodarzi, 1993b; and

Gentzis and Goodarzi, 1991). The Heiberg Formation is a thick, widespread sandstone unit that is the best potential reservoir in the study area as indicated by previous discoveries from plays in this unit (Chen *et al.*, 2002).

Deep burial, mafic igneous intrusions, and exhumation have strongly affected the eastern and central regions of the Sverdrup Basin (Balkwill, 1978). Axel Heiberg and Ellesmere Islands are within a region of reduced oil and natural gas potential as the most probable reservoirs have been exhumed and eroded and the hydrocarbon system components have been affected by magmatic activity. The burial history model of the Depot Point L-24 well on Axel Heiberg Island provides further insight into the processes which affected the hydrocarbon system in this region.

2.4 System Integration

Hydrocarbon generation predictions in the Sverdrup Basin require the geological characteristics of volcanic and hydrocarbon systems to be integrated and their interactions explored. Schutter (2003) states that complete exploration strategies should include hydrocarbons found in and around igneous lithologies. Sill emplacement causes heating, pore fluid expulsion, and metamorphic reactions which affect basin evolution (Malthe-Sørenssen *et al.*, 2004). Igneous activity may initiate oil and/or gas generation as a product of this heating, and solidified igneous units will alter the permeability structure in the basin and may constitute effective seal rocks once emplaced (Schutter, 2003). Contrary to this, if the igneous rocks fracture during cooling, they may be permeable to fluids. However, the heat introduced into the basin by igneous activity could also lead to hydrocarbon over-maturation (Schutter, 2003).

In the Karoo Basin, South Africa, several interactions between the magmatic system and other basin components have been recognized. Contact aureoles around intrusive bodies show the development of hornfels units, which in some cases are fractured and act as aquifers. These fractured hornfels have reservoir potential. Some wells within the Karoo Basin intersect source rocks which produced petroleum upon introduction of sill complexes (Svensen and Planke, 2003).

Although large volumes of basalt erupted as lava flows, very little effect on the hydrocarbon systems is expected because of rapid cooling into air. In addition, most of the lava flows are thin and cool rapidly prior to burial by subsequent flows. The sills and dykes are predicted to have a greater effect on the surrounding strata because the excess heat of intruded magma is transferred efficiently to adjacent rocks during the cooling process (Schutter, 2003). The contact aureoles of metamorphosed rock documented on the Depot Point L-24 well litholog are effects of sill intrusion and are discussed in Chapters 3 and 4. These metamorphosed zones formed in response to the increased temperature caused by the intrusion, which allows crystallization and the formation of new mineral phases, especially in clay-rich deposits.

The thermal effects of the sills have a further reach than these metamorphic contact zones, although this is not obvious from field observations and well logs. Beyond the visible contact aureoles there is likely enough heat to affect source rocks or hydrocarbon reserves. As a result, igneous activity adds another level of complexity to the hydrocarbon system. The proximity of sills to source rocks and reservoirs determines the magnitude of the effects because the heat decreases away from the heat source. The situation can be further complicated if magmatism is accompanied by hydrothermal

circulation (Schutter, 2003). The intrusion of sills into sediments rich in organic carbon has been suggested as a cause for explosive activity in hydrocarbon-rich volcanic basins that results in catastrophic methane release into the atmosphere (Svensen *et al.*, 2004).

It is expected that sill intrusion will have greater effects on the surrounding host rocks than extrusive magmatism. Therefore, it is essential to understand the characteristics of the intrusive feeder systems to flood basalts of the Sverdrup Magmatic Province when determining the thermal history of the Depot Point L-24 well and subsequently the hydrocarbon generation potential.

2.5 Summary

The Sverdrup Basin is an upper Paleozoic and Mesozoic depositional centre (Trettin, 1989) which likely developed as a result of Carboniferous to Permian rifting (Balkwill *et al.*, 1983). Renewed rifting in the Cretaceous caused by the opening of the adjacent Arctic Ocean resulted in intrusive and extrusive igneous activity that affected the Paleozoic and Mesozoic strata in the Sverdrup Basin (e.g. Embry, 1991; Harrison, 2005). The Cretaceous volcanic and intrusive rocks are collectively referred to as the Sverdrup Basin Magmatic Province, SBMP (Williamson, 1998).

So far, twenty-five pools with gas and eight pools with oil were discovered (Chen *et al.*, 2002). Most of the discoveries are present in the upper Triassic to Lower Jurassic Heiberg sandstone (Chen *et al.*, 2002). Strata within the Blaa Mountain, Ringnes, and Awingak Formations have good source rock potential and strata within the Hare Fiord, Van Hauen, Jameson Bay, Deer Bay, and Christopher Formations have lower source rock potential (Gentzis and Goodarzi, 1993a; Gentzis and Goodarzi, 1993b; and Gentzis and Goodarzi, 1991).

Hydrocarbon generation predictions in the Sverdrup Basin require the geological characteristics of volcanic and hydrocarbon systems to be integrated and their interactions explored. The intrusion of igneous rocks introduces heat and therefore, may initiate hydrocarbon generation (Schutter, 2003). The Karoo Basin in South Africa has been studied extensively and shows evidence of hydrocarbon generation related to igneous intrusions. The Karoo Basin has been compared with Arctic basins in the Norwegian Sea (Svensen and Planke, 2003). This emphasizes the importance of understanding the igneous rocks within the Sverdrup Basin and introducing the igneous rocks into a hydrocarbon systems model.

CHAPTER 3: ATTRIBUTES OF VOLCANIC AND INTRUSIVE ROCKS IN THE SVERDRUP BASIN MAGMATIC PROVINCE

3.1 Distribution of Igneous Rocks on Axel Heiberg Island

The purpose of the numerical model is to determine the effects of igneous intrusions on hydrocarbon generation. The numerical model requires the Depot Point L-24 well litholog, but also relies on a good understanding of the stratigraphy in the Mesozoic succession in the local area. The characteristics of the sedimentary units that form the basis of the numerical model are listed in Chapter 4. In this chapter, emphasis is placed on volcanic and intrusive rocks in the Mesozoic succession of central Axel Heiberg Island. It is beyond the scope of this thesis to describe the features of all of the volcanic and intrusive rocks in the Sverdrup Basin Magmatic Province.

The Sverdrup Basin Magmatic Province records the characteristics of large igneous provinces (Coffin and Eldholm, 1994). The episodes of voluminous mafic magmatism are associated with rifting and the opening of the Arctic Ocean (Williamson *et al.*, 2005). The volume of erupted magma is estimated to range from 10,000-20,000 km³ which is comparable to the western American Columbia River Basalt. The system of intrusive dykes and sills totals a volume at least one order of magnitude larger than that of the extrusive rocks (Williamson, 1998; Villeneuve and Williamson, in press). Figure 2.1 illustrates the extent of the Sverdrup Basin Magmatic Province and highlights the locations of the study area and the Depot Point L-24 well. Flood basalts and sills on Axel Heiberg Island are well exposed in the Princess Margaret Range which stretches north-south across the length of the island. To summarize the main features of the volcanism, field data from 2003-4 expeditions to Axel Heiberg Island are illustrated through the use of maps, stratigraphic columns, and

field photographs. Key petrographic observations are discussed in this chapter to highlight the characteristics of the intrusive igneous rocks. The Depot Point L-24 well is located on eastern Axel Heiberg Island and the described igneous units are from the western part of the island. The difference in location is because the lava flows that are best exposed in the Princess Margaret Range have been eroded in the east (Balkwill and Fox, 1982). Figure 3.1 is a location map which shows East Fiord, Strand Fiord, Expedition Fiord, Bunde Fiord, the Amarok River, Buchanan Lake, Eureka Pass, the Geodetic Hills, the Princess Margaret Range (PMR), the Wolf Intrusion, and the Depot Point L-24 well. Igneous units from these locations will be discussed throughout this chapter.

3.2 Field Setting

3.2.1 Volcanic Rocks

The volcanic rocks on Axel Heiberg Island belong to the Strand Fiord Formation, a sequence of mafic flows with minor volcanoclastic components (Tozer, 1960). The Strand Fiord Formation has a maximum recorded thickness of 998m in Bunde Fiord on northern Axel Heiberg Island (MacRae *et al.*, 1996). This is the highest stratigraphic unit in the area, implying that the original thickness was greater and what we see is a post-erosional remnant not its original extent (Ricketts, *et al.*, 1985). The thickest sequence of the formation on central Axel Heiberg was measured to be 701 m in East Fiord. The Strand Fiord Formation becomes thinner to the south and east and is not preserved at the Depot Point L-24 well location more likely due to erosion and lack of preservation rather than relating to its absolute extent (e.g. Ricketts, *et al.*, 1985). Figure 3.2 shows a set of stratigraphic sections that demonstrate the variance in thickness as well as trend of decreasing thickness towards the east. Figure 3.3 shows the basalt flows as East Fiord, located on western Axel Heiberg

Location Map: Axel Heiberg Island

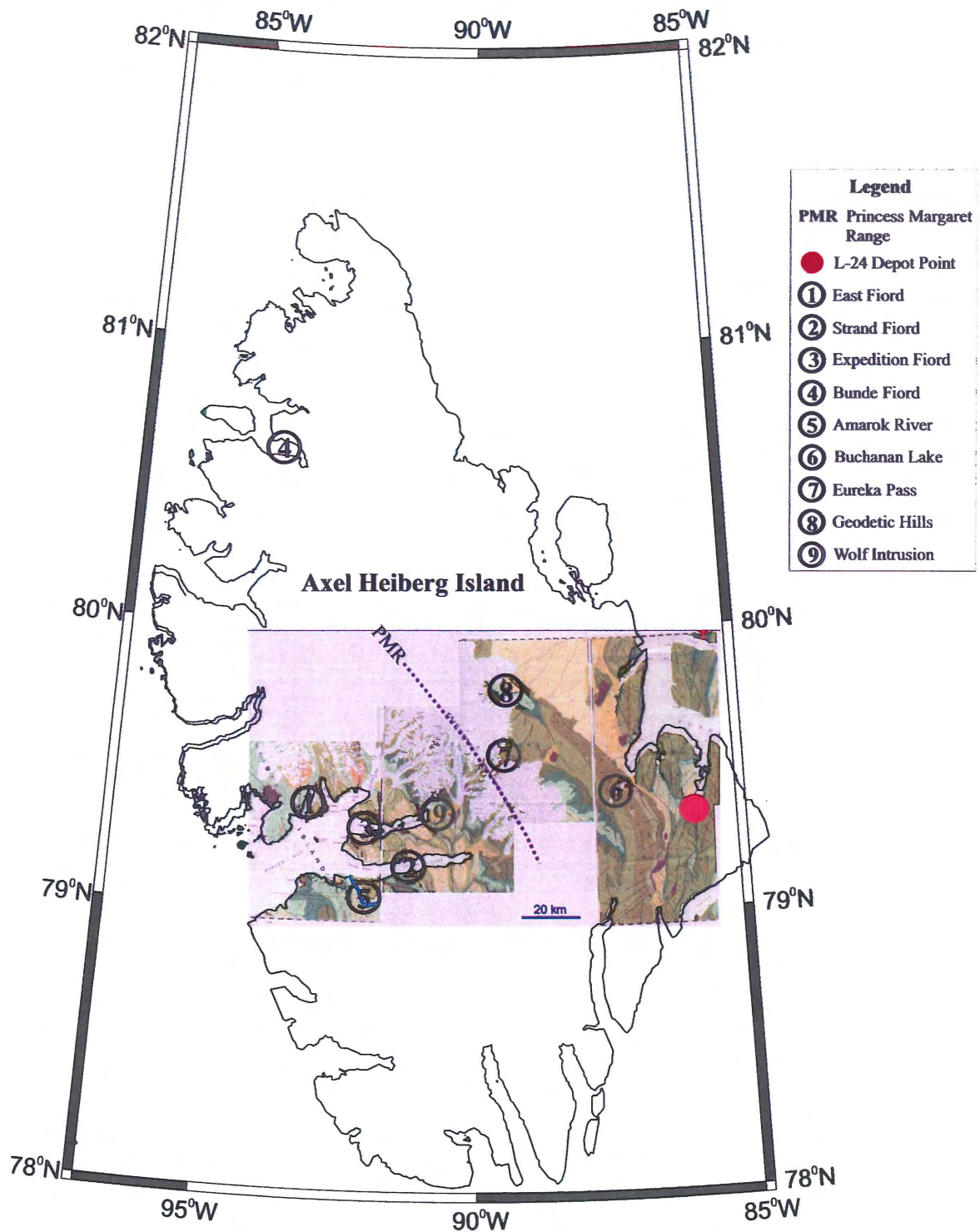


Figure 3.1: This location map shows East Fiord, Strand Fiord, Expedition Fiord, Bunde Fiord, the Amarak River, Buchanan Lake, Eureka Pass, the Geodetic Hills, the Princess Margaret Range (PMR), the Wolf Intrusion, and the Depot Point L-24 well. Igneous units from these locations will be discussed throughout this chapter. The geological maps are from Thorsteinsen (1971a, 1971b, and 1971c) and a detailed legend and approximated coordinates are provided in Figure 2.2.

Island. Figures 3.4 and 3.5 show columnar jointing in members of the Strand Fiord basalt flow sequence.

Both extrusive and intrusive rocks are present in the stratigraphic sections by MacRae et al. (1996; Figure 3.2). Although the volume of intrusive rocks in the Sverdrup Basin is larger than the volume of extrusive flows (Williamson, 1998; Villeneuve and Williamson, in press), the volume of lava flows in these stratigraphic sections is much larger than that of the sills, which have intruded the underlying mudstone and sandstone-dominated Bastion Ridge Formation (MacRae et al., 1996). These units were interpreted as invasive flows (Muecke et al., 1991). The Strand Fiord Formation has not been preserved on eastern and southern Axel Heiberg Island due to exhumation and erosion, if it was ever present there.

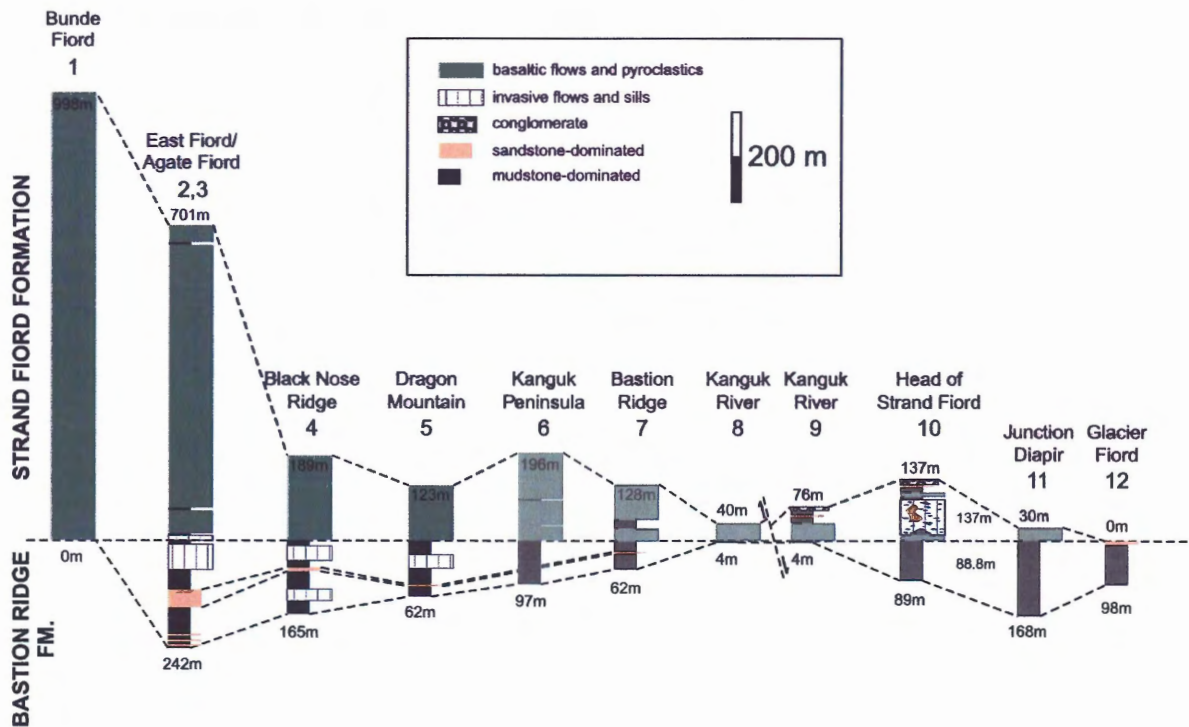


Figure 3.2: Stratigraphic correlation diagram showing the thinning of the Strand Fiord towards the east from East Fiord/Agate Fiord to Glacier Fiord. To clarify confusing nomenclature, East Fiord is located on western Axel Heiberg. (From MacRae et al., 1996) The data represented by the figure is from MacRae et al., 1996 and Ricketts et al., 1985 and references therein.

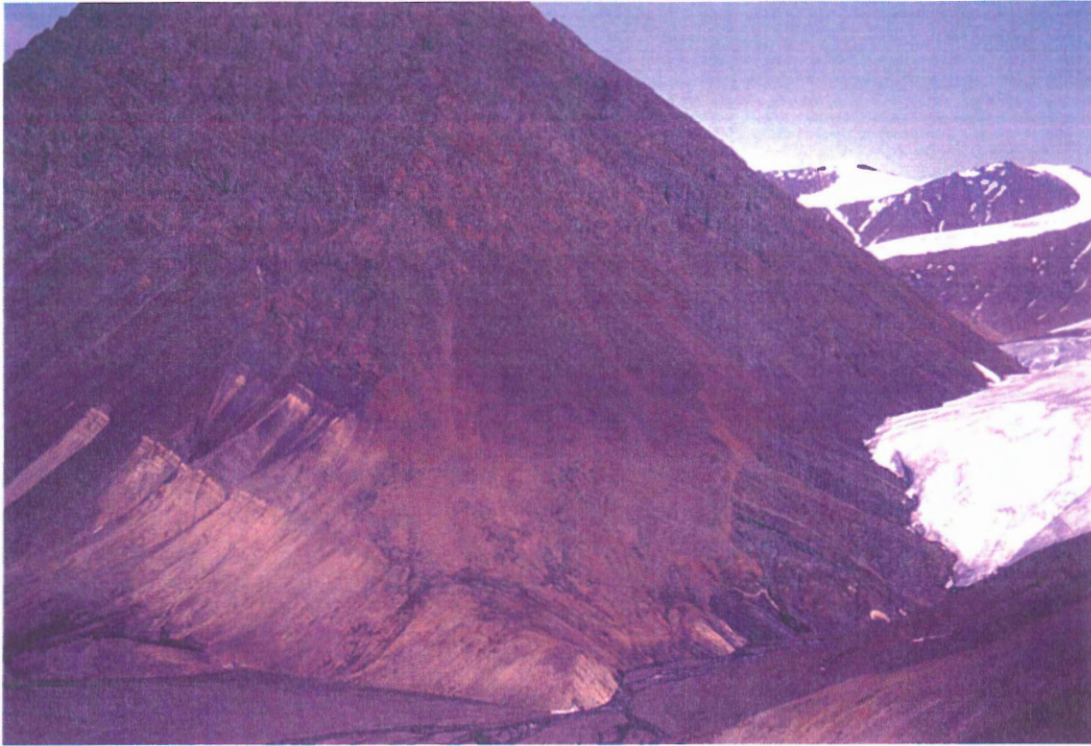


Figure 3.3: Aerial view of the Strand Fiord Formation at the head of East Fiord, western Axel Heiberg Island (see also Fig. 3.2; Composite section 2,3). Greyish flow tops are visible in the upper left corner of the photograph. The river flows from the northeast. (MacRae, 1996).



Figure 3.4: Columnar jointing is a prominent feature of lava flows in the Strand Fiord Formation. Joints develop during the cooling process, and are oriented perpendicular to the base of the flow. Amarok River, south shore of Strand Fiord (Photo M.-C. Williamson).

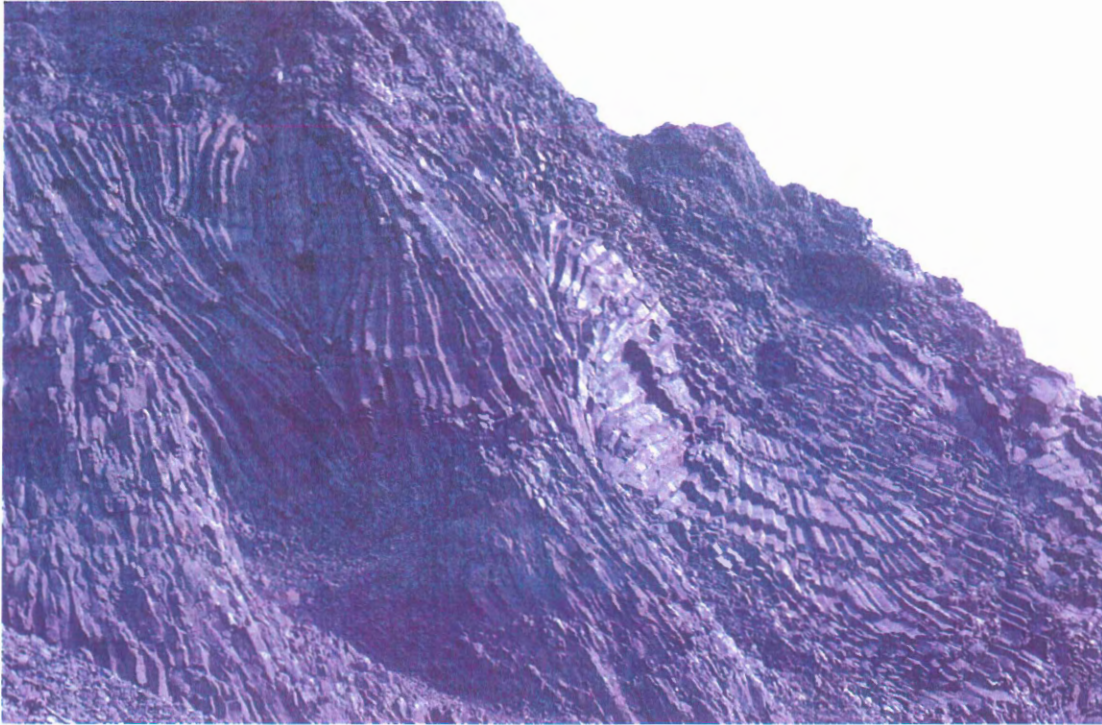


Figure 3.5: Thin, fan-shaped columns develop when lava flows advance over poorly consolidated, water-saturated sediments, resulting in a continuous change of orientation of cooling surfaces at the base of the flow, or within the entablature. Glacier Fiord Syncline, head of Strand Fiord (Photo M.-C. Williamson)

The lack of preservation in the rock record means that the absolute lateral extent of the Strand Fiord Formation upon emplacement cannot be determined (Ricketts, *et al.*, 1985).

3.2.2 Intrusive Rocks

Abundant sills and dykes intrude Carboniferous to Cretaceous strata on Axel Heiberg Island. The dykes have documented thicknesses of a few meters and are generally located in proximity to faults (Balkwill, 1978). Some of the dykes in the western Sverdrup Basin can be traced over tens to hundreds of kilometres using aeromagnetic anomalies (Buchan and Ernst, submitted), others occur in swarms (Jollimore, 1986). The sills are much larger, sometimes 100 m thick and can be traced laterally for tens of square kilometres by outcrop correlation and geophysical anomalies (Balkwill, 1978). Despite the prominence of intrusive rocks in the landscape, sills have not yet been included on the current GSC 1:250,000 scale

geologic maps. Figure 3.6 illustrates the density of sills intruding the Blind Fiord, Blaa Mountain, and Heiberg formations in the Buchanan Lake region. Aside from their high density spacing, the Buchanan Lake sills are characteristically thick as shown in figures 3.7 and 3.8. Thinner, more sparsely distributed sills were documented at Eureka Pass in the Geodetic Hills (Fig. 3.9). Weathering patterns of olivine-bearing sills are evident at Eureka Pass, as shown in figure 3.10. There are no complete stratigraphic sections of the subsurface sills in eastern Axel Heiberg Island. The best way to illustrate these sills for the purpose of this thesis is through the use of the Depot Point L-24 well log discussed later in this chapter.

The country rocks hosting intrusions show contact zones where local metamorphism has produced hornfels from shale and siltstone, and has cemented sandstones with silica (Balkwill, 1978). This contact zone description is consistent with the contact-metamorphism documented in the Depot Point L-24 litholog discussed in section 3.6.

3.3 Age Determination of Igneous Units in the SBMP

The age dates of the igneous units are particularly important when creating a numerical model. This is especially true for the intrusive units which are introduced into the basin at a specified time. Varying the age of sill emplacement produces different model results, discussed in Chapter 5. This emphasizes the importance of acquiring absolute age dates for igneous bodies within the study area. The sills intersected by the Depot Point L-24 well have not been dated; therefore the date assigned to them in the numerical model is based on the ages of emplacement of other igneous units of similar character on Axel Heiberg Island. The age of the magmatic system in the Sverdrup Basin was discussed in Chapter 2. This chapter investigates the age dates of rocks within the study area on Axel Heiberg Island and on neighbouring Ellesmere Island.

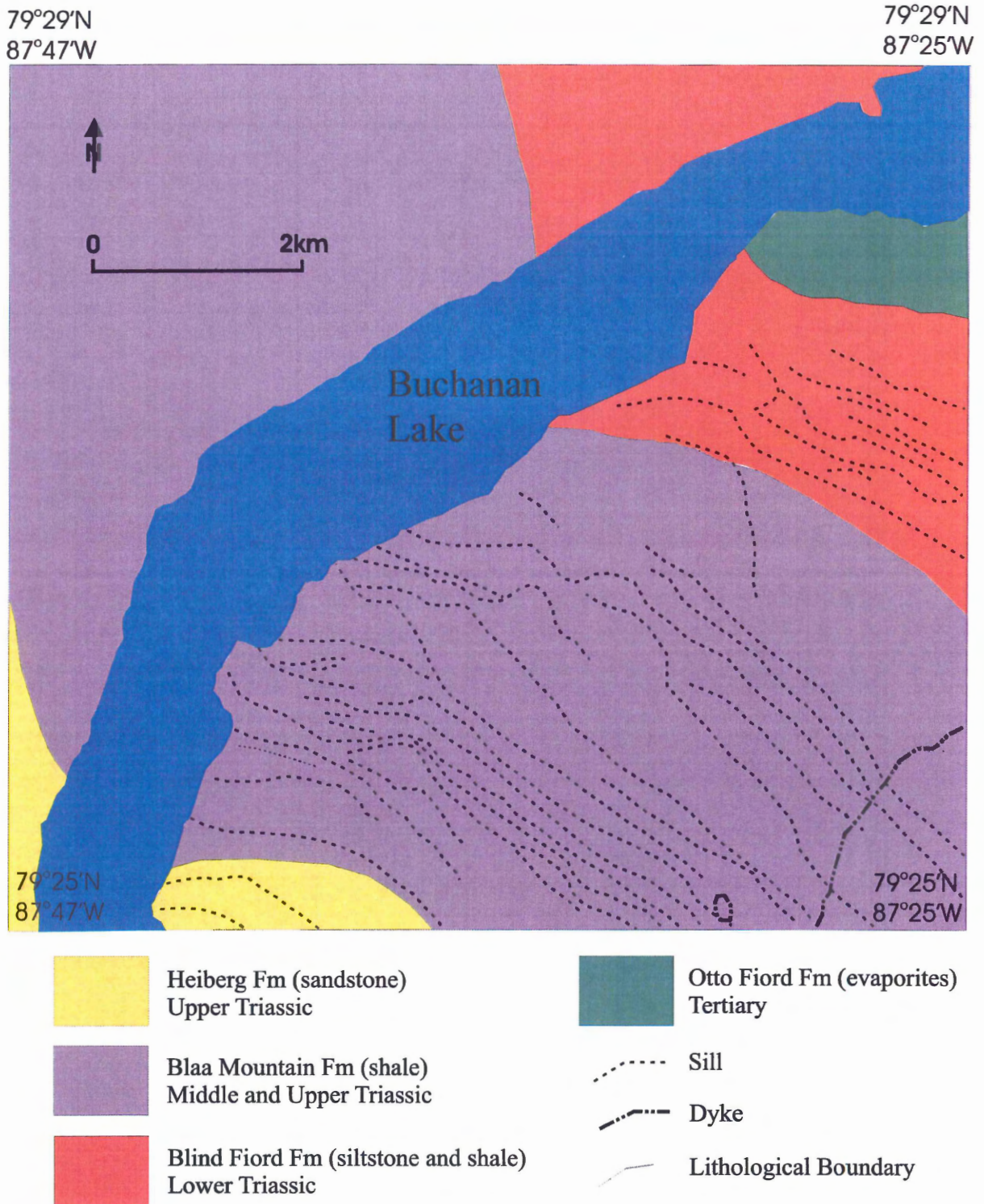


Figure 3.6: Geological map of the Buchanan Lake area showing the density of sill spacing on the south shore. The formations in this area are intersected by the Depot Point L-24 well which is to the east of Buchanan Lake. (Modified from Williamson, 1988)



Figure 3.7: View of densely-spaced sills located on the north shore of Buchanan Lake (Locality 6, Figure 3.1). Geochronological studies of the sills by Avison (1987) yielded ages of 126 ± 2 Ma and 129 ± 2 Ma. (Photo M.-C. Williamson)



Figure 3.8: Thick, massive sills of the Buchanan Lake area (north shore; up to 50 m in width) are characterized by columnar jointing and light-coloured zones where poorly-consolidated Triassic shales of the Blaa Mountain Formation are slightly baked. Contact planes are offset along regularly-spaced faults. (Photo M.-C. Williamson).

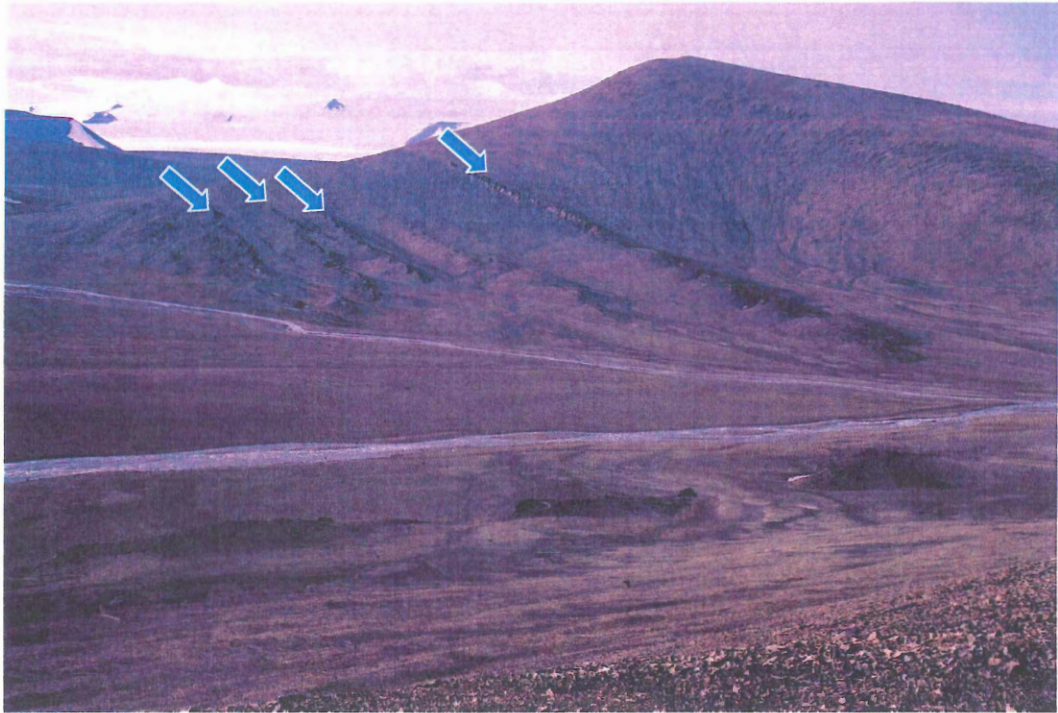


Figure 3.9: Sills in the Eureka Pass area (shown by blue arrows; Locality 7, Fig. 3.1) are thinner and more widely-spaced than in the Buchanan Lake area. These sills are typically 10 to 20 m in thickness, and intrude sandstones of the Triassic Heiberg Formation. (Photo M.-C. Williamson; view to Northwest).

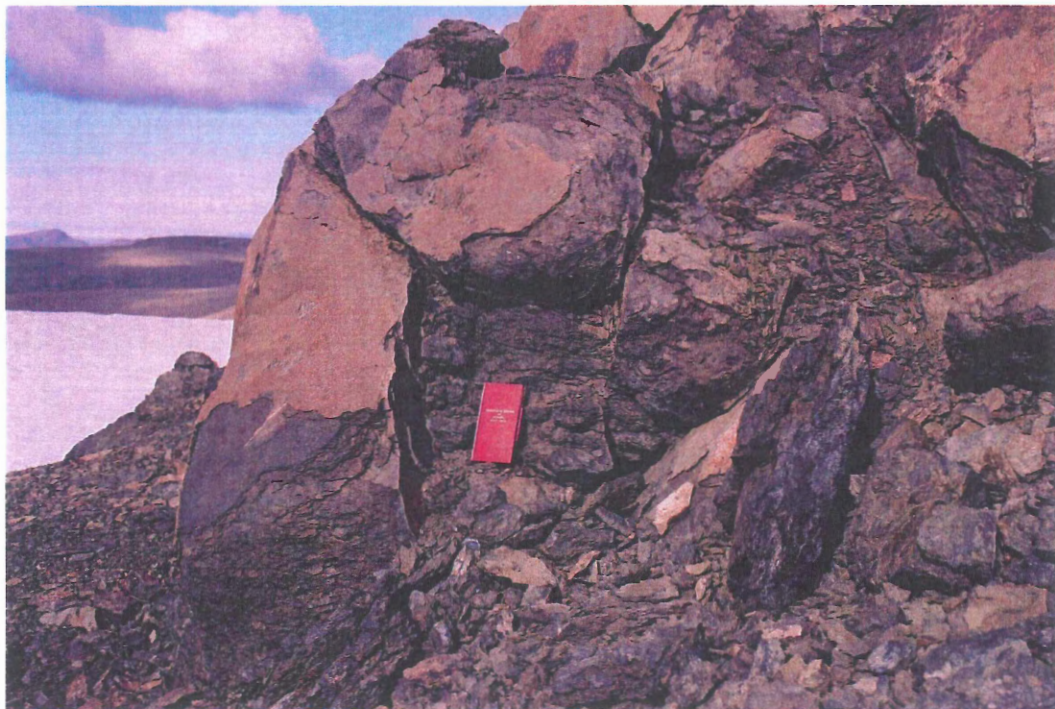


Figure 3.10: Distinctive “sheet-like” weathering pattern characteristic of olivine-bearing sills in the Eureka Pass area of central Axel Heiberg Island. (Photo M.-C. Williamson; view to South).

The Strand Fiord Formation has been dated stratigraphically and by absolute age dating techniques. The relative age can be determined by relating the basalt flows with the associated lower Upper Cretaceous marine rocks on western Axel Heiberg Island (Balkwill, 1978) and the overlying uppermost Cretaceous to Lower Tertiary Kanguk and Eureka Sound Formations (Ricketts *et al.*, 1985).

Absolute dating techniques have been used several times to assign ages of peak magmatic activity. The most recent study used whole rock laser $^{40}\text{Ar}/^{39}\text{Ar}$ geochronology to obtain ages for both volcanic and intrusive igneous rocks. Volcanic rocks from the Strand Fiord Formation on western Axel Heiberg, Celluloid Creek (near Bunde Fiord), and the south shore of Bunde Fiord have been dated (Figure 3.1). Intrusive rocks from northeastern Axel Heiberg and northern Ellesmere Island were dated using the same method (Villeneuve and Williamson, in press). Biostratigraphy has been used to date the strata above and below the Strand Fiord Formation; the overlying Kanguk Formation and the underlying Bastion Ridge Formation (MacRae and Hills, 2006).

The biostratigraphic constraints give an age range of 104.4-93.5 Ma for the extruded Strand Fiord Basalt (MacRae and Hills, 2006). The ages as given by Villeneuve and Williamson (in press) represent extrusive and intrusive units and show magmatic pulses of dominantly intrusive rocks at 127-129 Ma and 92-98 Ma for the rocks on Axel Heiberg Island and northern Ellesmere Island. Vogt *et al.* (2006) reported extrusive and intrusive rocks from Axel Heiberg Island and northern Ellesmere Island to have age dates ranging from 130-90 Ma. The numerical model requires an age of emplacement for the sills penetrated by the Depot Point L-24 well. Assuming the sills intersected by the Depot Point L-24 well are associated with the Strand Fiord Formation, assigning an age within that 130-

90 Ma range is acceptable. The effects of varying emplacement ages in the numerical model are discussed in Chapter 5.

There are some challenges associated with dating the intrusive rocks. Lava flows have been dated with radiometric methods, but can also be constrained using stratigraphic techniques (Buchan and Ernst, submitted). Intrusive units require radiometric dating. Large samples, which cannot always be recovered from drilled wells, are required for the dating process. When radiometric dating is not possible, geochemical studies can provide a first order approximation of the age of emplacement. The intrusive feeder networks and their extrusive equivalents are expected to share similar geochemistry, thus geochemical comparisons could correlate intrusive units of unknown age with related igneous rocks that have assigned radiometric ages (e.g. Buchan and Ernst, submitted).

3.4 Magma Types in the SBMP

The Sverdrup Basin Magmatic Province has three principal magma types, tholeiites, ferrobasalts, and alkali basalts (Williamson, 1998). Tholeiites have clinopyroxene (augite) and very rare pigeonite, but usually lack olivine. They do not have alkali feldspar, but plagioclase is common. Alkali basalts have titaniferous clinopyroxene, alkali feldspar, and olivine. Plagioclase is less common, and orthopyroxene is usually absent (Winter, 2001). The ferrobasalts are composed of salitic clinopyroxene, plagioclase, olivine, common Ti-magnetites, and are mildly alkaline to alkaline in character (Williamson, 1998).

In the eastern part of the Sverdrup Basin there is a strong relationship between age dates, spatial location, and magma type. In both extrusive and intrusive forms, the sequence of emplacement of magma types is: tholeiites, ferrobasalts, and alkali basalts (Williamson, 1998). The tholeiitic lavas and associated intrusives are located on Axel Heiberg Island; the

ferrobasalts and alkali basalts are found on Ellesmere Island. This shows that the variation in magma composition over time occurs spatially from southwest to northeast in the eastern part of the Sverdrup Basin (Williamson, 1988). Based on this distribution of magma types across the east-central Sverdrup Basin, it is expected that the units in the Depot Point L-24 well on Axel Heiberg Island consist of gabbroic sills likely emplaced between 129-127 Ma (Villeneuve and Williamson, in press).

Samples representative of tholeiitic sills and dykes from central Axel Heiberg Island have been analysed and described. A list of sample descriptions and sample locations are included in Appendix A. Most of these samples show similar mineralogy and textures. Grain size ranges from very fine to medium and the samples have plagioclase, clinopyroxene, and Fe-Ti oxide mineralogy. The samples are generally inequigranular, aphyric, and show varying degrees of alteration. Each sample is assigned a numerical alteration index based on Williamson (1988), which is explained in Appendix A. All locations are listed on Figure 3.1.

Petrographic descriptions for a selection of samples from the Wolf Intrusion and other intrusive units in central Axel Heiberg Island are summarized in Appendix A. The primary mineralogy is plagioclase, clinopyroxene, and Fe-Ti oxide. Accessory minerals include apatite and biotite (which may be secondary). The secondary minerals chlorite, iddingsite, sericite, and clays are minor components of the rocks. Samples are fine to medium grained, holocrystalline, inequigranular, and aphyric. The plagioclase is generally subhedral and lath shaped. The clinopyroxene is rounded to irregular in shape and has anhedral to subhedral grain boundaries. The plagioclase and clinopyroxene show subophitic to ophitic texture. Subophitic texture is an intergrowth of the two phases and ophitic texture occurs when the

intergrowth includes plagioclase grains completely isolated within clinopyroxene grains (Winter, 2001). The Fe-Ti oxide grains have anhedral to subhedral grain boundaries and range from equant to irregular and skeletal shapes. Olivine is present in most of the samples and shows varying degrees of alteration into iddingsite. The olivine crystals are irregular in shape and have anhedral grain boundaries. The iddingsite forms alteration rims around some of the olivine crystals and fills the cracks in others. Apatite is an accessory mineral with acicular habit found in several of the samples occurring as inclusions within other mineral grains. Secondary minerals include iddingsite, chlorite, sericite, biotite, and some interstitial clay minerals. All of the Wolf Intrusion samples have an alteration index of one, indicating the presence of few secondary minerals and clays and very minor alteration. The alteration index scale, defined by Williamson (1988), is included in Appendix A. Low alteration rank is supported by the presence of olivine, an easily weathered mineral, in four of these samples.

Samples from the Geodetic Hills, central Axel Heiberg Island, represent very fine to medium grained dykes and sills (Locality 8, Figure 3.1). All of these samples have similar mineralogy; plagioclase, clinopyroxene, and Fe-Ti oxide. The plagioclase ranges from very fine microlites up to medium grained tabular, lath-shaped crystals. Some samples show major saussurite and sericitic plagioclase alteration, but the tabular primary grain shape is still evident. Small quantities of olivine are present in several of the samples from both sills and dykes. The olivine grains have alteration rims or show alteration to iddingsite within the grain itself. Accessory minerals include acicular apatite that is present in both sill and dyke samples and zircon found within biotite grains. Secondary minerals include chlorite, amphibole, biotite, iddingsite, saussurite, sericite, carbonate, and clays.

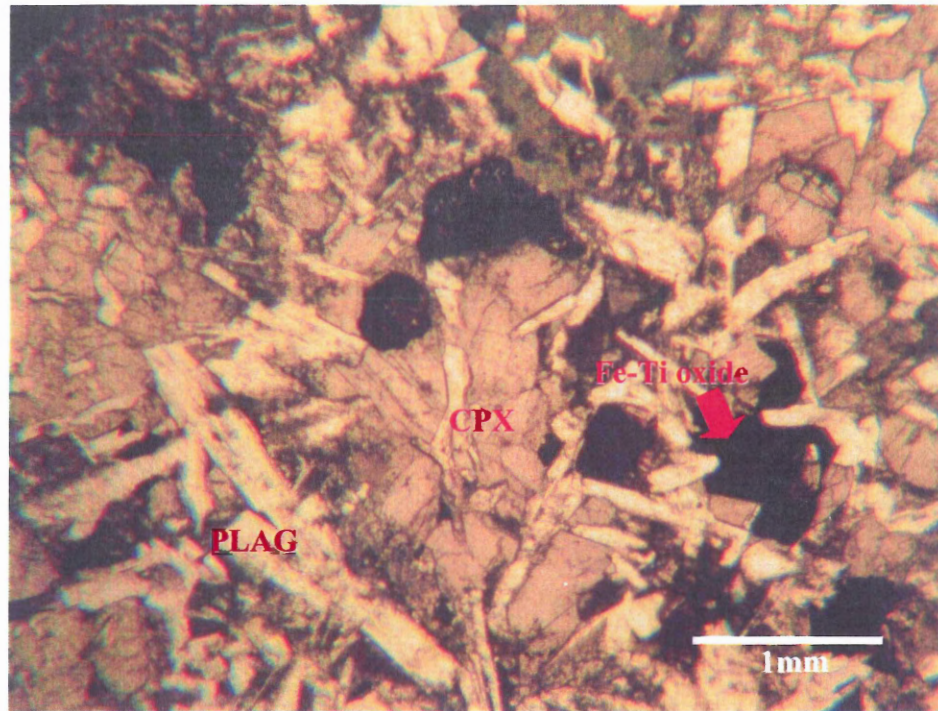


Figure 3.11: This coarse-grained igneous intrusive rock is in plane, polarized light. It shows subophitic interactions of clinopyroxene and plagioclase. Clinopyroxene, plagioclase, Fe-Ti-oxides are labelled on the image. Photomicrograph by Sheri Lyon.

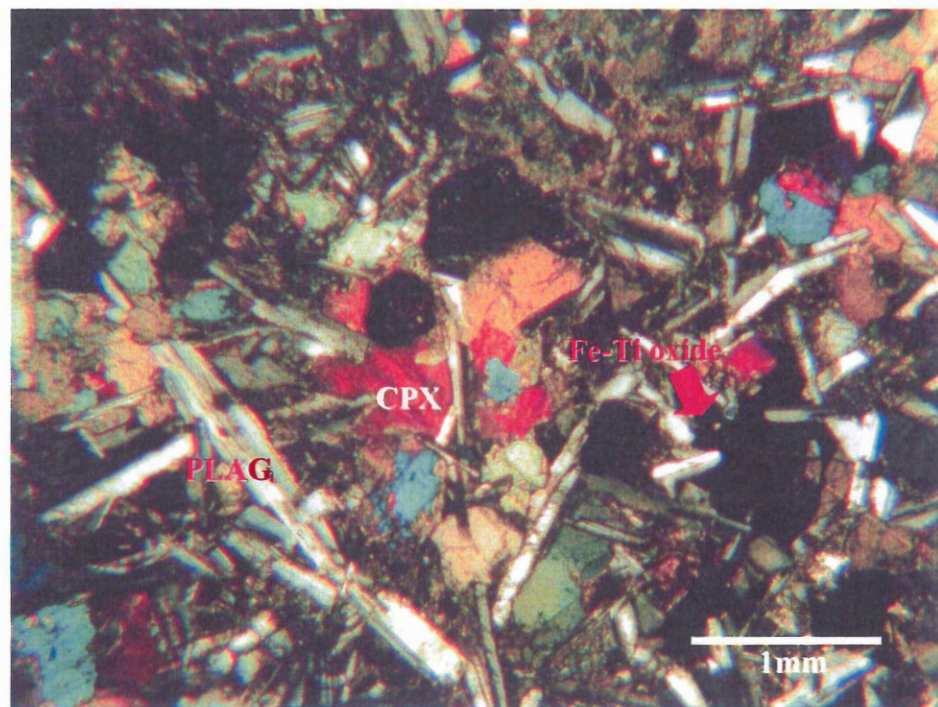


Figure 3.12: This is the crossed-nicols view of the sample shown in figure 3.11. Photomicrograph by Sheri Lyon.

Figures 3.11 and 3.12 show a typical sample of an intrusive gabbroic rock from Axel Heiberg Island in plain, polarized light and crossed-nicols respectively. The sub-ophitic texture exhibited by the plagioclase and clinopyroxene and the xenoblastic Fe-Ti oxides are present. This sample has tholeiitic mineralogy; plagioclase, clinopyroxene, and common Fe-Ti oxides.

3.5 Magma Emplacement

Magmatism in the Sverdrup Basin occurred as a result of Cretaceous rifting (Williamson, 1998). The intrusive rocks likely moved towards the earth's surface as vertical or nearly vertical dykes, perhaps along fault planes, and moved horizontally as sills in weak strata such as under-compacted shale or siltstone (Balkwill, 1978). It is most likely that magma and fluids rose over time, possibly episodically, thus producing a range of intrusive ages (Balkwill, 1978). Age date studies by Villeneuve and Williamson (in press) and MacRae and Hills (2006) discussed in section 3.3 support this hypothesis.

3.6 Igneous Rocks Intersected by the Depot Point L-24 Well

The Depot Point L-24 well is an important source of stratigraphic information. Figure 3.13 presents a simplified version of the Canadian Stratigraphic Services Ltd. Depot Point L-24 well litholog. The well intersects six igneous units as described in Table 3.1. The well also documents several sedimentary formations, which are discussed in Chapter 4 as model input. This section will describe the characteristics of the igneous units intersected by the well.

The intrusive rock types have gabbroic to dioritic compositions. All of the igneous units are coarse grained. Their thicknesses range from 9-68 m. The igneous rocks intrude country rocks of varying lithologies: sandstone, siltstone, and shale in concordant fashion.

The well litholog does not provide any information about mineralogy or textures. Age dates are not available for any of the igneous units intersected in the well.

The zones of contact metamorphism at the upper and lower contacts between the sills and country rocks are used as evidence of concordant intrusion. The stratigraphically highest sill intersected by Depot Point L-24 is associated with metamorphism only at the lower contact with country rocks. However, this unit is assumed to be a sill, based on the thick nature of the lower contact metamorphic zone (almost half of the sill thickness) and the presence of other sills within the same country rock (Blind Fiord Formation).

The contact-metamorphic rocks documented in the well log are very fine grained quartzite, meta-siltstone, and hornfels. Some of the contact zones show fracturing, chloritization, and/or silicic and dolomitic cement. Table 3.1 outlines depths and thicknesses of sills and contact-metamorphosed zones.

Sill No.	Thickness (meters)	Formation Intruded	Upper contact (depth in meters)	Lower contact (depth in meters)	Upper Contact Zone Thickness: (meters)	Lower Contact Zone Thickness: (meters)
1	13.7	Blind Fiord	384.0	397.8	N/A	6.4
2	12.8	Blind Fiord	835.2	848.0	4.6	3.0
3	9.1	Blind Fiord	960.1	969.3	1.5	1.5
4	32.9	Blind Fiord	1028.7	1061.6	1.5	0.6
5	20.7	Blind Fiord	3064.2	3084.9	7.9	9.8
6	68.6	Van Hauen	3602.7	3671.3	7.9	3.4

Table 3.1: The thicknesses of the sills and contact metamorphic zones, position of sills, and the formations intruded indicated by the Depot Point L-24 litholog are summarized in tabular format.

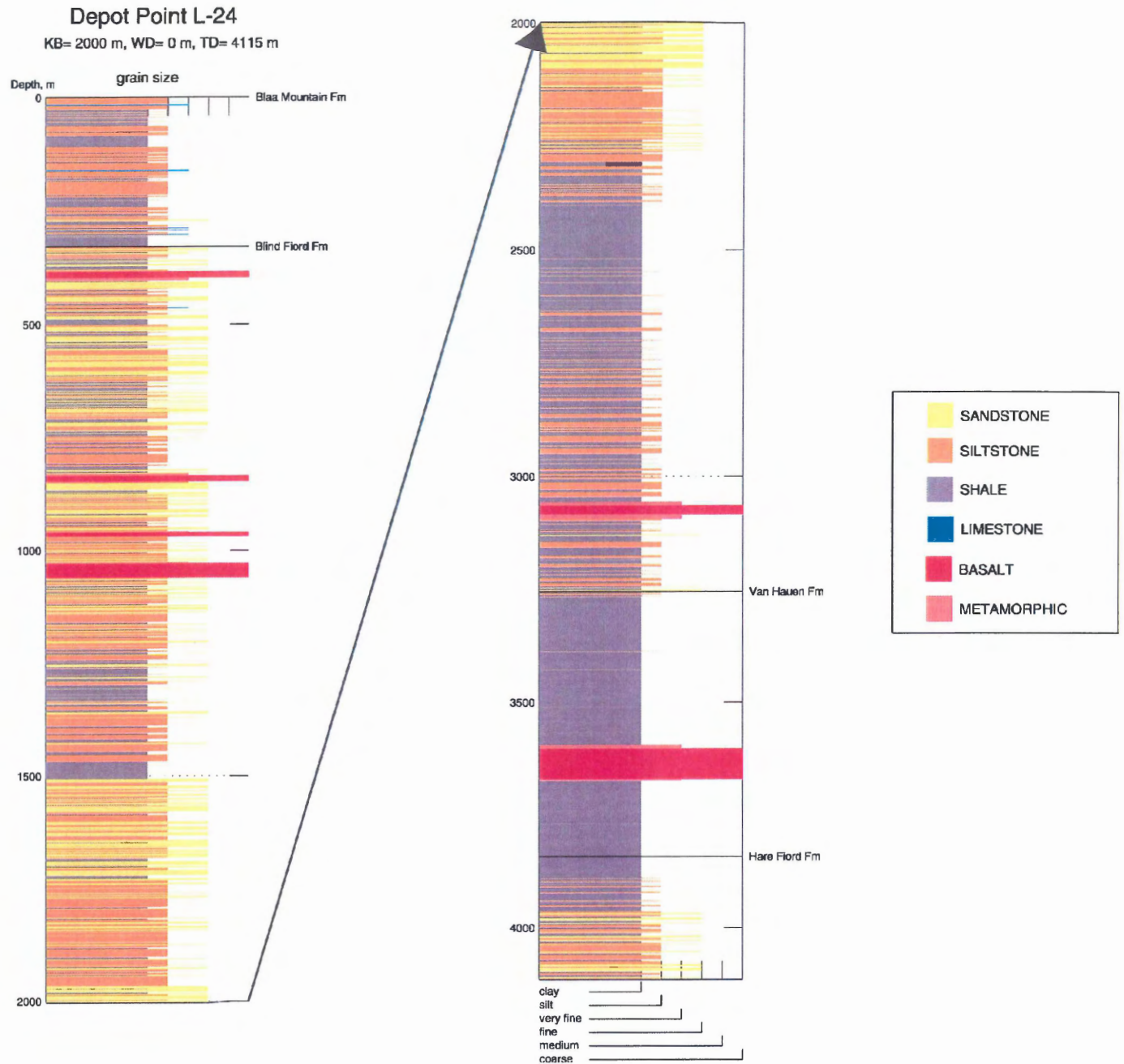


Figure 3.13: Complete litholog for the Depot Point L-24 well. The igneous intrusive units are shown in red. Data were collected by Horn River Resources and originally compiled by Canadian Stratigraphic Services Ltd.

3.7 Summary

The Sverdrup Basin Magmatic Province (SBMP) exhibits the characteristics of large igneous provinces (LIPs) (Coffin and Eldholm, 1994). The episodes SBMP is associated with rifting and the opening of the Arctic Ocean (Williamson *et al.*, 2005). The volume of extrusive rocks is comparable to the western American Columbia River Basalt and the intrusive feeder system of dykes and sills has a volume at least one order of magnitude larger than that of the extrusive rocks (Williamson, 1998; Villeneuve and Williamson, in press).

Abundant sills and dykes intrude Carboniferous to Cretaceous strata on Axel Heiberg Island and the related Strand Fiord Formation forms thick flood basalt successions (e.g. Balkwill, 1978). Biostratigraphic studies by MacRae and Hills (2006) assign an age range of 104.4-93.5Ma for the extruded Strand Fiord Basalt. Villeneuve and Williamson (in press) report an age range from 130-90Ma for the related intrusive rocks on Axel Heiberg and Ellesmere Islands. The igneous rocks have gabbroic to dioritic compositions, and are tholeiites. All of the igneous units are coarse grained and have contact aureoles. The sills intrude country rocks of varying lithologies within the Blind Fiord and Van Hauen Formations: sandstone, siltstone, and shale.

The purpose of the numerical model is to determine the effects of magmatism on hydrocarbon generation. The L-24 Depot Point well intersects six sills, thus intrusive rocks are emphasized in this chapter. In order to properly represent the sills in the model, their physical, chemical, and geochronological characteristics must be understood.

CHAPTER 4: MODEL CONSTRUCTION AND INPUT DATA

4.1 Introduction

The construction of a numerical model requires specific information about the study area and boundary conditions; e.g. geological formations, lithologies, formation thicknesses, formation ages, erosion rates, and age of sill emplacement. Other input data specific to individual well sites including vitrinite reflectance, sea level, heat flow, and porosity, can be added into the model in order to provide boundary conditions which are used to constrain the model simulation to defined parameters exhibited within the study area. In this thesis, only a single well is used and the model itself is one-dimensional, it looks at the evolution of the Depot Point L-24 well over time.

This chapter discusses the software program PetroMod[®] written and distributed by Integrated Exploration Systems (IES). PetroMod[®] is used for model construction and simulation in this study and also provides listings of the input data and assumptions. PetroMod[®] contains a set of built-in physical properties such as values of conductivity, porosity decline with depth, and source rock kinetics.

The Depot Point L-24 well intersects six igneous units, making it a prime candidate for a numerical simulation to test the effects of intrusions on hydrocarbon systems. The framework of the model consists of the rock formations, their lithologies, depositional ages, erosional ages, thicknesses of eroded sections, and stratigraphic thicknesses. Vitrinite reflectance, heat flow, sea level, porosity, and sediment-water interface temperatures are included as additional data sets which constrain the model to the characteristics exhibited by the study area. Fission-track data are used in constraining the time of basin inversion. The most reliable data are the lithologies, thicknesses, and

sill characteristics which have been well documented on Axel Heiberg Island and are intersected by the Depot Point L-24 well. These data provide a foundation for model construction. It is more difficult to rate the reliability of the heat flow data. Present-day heat flow values are highly variable on regional and local scales, as discussed later in this chapter.

4.2 Using PetroMod[®] for 1D Modeling

PetroMod[®] is a tool that is well-suited to simulate the late Paleozoic and Mesozoic evolution of the Depot Point L-24 lithologic column because it is designed to predict the temporal and spatial framework of hydrocarbon generation, based on the data and controls input by the user. IES defines a hydrocarbon systems model as a digital model that encompasses all of the processes and characteristics of a hydrocarbon system, integrates these processes and characteristics with one another, and simulates their behaviour to yield a prediction that includes hydrocarbon generation, migration, accumulation, and loss over time. It also simulates processes such as compaction of the sediments over time, and the related porosity reduction. PetroMod[®] 1D is the particular package used for this thesis. It is capable of simulating pressure, temperature, hydrocarbon generation, and maturation histories of single or multiple wells. Migration and accumulation are not simulated by the one-dimensional software. The program contains default values for many factors such as conductivity, porosity reduction with depth, and compaction susceptibility for the various lithologies. The user inputs all of the data sets in a series of tables. The software is then able to simulate the burial history, thermal history, and hydrocarbon generation potential based on the input information.

Darcy's Law, the Arrhenius equation, kinetic models, and geothermal gradient equations are key factors used in producing the simulation.

4.3 Lithologies

The numerical model requires details concerning the different formations intersected by the well. The formation names, lithologies, thickness, and depositional age used in model construction are in Table 4.1. Information about the rocks that have been eroded from the location and units below the penetration depth of the well must be included. The information in the shaded rows is from the Depot Point L-24 well log (Figure 4.1). The other data were compiled from Embry (1991), Trettin (1989), Balkwill *et al.* (1983), and Gentzis and Goodarzi (1991). Aside from the data sets presented in Table 4.1, porosity values recorded on the original litholog were incorporated into the model. The characteristics of the formations above and below the units intersected by the well have been inferred from the local stratigraphy, neighbouring wells, generalized cross sections, and lithology isopach maps. The Depot Point L-24 well intersects 4033 m of rock. These intersected units are referred to as the Depot Point L-24 well in this chapter and following. The estimated thicknesses of the eroded units are summarized in Table 4.1. The eroded rock units will have had a significant effect on the burial history and consequently the thermal maturity of the sediments intersected by the well. The entire modeled column, intersected and inferred units, is referred to as the Depot Point L-24 lithologic column.

4.4 Source Rock Properties

Historically, the western Sverdrup Basin has been the focus of hydrocarbon research due to the assumption that igneous intrusions and orogenic processes were not as

Formation Name	Dominant Lithology	Thickness (meters)	Depositional Environment	Age
Expedition Fm	Sandstone	500	delta front	Late Cretaceous; Campanian - Maastrichtian
Kanguk Fm	Shale & Siltstone	150	offshore shelf	Late Cretaceous; mid Cenomanian - Santonian
Strand Fiord Fm	Basalt	300	N/A	Early Cretaceous; late Albian - mid Cenomanian
Bastion Ridge Fm	Silty Shale	50	offshore marine	Early Cretaceous; late Albian
Hassel Fm	Sandstone	150	delta front	Early Cretaceous; mid Albian
Christopher Fm	Shale & Siltstone	600	offshore then shelf	Early - Late Cretaceous; late Aptian - mid Albian
Isachsen Fm	Sandstone	200	nearshore shelf	Early Triassic; Valanginian - late Aptian
Deer Bay Fm	Shale & Siltstone	100	outer shelf	Late Jurassic - Early Cretaceous; mid Tithonian - Berriasian
Awingak Fm	Sandstone	250	shallow shelf	Late Jurassic; mid Oxfordian - Tithonian
Ringnes Fm	Shale & Siltstone	100	basinal	Mid - Late Jurassic; Bajocian - Oxfordian
Jameson Bay Fm	Shale & Siltstone	50	offshore shelf	Early - Mid Jurassic; Toarcian - Aalenian
Heiberg Fm	Sandstone	2000	delta front to nearshore shelf	Late Triassic - Early Jurassic; mid Norian - Pliensbachian
Blaa Mountain Fm	Calcareous Shale	1000	basinal	Mid - Late Triassic; Anisian - mid Norian
Blind Fiord Fm	Siltstone and Shale	2926	slope	Early Triassic; Indusian - Oienekian
Van Hauen Fm	Silty Shale	587	slope	Roadian
Hare Fiord Fm	Shale	303	basinal	Moscovian - Roadian
Otto Fiord Fm	Halite	200	evaporite deposits	Upper Carboniferous
Basement	Basement	N/A	N/A	N/A

Table 4.1: Lithologies intersected by the Depot Point L-24 well (shaded rows) and inferred units used for the construction of the one-dimensional model framework. The depositional ages and environment for each formation were used to recreate the burial history and construct a sea level curve. The data were compiled from Embry (1991), Trettin (1989), Balkwill *et al.* (1983), and Gentzis and Goodarzi (1991).

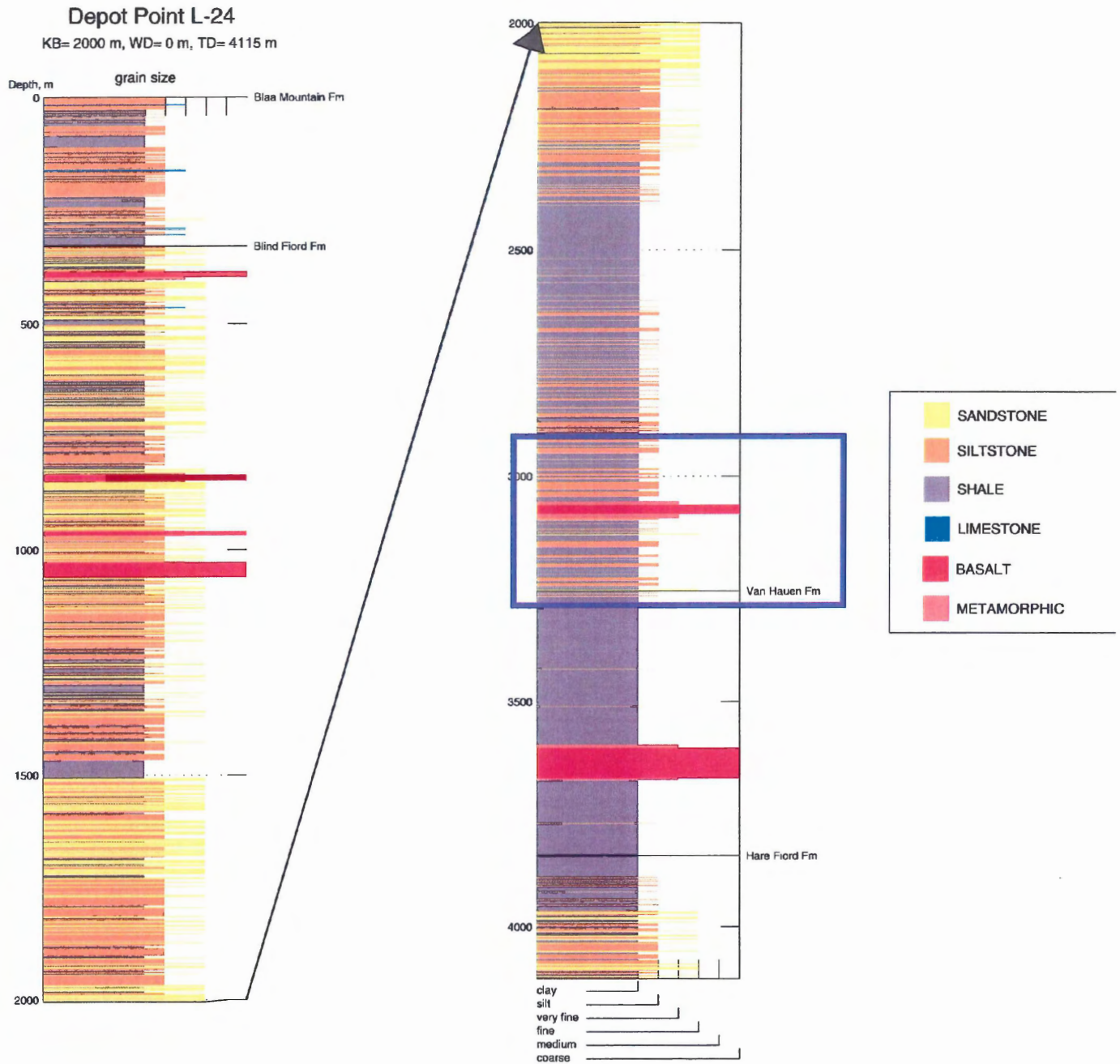


Figure 4.1: Depot Point L-24 well log showing the lithologies intersected by the well and the grain sizes. The formation names and depths are listed alongside the well. See figure 4.2 for an enlargement of the section in the blue box. Data collected by Horn River Resources and originally compiled by Canadian Stratigraphic Services Ltd.

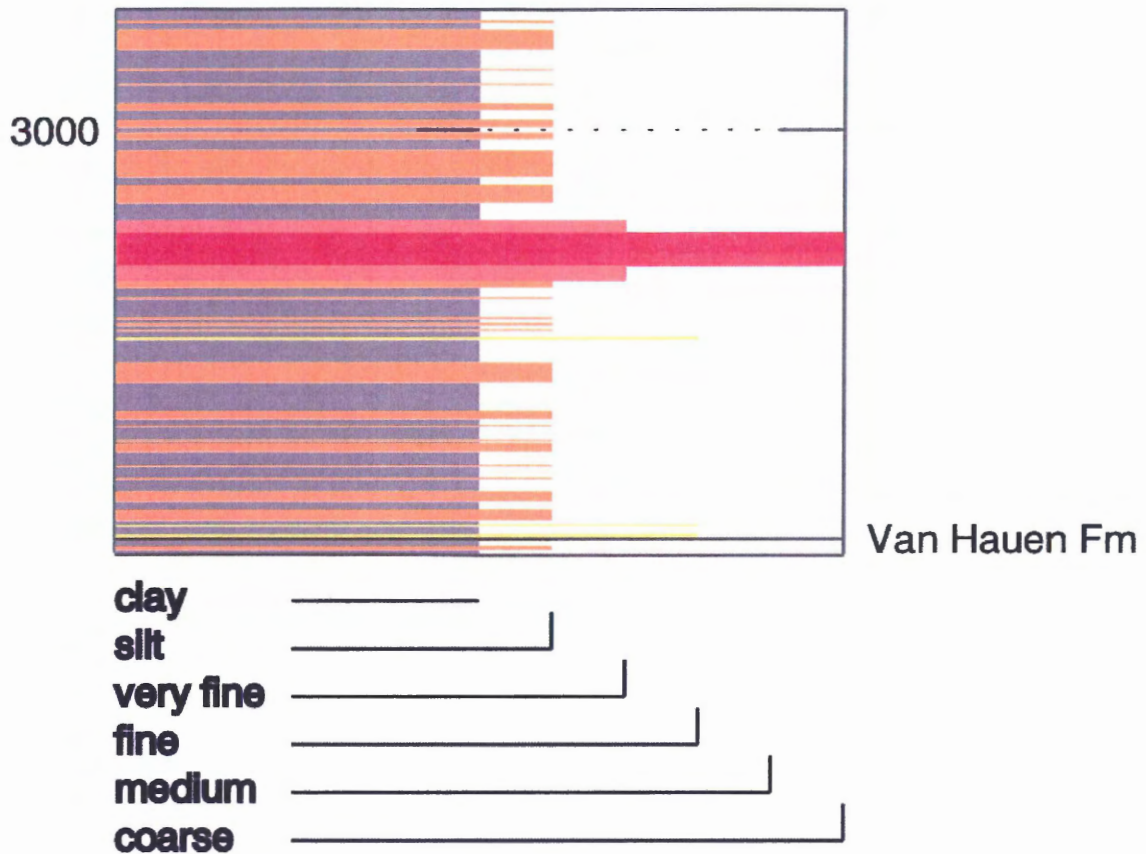


Figure 4.2: Enlarged section of Depot Point L-24 lithology log showing a basaltic sill and the bordering contact-metamorphic zones. See figure 4.1 for legend and data sources.

prominent as in the eastern Sverdrup Basin (e.g. Balkwill, 1978). No Rock-Eval data are available for the Depot Point L-24 well, therefore source rock properties of the strata in the study area must be inferred from data collected from other locations within the basin. Rock-Eval pyrolysis involves the passing of helium through crushed rock which is progressively heated. Vapours are collected and analyzed for hydrocarbons. This method allows determination of organic matter type and maturity and allows recognition of good and poor source rocks (Hunt, 1996).

Several units intersected by the well have source rock properties. The hydrogen index (HI) and the total organic carbon (TOC) for these formations are important model

input parameters and will largely determine the potential to generate hydrocarbon. The source rock properties of the Mesozoic Ringnes, Awingak, and Blaa Mountain Formations have been documented within the western Sverdrup Basin (e.g. Gentzis and Goodarzi, 1993a; Gentzis and Goodarzi, 1993b; Gentzis and Goodarzi, 1991). These rocks range from marginally mature to immature; the main limiting factor controlling oil generation is the significant amount of terrestrial organic material, which is more likely to produce gas. There are also a number of formations that have been identified as poor source rocks, such as the Permian Van Hauen and Hare Fiord Formations and the Mesozoic Jameson Bay, Deer Bay, and Christopher Formations (Gentzis and Goodarzi, 1993a; Gentzis and Goodarzi, 1993b; Gentzis and Goodarzi, 1991). Table 4.2 lists the estimated TOC and HI values used as input for the model. These estimates are based on source rock data in the western and southern Sverdrup Basin.

The numerical model requires a kinetic model which dictates the rates of generation and the types of hydrocarbons produced. Kinetic style has not been reported for the source rocks on Axel Heiberg Island, thus the Burnham type II model (Burnham and Sweeney, 1989), one of several kinetics options available for use in PetroMod[®], is chosen for the purpose of this thesis.

There are several sandstone units intersected by the modeled Depot Point L-24 well: the Heiberg, Awingak, Isachsen, Hassel, and Expedition Formations. All of these sandstones are potential reservoirs, but the Heiberg sandstone is the thickest and most extensive, making it the most likely candidate (e.g., Balkwill *et al.*, 1983; Embry, 1991). Shales are common in the Depot Point L-24 lithologic column, providing strata that could represent the seal rock component of the hydrocarbon system. It is important to

Formation	TOC (wt. %)	HI (mg HC/TOC)
Hare Fiord	1.0	50
Van Hauen	1.0	50
Blaa Mountain	5.0	400
Jameson Bay	0.5	150
Ringnes	6.0	400
Awingak	4.0	100
Deer Bay	2.5	50
Christopher	2.5	300

Table 4.2: Total Organic Carbon (TOC) and Hydrogen Index (HI) values used in the model. Values were not measured directly from the Depot Point L-24 well. Rather, average values were inferred from other locations in the Sverdrup Basin for the purpose of this study. In addition, the values are estimates that are not reported in the literature but calculated from the trends reported by Gentzis and Goodarzi (1991, 1993a, 1993b).

recognize that the one-dimensional model process focuses on the generation of oil and gas. Modeling of the migration pathways and hydrocarbon traps would require the construction of a 2D or 3D model which is outside of the scope of this thesis.

4.5 Vitrinite Reflectance

Vitrinite reflectance measurements are valuable for constraining the thermal history of the Depot Point L-24 well. Vitrinite is an organic compound derived from plant material. The light reflected by the polished vitrinite surface can be measured petrologically under immersion oil (R_o = reflectance in oil). The amount of reflection is proportional to the maximum temperature to which strata have been heated (Hunt, 1996). A table of R_o values for the Depot Point L-24 well is presented in Table 4.3; the data are from and were discussed by Arne and others (2002). Table 4.3 shows the data used, whereby the depth of the measurement was converted into meters, the R_o values are percentages, and n refers to the number of measurements taken on each sample. The high

Depth (m)	R_o (%)	n
229	0.99	15
329	1.44	8
503	1.10	12
716	1.09	10
1268	1.81	2
1493	1.40	4
2316	1.72	4
2675	0.66	2
3414	2.81	8
3551	3.80	17
3719	3.51	11
3801	3.44	22
3871	3.95	30
3962	3.23	13

Table 4.3: Vitrinite reflectance (R_o) values from Arne et al. (2002). The data were used in the model for calibration purposes, and to determine the thermal history of the Depot Point L-24 succession. The n values represent the number of analyses completed at the specified core depth.

vitrinite reflectance values near the base of the well reflect the deep burial of the Permian formations as well as the intrusion of igneous rocks (Arne *et al.*, 2002).

4.6 Heat Flow

Heat flow, or heat flux, is the amount of heat moving up towards the Earth's surface expressed as mW/m² (Musset and Khan, 2000). Heat flow studies are important in the Sverdrup Basin because they yield information about Arctic tectonic and basinal processes. Reconstruction of the thermal history of any part of the basin requires knowledge of present and paleo-heat flow and directly relates to the generation, migration, and maturation of oil and natural gas. Present day heat flow values are determined through the analysis of bottom-hole temperature (BHT) data (Jones *et al.*, 1989) and paleo-heat flow and paleo-gradient values are estimated from Vitrinite reflectance profiles and coalification parameters (Majorowicz and Embry, 1998).

Table 4.4: Thermal Environment Data		
	Jones <i>et al.</i>, 1989	Majorowicz and Embry, 1998
Heat Flow	42 mW/m ²	68 mW/m ²
Effective Conductivity	1.9 W/m/K	1.9 W/m/K
Paleo-heat Flow (Tertiary)	-	57 mW/m ²
Paleo-geothermal Gradient (Tertiary)	-	30 mK/m

Table 4.4: Present-day and paleo-heat flow values for the Depot Point L-24 well. The range of values reflects the variability in measurement techniques and interpretation.

Table 4.5: Heat Flow Input Data			
Age (Ma)	Heat Flow (mW/m²)	Age (Ma)	Heat Flow (mW/m²)
0.00	39.00	100.00	66.00
18.00	41.00	102.00	67.00
30.00	43.00	104.00	68.00
50.00	47.00	108.00	71.00
55.00	48.00	110.00	73.00
60.00	50.00	112.00	75.00
65.00	51.00	114.00	76.00
70.00	53.00	116.00	78.00
75.00	54.00	118.00	81.00
80.00	56.00	120.00	83.00
88.00	59.00	122.00	85.00
90.00	60.00	124.00	88.00
92.00	61.00	125.00	90.00
94.00	62.00	127.00	45.00
96.00	63.00	312.00	45.00
98.00	65.00		

Table 4.5: Heat flow data act as a boundary condition for the simulation process. The input values are based on a rifting event at 125 Ma; the subsequent heat flow decay was calculated according to the equation cited in Turcotte and Schubert (2002). The result is a present day heat flow value of 39 mW/m², close to the heat flow value reported by Jones *et al.* (1989).

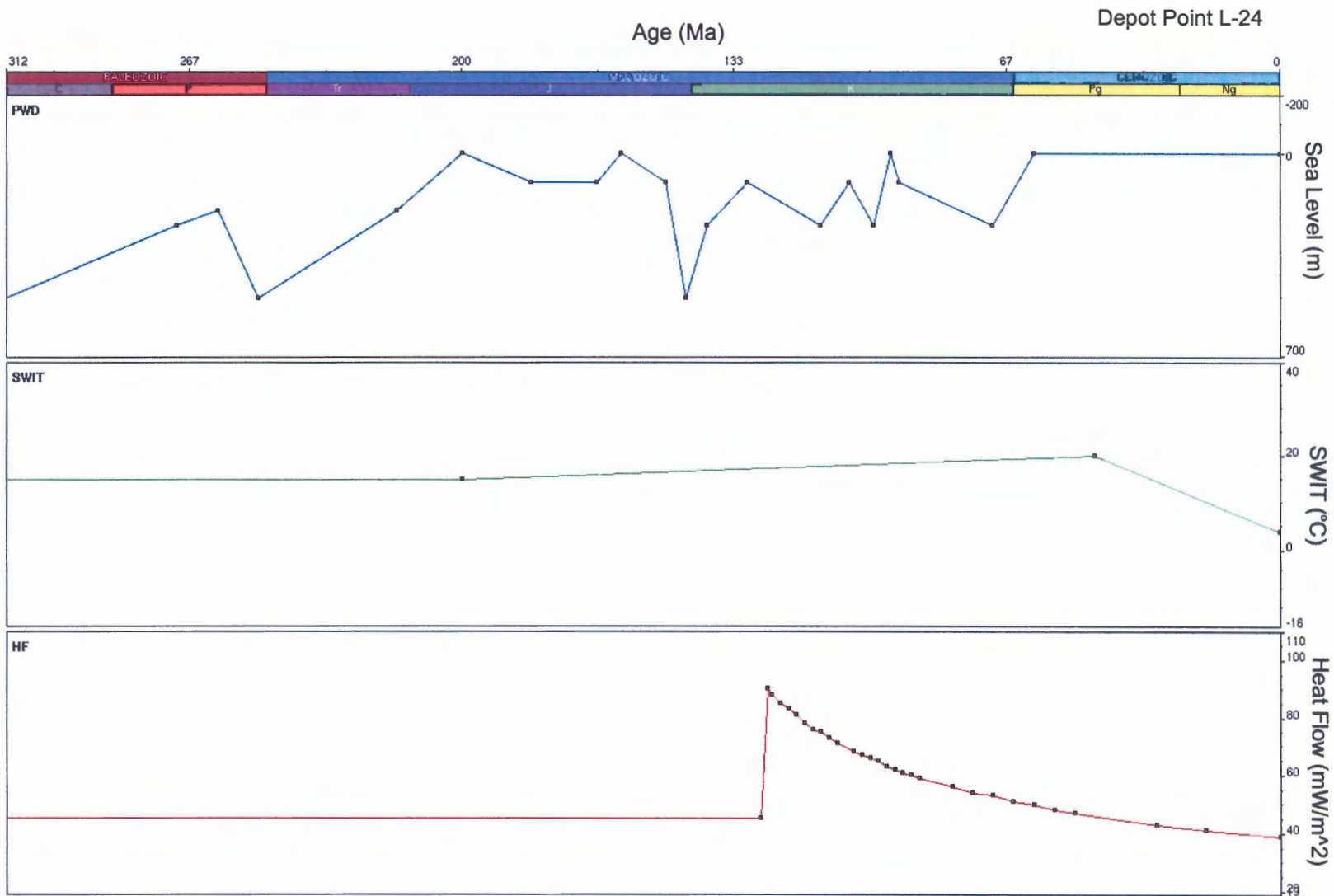


Figure 4.3: The model refers to the following three data sets as boundary conditions as they define the depositional environment: a) a sea level curve, b) the sediment-water interface temperature, and c) the heat flow values.

Heat flow, effective thermal conductivity, and geothermal gradient values for the Depot Point L-24 well were determined by Jones et al. (1989) to be 42 mW/m², 1.9 W/m/K, and 22 mK/m respectively. Higher values are reported in a more recent study by Majorowicz and Embry (1998). Table 4.4 compares the data presented by both studies. Over the entire Sverdrup Basin, present-day heat flow values range from values around 40 mW/m² to values 90 mW/m² (Majorowicz and Embry, 1998). Current heat flow patterns are influenced by lateral fluid flow and thermal refraction within this basin (Jones *et al.*, 1990). The basin has reached a thermal equilibrium and is no longer affected by past magmatic episodes (Jones *et al.*, 1989).

Table 4.5 lists the heat flow input values used in the numerical model. The 90 mW/m² value at 125 Ma estimates the heat flow during the onset of Cretaceous rifting. In this situation, this best guess is acceptable; there are no published values for the heat flow during rifting on Axel Heiberg Island. The other heat flow values were calculated through the use of a heat flow decay formula presented by Turcotte and Schubert (2002) and give a present day heat flow of 39 mW/m², which is comparable to the present-day heat flow value reported by Jones et al. (1989). Figure 4.3 graphically displays the heat flow values over time for the Depot Point L-24 well.

4.7 Erosion Rates and Fission-track Data:

Fission-track studies have been applied to the Sverdrup Basin to constrain the time of thrust faulting, which correlates with exhumation of the strata in the basin. This is the time where erosion would have replaced deposition as the dominant process in the eastern Sverdrup Basin. For example, the Vesle Fiord Thrust belt, located on

neighbouring Ellesmere Island initially became active in the Paleocene (Arne *et al.*, 1998). Fission-track data from the Depot Point L-24 well yield a near constant age, ranging from 51-59 Ma, for a depth of 1.5 km. This indicates rapid cooling and exhumation during the early Tertiary (Arne *et al.*, 2002).

Erosion occurred on Axel Heiberg Island from around 60 Ma to the present day. Based on the lithologic column entered into the model, approximately 5100 meters of strata have been eroded. Most of this thickness was removed between 60-40 Ma during the period of most rapid erosion. Less than one kilometre of rock was eroded between 40-0 Ma as basin inversion slowed (Zentilli, *pers comm.* 2005-2006). In the numerical model, each period of erosion assumes a constant erosion rate. This is a highly simplified summary of the erosional history in the study area. This simplified approach is the most appropriate. A larger number of assumptions in the numerical modeling increases the complexity of model processes and range of possible solutions.

4.8 Sea Level:

A sea level curve can be input into PetroMod[®] and allows the weight of the water column and the presence of water within the sediments to be considered in simulated processes such as compaction. The sea level data used are largely qualitative and were compiled from Balkwill *et al.* (1983) and Embry (1991). The lithologies intersected by the Depot Point L-24 well and the units that have been eroded provide clues about the depositional and erosional environments as well as changing heat flow regime; thus they provide information about the local relative sea level.

Balkwill *et al.* (1983) constructed a sea level curve based on observed transgressive and regressive cycles in the Canadian Arctic Islands. This qualitative curve

and the authors' explanation along with the lithologies intersected by the Depot Point L-24 well were used to construct a general sea level curve for this part of Axel Heiberg Island. The assigned boundary conditions are shown in Figure 4.3. PetroMod® will not accept a qualitative sea level curve, so water depths need to be assigned at different times in the Cenozoic, Mesozoic, and uppermost Paleozoic. Water depths were estimated to be fairly shallow due to the nature of the basin, an intracontinental sea (e.g. Balkwill *et al.*, 1983; Trettin, 1989). For example, basinal conditions are input as 500 m, slope conditions between 400-250 m, shelf at 100 m water depth, and non-marine deposits and periods of erosion at or above sea level, 0 m. Further research regarding paleo-sea levels in the study area, perhaps using isotopic or biostratigraphic studies, would improve the constraints on this sea level curve.

4.9 Sediment-Water Interface Temperature:

Detailed information regarding the sediment-water interface temperature (SWIT) is not essential in the simulation of the Depot Point one-dimensional column; however some simple data were included. A present day SWIT of 4°C is commonly assumed at the bottom of northern oceans. Fossil forests on Axel Heiberg and Ellesmere Islands (Kuagai *et al.*, 1995; Greenwood and Basinger, 1994) and vertebrate fossils on Axel Heiberg Island (Tarduno *et al.*, 1998) indicate an Eocene thermal high. Model input SWIT values of 20°C during the Eocene and 15°C during the Jurassic were used to illustrate generalized climate trends. These three data points are connected as shown in figure 4.3, producing a linear decrease in the SWIT from the Eocene to present day.

4.10 Sill Characteristics:

The sills intruded into the Depot Point L-24 well location were discussed in

Chapter 3. The thicknesses and depths of the six sills intersected by the Depot Point L-24 well are listed in Table 3.1. Several assumptions are made in the process of defining the nature of the intruded igneous units. For example, the time of intrusion, number of sill populations, and magma temperature.

In this thesis, the sills are assumed to belong to a single population and behave as instantaneous events in geologic history. The number of sills intruding the modeled one-dimensional column is restricted to six, as intersected by the Depot Point L-24 well. It is possible that sills may have intruded some of the other Mesozoic formations; however, this cannot be established due to erosion. In all simulations a typical basaltic melt temperature of 1000°C (Winter, 2001) is used as the temperature of sill emplacement.

The age of sill emplacement and lava flow extrusion is discussed in Chapter 3, Section 3.4: Age Determination of Igneous Units. The igneous rocks on Axel Heiberg Island have an age range of about 130-90 Ma (Villeneuve and Williamson, in press and references therein). The effects of different ages of emplacement were explored in this study. Several one-dimensional simulations with different ages of sill emplacement comprise a short sensitivity study that identifies variations in the model results as a function of emplacement age. These trials are presented in Chapter 5.

4.11 Summary

Construction of the Depot Point L-24 model requires information about the study area including geological formations, lithologies, formation thicknesses, formation ages, erosion rates, and age of sill emplacement. Other input data specific to the Depot Point L-24 well site including vitrinite reflectance, sea level, sediment-water interface temperatures, heat flow, and porosity, are also added to the model. PetroMod[®] is the

software program used to simulate the late Paleozoic and Mesozoic thermal evolution of the Depot Point L-24 well. The model simulation predicts the temporal and spatial frameworks of hydrocarbon generation, according to the values and assumptions that best reflect the depositional environment and igneous history.

The formation names, lithologies, thickness, and depositional ages of the units intersected by the Depot Point L-24 well form the framework of the model. The characteristics of the formations above and below the units intersected by the well have been inferred from the local stratigraphy, neighbouring wells, generalized cross sections, and lithology isopach maps. Estimated hydrogen index and total organic carbon are input for each of the potential source rocks intersected by the modeled lithologic column. Information about the sills intersected by the Depot Point L-24 well is essential in model construction. The sill depths, thicknesses, age of emplacement, and temperature of emplacement are used in the reconstruction of the burial and thermal history of the Depot Point L-24 lithologic column.

CHAPTER FIVE: ONE-DIMENSIONAL MODEL RESULTS

5.1 Introduction

The model output by the PetroMod[®] 1D simulator yields information about the evolution of Depot Point L-24. In this thesis, the burial history, thermal history, and hydrocarbon generation potential are investigated. This information is presented to the user as a series of plots and images. This chapter begins with an introduction to the interpretation of PetroMod[®] output plots, using three simple models relevant to the Depot Point L-24 model. That is followed by the model results, focusing on the burial and thermal histories and hydrocarbon potential of the Depot Point L-24 well. The chapter concludes with a sensitivity study limited to a) comparison with models without sills and without rifting, b) varying the age of sill emplacement, and c) a discussion about other important variables which are not explored in detail in this study.

5.2 Interpreting Data Displays

Before the model results are presented, it is useful to understand some of the graphical displays used in this chapter. Figure 5.1 is a simple three-layer model that illustrates the evolution of a one-dimensional lithologic column over time. The following three lithologies are shown: (1) basement rock 'Alpha', (2) shale 'Beta', and (3) sandstone 'Gamma'. The graph shows the evolution of a one-dimensional lithologic column over time. This type of diagram is called a burial history plot. The x-axis shows time in millions of years and the y-axis shows burial depths. It is important to keep in mind that this plot is not a cross-section. The bold blue, vertical line represents the lithologic column at present, 0 Ma. Rock formations and their unit thicknesses in a well bore would, therefore, correspond to the sequence illustrated along the blue line. The

green line represents the column at 7 Ma before present. The figure shows that at that time the Gamma sandstone is being deposited and the Alpha and Beta units are already in place. The red line goes further back in time to 15 Ma before present. At this time the Beta shale is being deposited and of course the Alpha basement layer is already in place. The red line represents a time prior to the deposition of the Gamma sandstone.

Figure 5.2 shows a three-layer model that includes a period of erosion. The Sydney gypsum and the Halifax limestone are deposited from 25-20 Ma and 20-15 Ma, respectively. From 15-10 Ma the system is static. Erosion of the Halifax limestone begins at 10 Ma and continues until 5 Ma. The Sydney limestone is then eroded from 5-0 Ma. The period of erosion is marked with a blue arrow along the time axis of the plot.

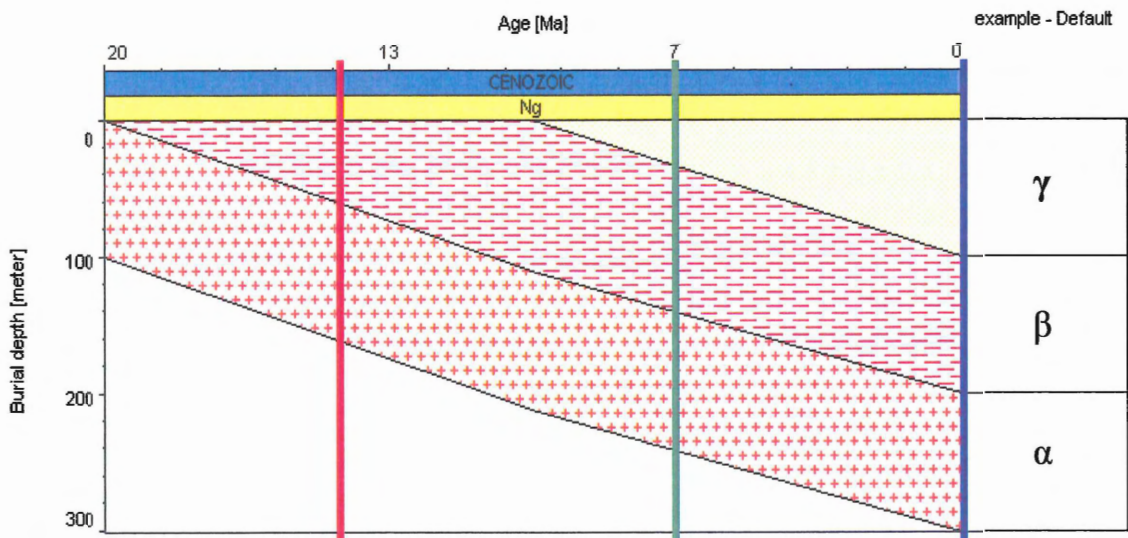


Figure 5.1: Schematic diagram showing the evolution of a lithologic column over time (*burial plot*) for basement α , shale β , and sandstone γ . See text for explanation.

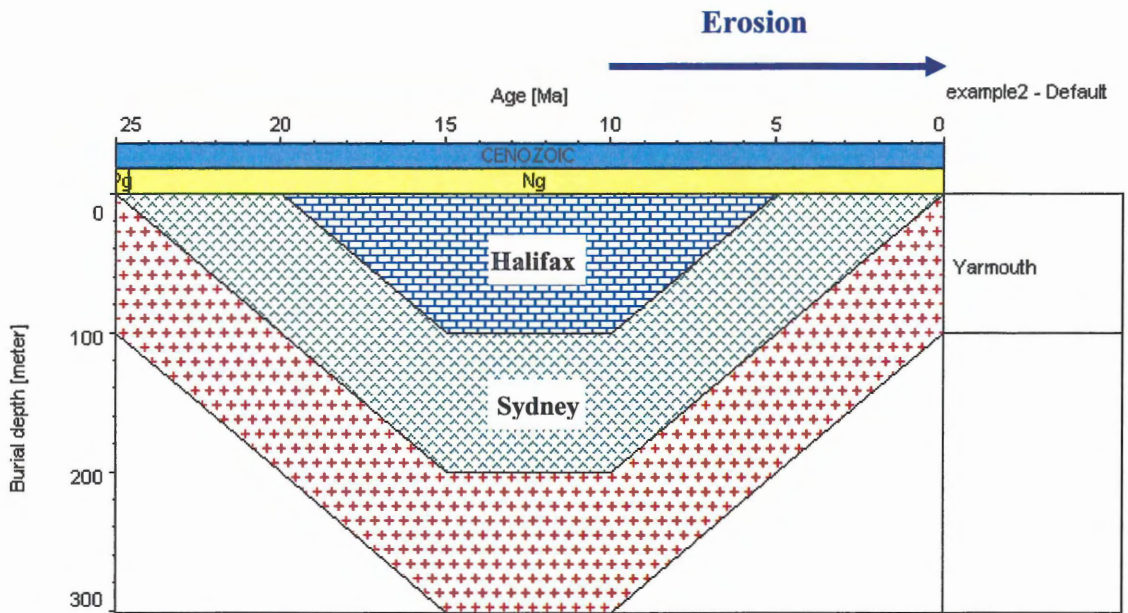


Figure 5.2: The Halifax limestone, the Sydney gypsum, and the Yarmouth basement are the three formations represented in this simple three-layer model. See text for the full explanation.

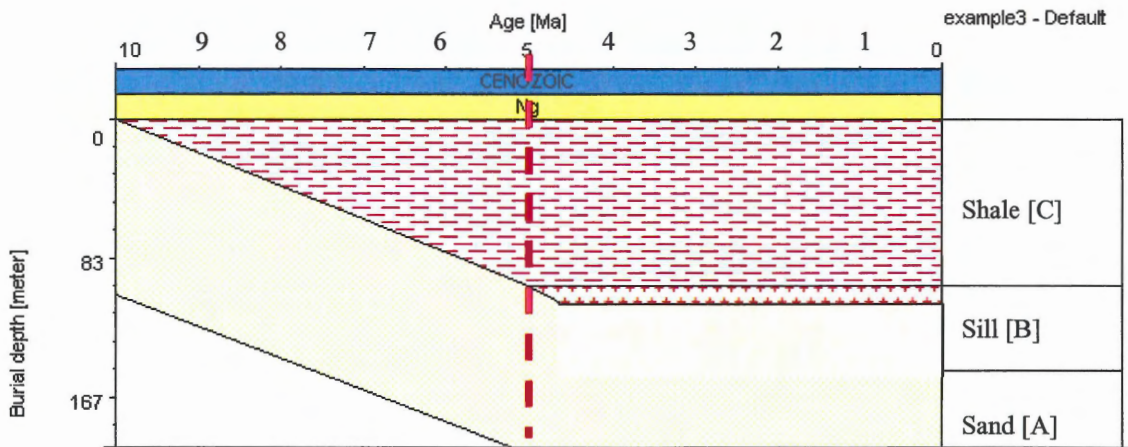


Figure 5.3: The C shale, the B sill, and the A sandstone are the three formations represented in this simple three-layer model. The B sill is intruded at 5 Ma, marked by the dashed red line. See text for the full explanation.

Figure 5.3 shows a sill emplaced between sandstone and shale strata. The shale is deposited from 10-5 Ma and then emplacement of the basaltic sill occurs at 5 Ma which is marked with a dashed red line.

5.3 Burial History

The burial history plot in Figure 5.4 shows the evolution of the Depot Point L-24 lithological column. Refer to Table 5.1 and Figure 5.1 for a detailed description of well lithologies. The plot includes a lithology legend that shows sandstone, siltstone, shale, basalt, and evaporites. The Blaa Mountain, Ringnes, and Awingak Formations are good potential source rocks, while the Van Hauen, Hare Fiord, Jameson Bay, Deer Bay, and Christopher Formations have poor source rock potential. The thick Heiberg Formation overlays the Blaa Mountain Formation and is a potential reservoir. Maximum burial occurs in the early Tertiary and is followed by basin inversion during the Eurekan orogeny. The youngest strata erode rapidly between 60 and 40 Ma; the Depot Point L-24 well is represented by the unit thicknesses at the 0 Ma point. The age of sill emplacement, at 125 Ma, is marked with a black dashed line and the sills themselves are traced in bright red.

5.4 Thermal Profile

The temperature overlay in figure 5.5 shows the thermal history of the rock strata in the Sverdrup Basin at the Depot Point L-24 well location. There is a strong temperature increase at 125 Ma, which represents the combined effects of rifting and sill intrusion. The geothermal gradient changes at 125 Ma and heats the basal strata, the Otto Fiord and Hare Fiord Formations, to near 500°C from previous temperatures of 175° to 200°C. The bands of constant geothermal temperature subside to deeper levels after the

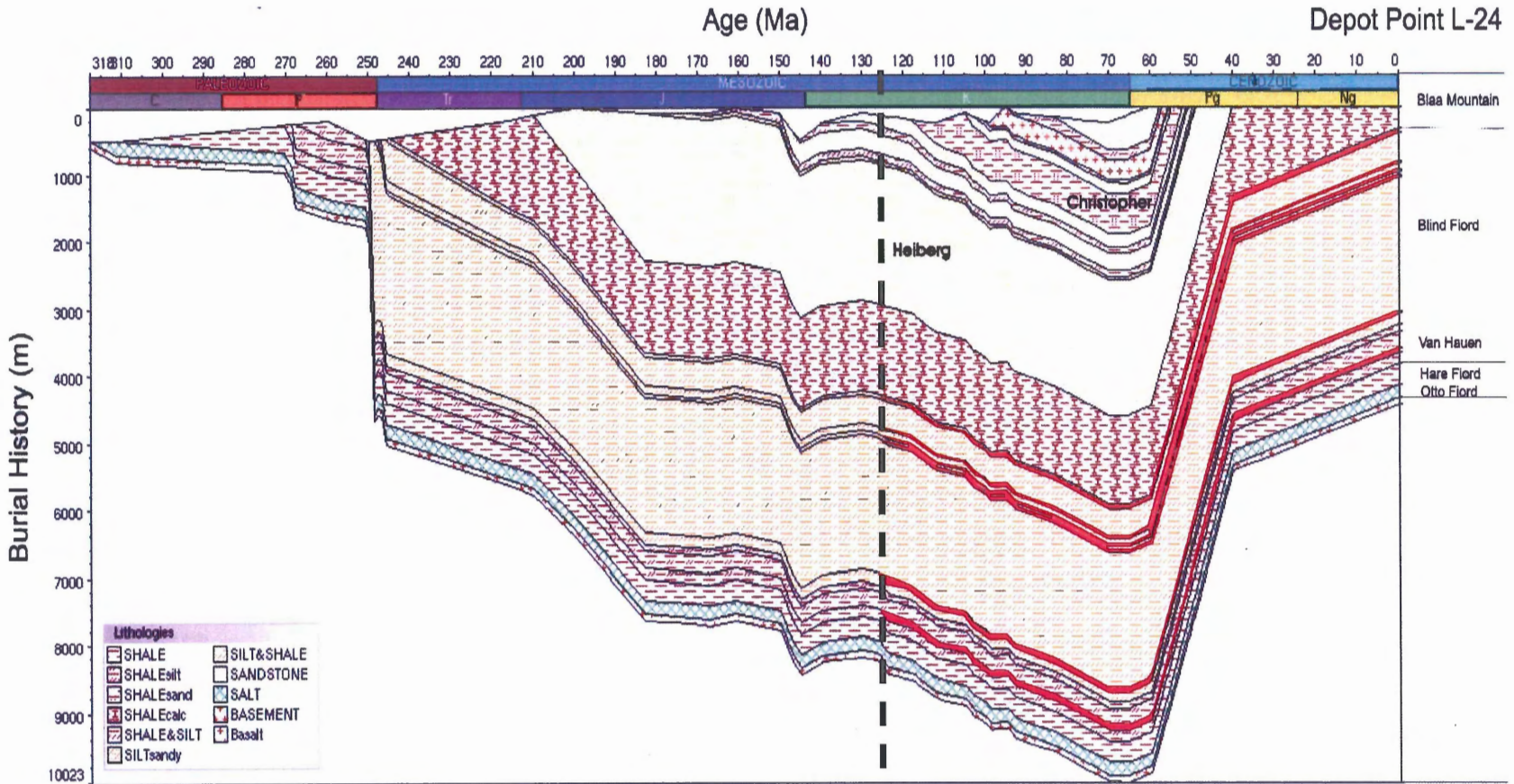


Figure 5.4: The burial history for the Depot Point L-24 includes Carboniferous to Cretaceous deposition, sill emplacement, and Tertiary basin inversion. The black dashed line shows the time of sill intrusion, 125 Ma, and the sills themselves are traced in bright red.

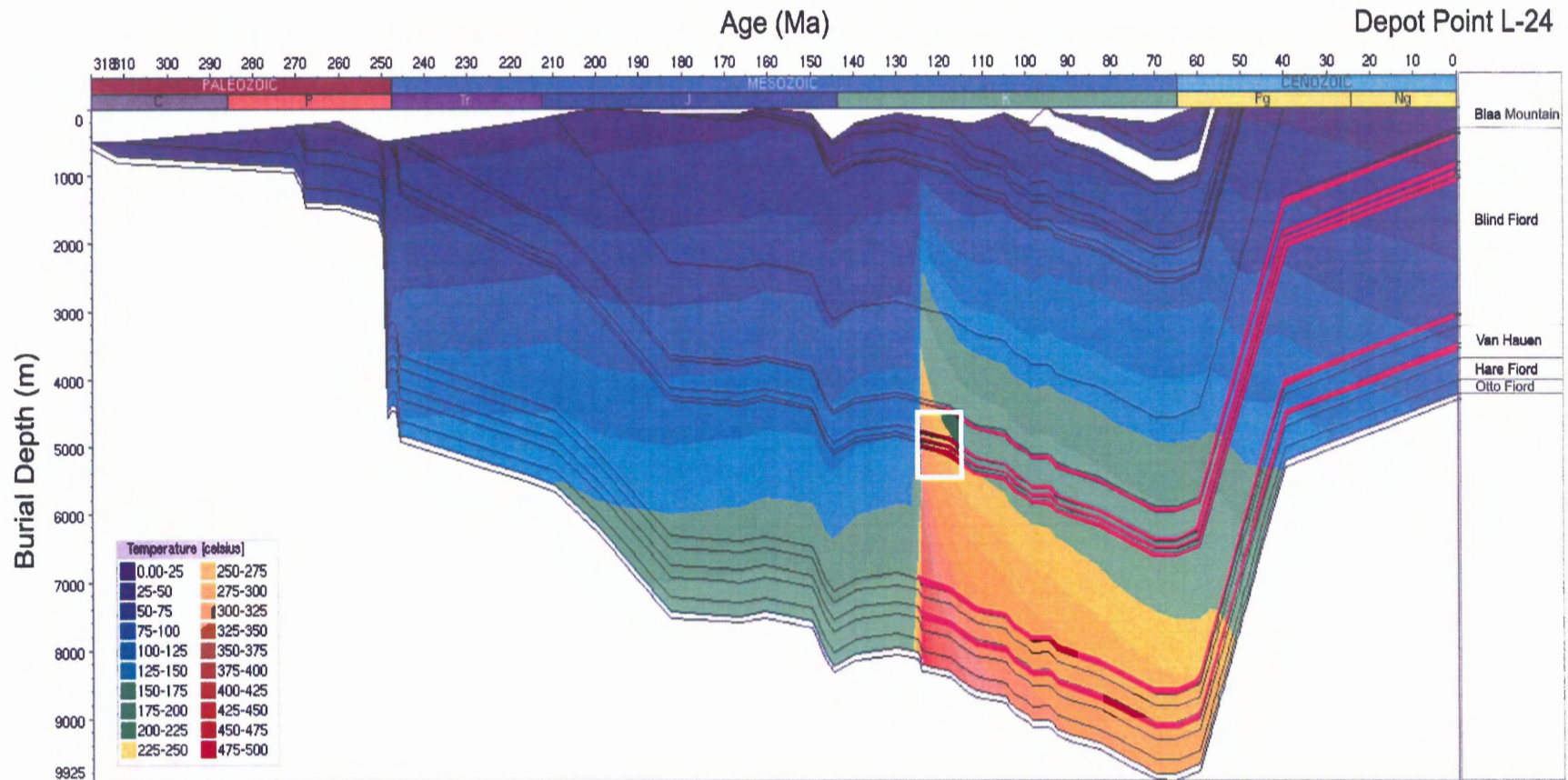


Figure 5.5: A temperature overlay can be added to the burial history plot shown in figure 5.4. There is a prominent temperature spike at 125 Ma, the time of rifting and sill emplacement. The basal strata reach temperatures around 500°C. After rifting and sill intrusion the modified thermal profile decays. The sills are traced with bold magenta lines. The white box outlines the area of the plot shown in figure 5.6.

rifting and intrusion events, and appear to have reached equilibrium by 0 Ma; this indicates that that temperature changes resulting from rifting and sill emplacement have dissipated.

Figure 5.6 zooms into an area where several sills intrude the well. This close up view clarifies the detailed structure of the temperature spike. The dashed black box outlines the initial changes in the geothermal gradient due to the onset of rifting before sill emplacement. The area of the plot to the right of 125 Ma indicates the time period of temperature decay after rifting and sill emplacement. This cooling period is indicated by the black arrow and increasingly lighter yellow zones. The purple line marks an area that reaches temperatures above 500°C . Notice that this area is in very close proximity to the intruding 1000°C magma.

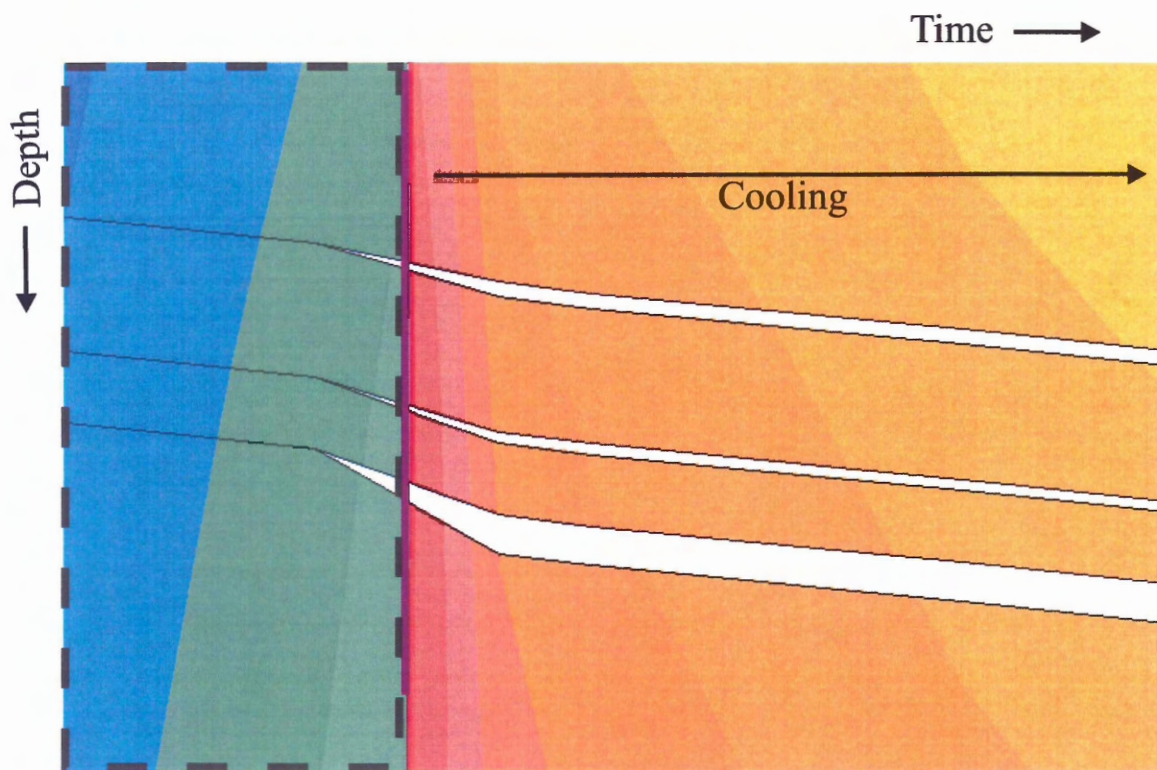


Figure 5.6: This image represents the area on the plot outlined by the white box in figure 5.5. The black dashed box traces changes in the temperature profile due to the onset of rifting. The white lines are the sills (the sills are red in Figure 5.5). The purple line shows the localized region around the intruding sills that is heated above 500°C and the period of cooling after rifting and sill emplacement is indicated.

Figure 5.7 highlights the formations that have source rock properties; their TOC and HI values were included as model input. Upon rifting and sill emplacement, the Blaa Mountain formation, a potential source rock at depth, reaches temperatures that range from 150-300°C, with the higher temperatures in rocks closest to the sills that intrude the underlying Blind Fiord Formation. Prior to rifting and sill emplacement, the Blaa Mountain Formation was at temperatures around 75-100°C. The immediate contact zones bordering the intrusive units, emplaced at 1000°C, were heated to significantly higher temperatures.

5.5 Hydrocarbon Potential

The model results demonstrate unequivocally that rifting and sill emplacement have profound effects on the thermal history of the Depot Point L-24 well and that oil and gas generation is possible in the strata intersected by the Depot Point L-24 well. Figure 5.8 shows a maturity-zone overlay onto the burial history of the Depot Point L-24 well. The blue, green, red, and yellow areas represent thermally immature, oil window, gas window, and over-mature zones respectively. The oil and gas windows are influenced by the kinetic parameters used in the model. In this thesis, the oil and gas windows refer to the green and red regions respectively, defined on the output maturity zone plots. The temperature ranges for the oil and gas windows as defined by the model are approximately 75°-125°C and 125°-150°C respectively. The temperature range given for the gas window is the optimal temperature range; gas may still be produced at temperatures higher than 150°C. *The most distinct feature in the maturity zone overlay is the jump in the position of the maturity zones at the time of rifting and sill intrusion.* The changes in temperature, and thus the geothermal gradient, allow rock that would

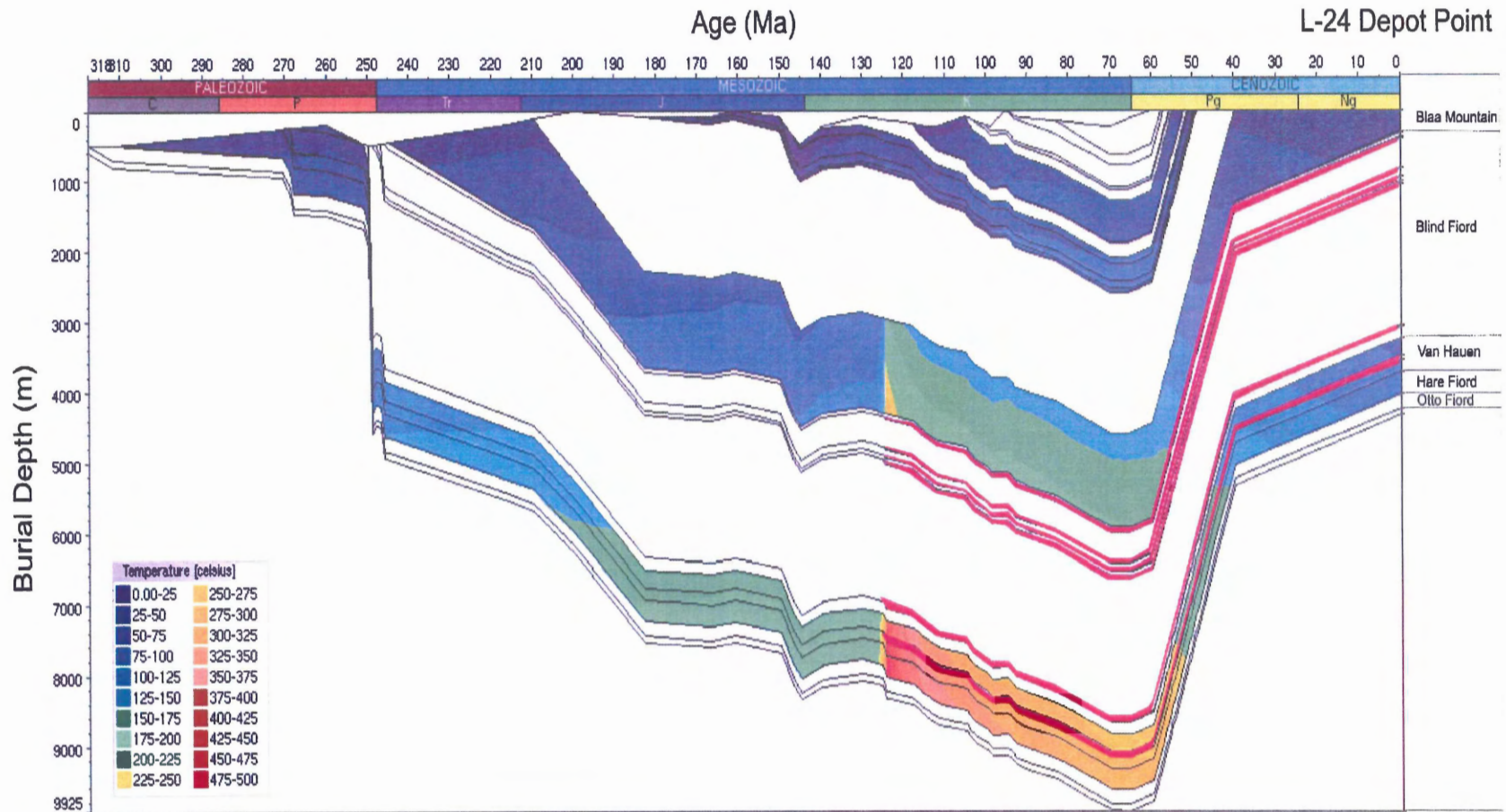


Figure 5.7: This image is essentially the same as Figure 5.5 except the temperature overlay is only displayed on the rock units that have source rock properties. It reveals the significant heating of potential source rocks at all levels within the lithologic column. The sills are traced with bold magenta lines. See text for more details.

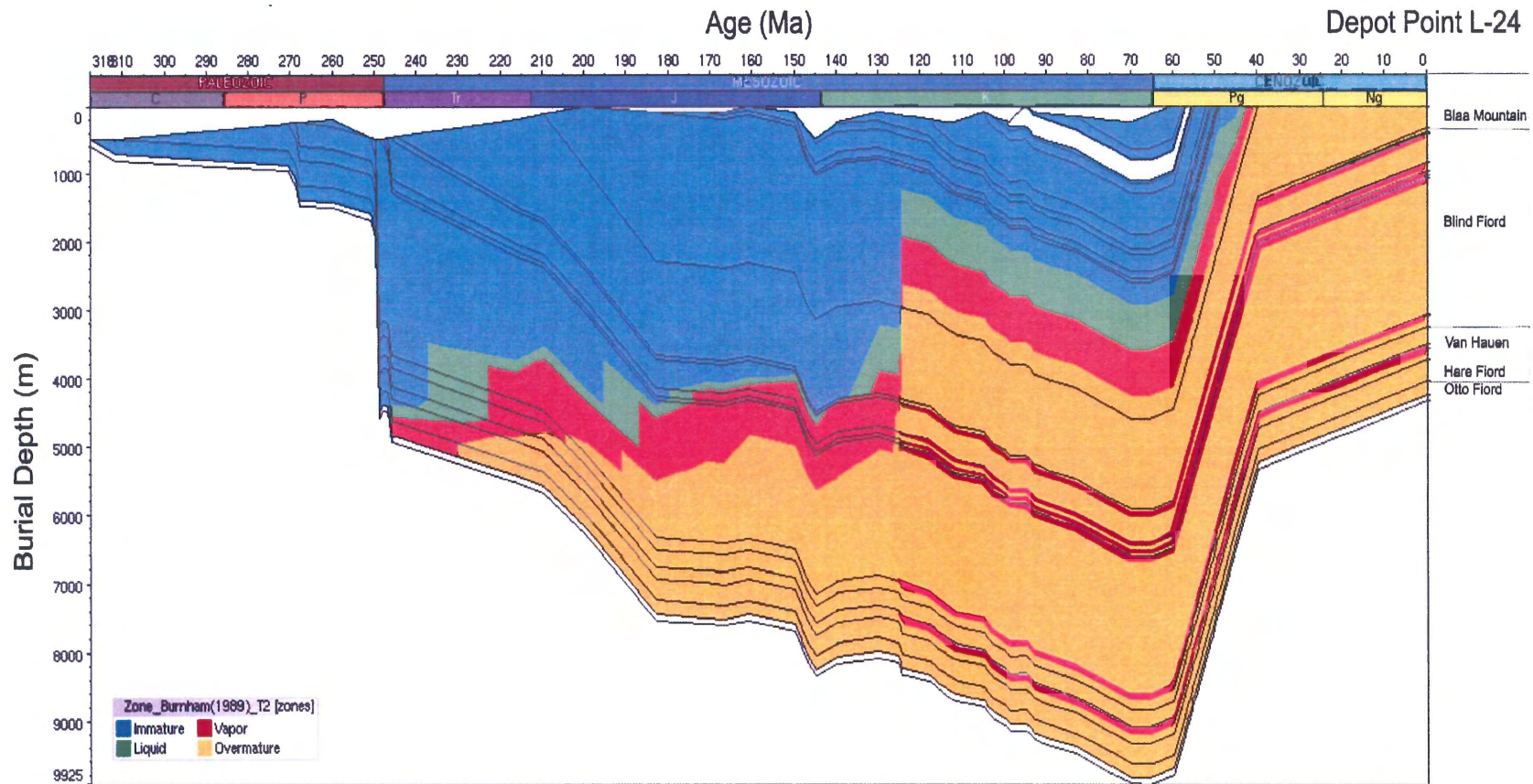


Figure 5.8: A maturity overlay can be placed on the burial history (Figure 5.4). The model shows thermally immature rocks in the blue regions and over-mature rocks in the yellow regions. Strata within the oil and gas windows are shown in green and red respectively. The distinct feature is the jump in the position of the mature rock region at 125 Ma, the age of rifting and sill emplacement. The sills are traced with bold magenta lines. See text for more details.

otherwise be immature, *in particular the Blaa Mountain Formation, to pass through the liquid-generating and gas-generating maturity zones and subsequently to produce hydrocarbons*. The deep source rocks, the Hare Fiord and Van Hauen Formations, pass through the oil and gas windows, and into over-mature zones prior to rifting and sill intrusion. This indicates that *the rifting and sill intrusion will not induce hydrocarbon generation in the deepest source rocks*. The shallow source rocks, for example the Awingak and Ringnes Formations, are not heated to temperatures high enough for hydrocarbon production; they remain thermally immature.

This model shows that the Hare Fiord, Van Hauen, and Blaa Mountain Formations produce hydrocarbons. The oil and gas generation overlays are presented in Appendix C. The Hare Fiord and Van Hauen Formations generate hydrocarbons prior to rifting and sill intrusion. In the Hare Fiord Formation, about 0.3 million tons of oil are generated between 245-220 Ma. The generation of 0.6 million tons of gas is coeval with oil generation in the Hare Fiord Formation. Rifting and sill emplacement occur at 125 Ma, much later than the generation of oil and gas from the Hare Fiord Formation; thus rifting and sill emplacement do not affect hydrocarbon generation within the Hare Fiord Formation.

The oil and gas generation in the Van Hauen Formation is very similar to that in the Hare Fiord Formation. Approximately 0.3 million tons of oil are generated between 240-210 Ma and 0.6 million tons of gas are produced during the same time period. The quantities of hydrocarbons produced directly reflect the model input parameters. Therefore, the numbers should not be quoted, rather the relative magnitudes of oil and

gas for different formations should be compared with one another to determine which source rocks are the most and least productive.

The Blaa Mountain formation is closer to the surface of the Earth than the Hare Fiord and Van Hauen Formations. Consequently, it remains at lower temperatures until rifting and sill emplacement. Prior to rifting and sill emplacement, less than 0.2 million tons of oil and 0.8 million tons of gas are produced by the Blaa Mountain Formation. Approximately 40 million tons of oil and 9 million tons of gas are generated rapidly at 125 Ma, as a result of rifting and sill emplacement. Oil generation ceases at about 124 Ma and gas generation doesn't occur after 123 Ma. The Blaa Mountain Formation produces more than one hundred times more oil and almost ten times more gas than the Hare Fiord and Van Hauen Formations.

5.6 Sensitivity Study

This section presents a sensitivity study limited to a) comparison with models without sills and without rifting, b) varying the age of sill emplacement, and c) a discussion about other important variables which are not explored in detail in this study.

5.6.1 Lack of Intrusive Activity and Lack of Rifting

When sills are omitted from the model the thermal history changes significantly. The temperature spike in Figure 5.9, the modeled scenario without sill intrusion, only represents rifting. The geometry of the temperature spike in Figure 5.9 is rounded due to the gradual nature of rifting, it is not considered instantaneous on the scale of geological time. The cooling and subsidence of geothermal isolines after the onset of rifting is more gradual than the decay after sill intrusion in the original model. The maximum

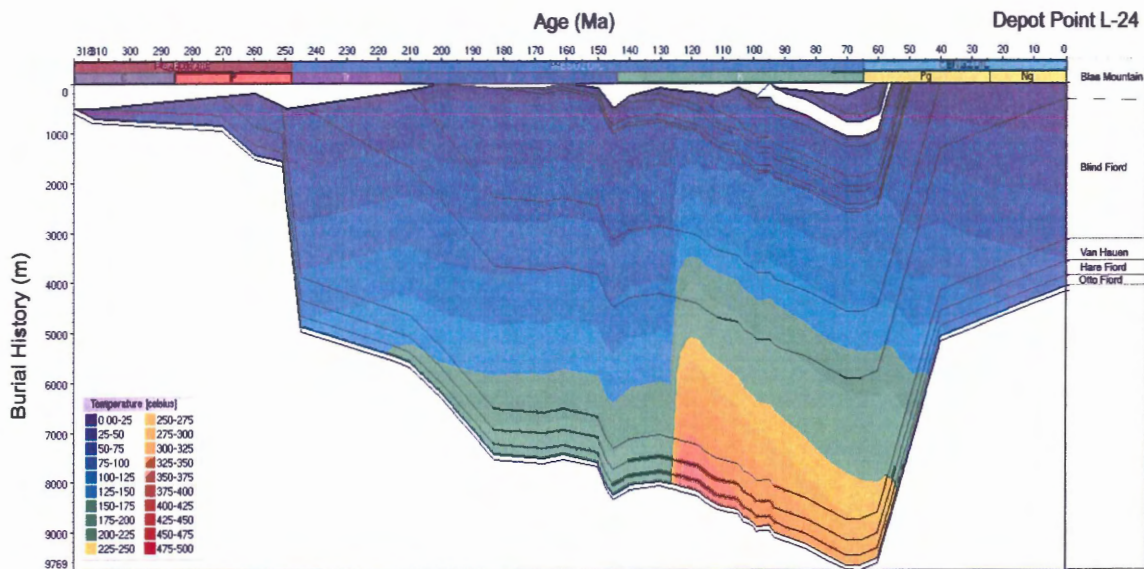


Figure 5.9: On this diagram, the temperature profile for the lithological column at Depot Point L-24 does not include take into account the additional heat provided by sill intrusion. As a result, the temperature spike observed on the plot is related to the *rifting event only*. Note that the peak is wider and more subdued than in the original model shown in Figure 5.5. The cooling trend indicated by geothermal isolines following rifting is also more gradual compared to the original model. See text for details.

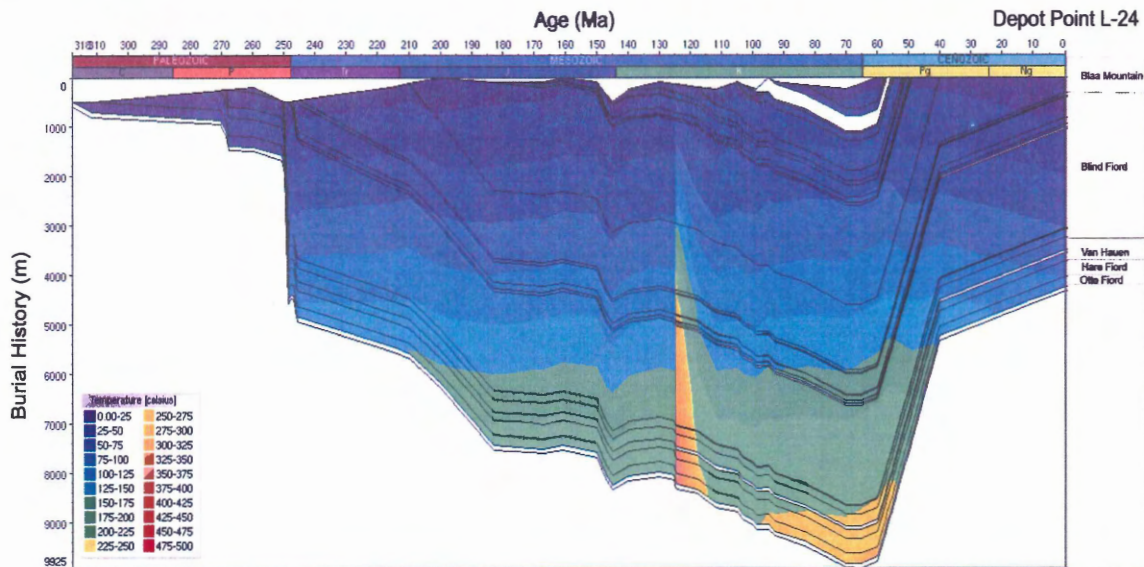


Figure 5.10: On this diagram, the temperature profile for the lithological column at Depot Point L-24 takes into account the additional heat provided by sill intrusion, without rifting. The observed temperature spike is sharp and decays rapidly following the intrusive event. See text for details.

temperatures reached by the Blaa Mountain Formation are between 200-225°C, which are significantly lower than the maximum temperatures produced in the model with the sills. Although the entire rock column is affected by rifting, the effects are less drastic than those recorded in the model with sill intrusion.

Figure 5.10 shows a version of the model where the sills are emplaced, but the rifting event is removed. This results in a sharp temperature spike, which decays relatively quickly after sill emplacement. The entire lithologic column is not heated evenly. The strata closest to the sills are heated to significantly higher temperatures than the strata far away from the sills. A comparison of Figures 5.9 and 5.10 shows rifting is responsible for heating the entire lithologic column. Rifting also produces a long-term change in the geothermal gradient, and thus the thermal profile of the region. Sill emplacement exhibits more localized effects, which decay soon after intrusion.

When sills are not intruded into the Depot Point L-24 well, the Blaa Mountain Formation produces hydrocarbons. This indicates that the thermal changes due to rifting are capable of inducing hydrocarbon generation. However, there are some significant differences in the hydrocarbon generation from the Depot Point L-24 model where the sills are intruded. When no sills are intruded, the thermal effects of rifting initiate oil generation. Approximately 40 million tons of oil are produced over a time period of 4 Ma, from 125-121 Ma. The Blaa Mountain Formation then enters the gas window and produces about 9 million tons of gas. Not all of the oil is converted into gas; much of it remains as a residuum. This gas will then diffuse away from the source rock.

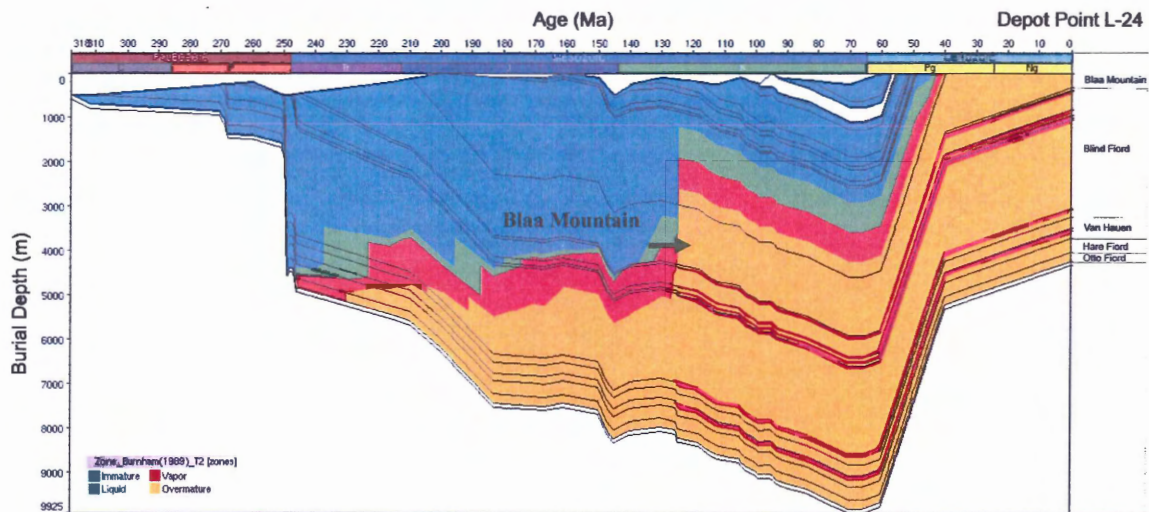


Figure 5.11 a): This image shows the maturity zones for the Depot Point L-24 well. This is the original model, which includes rifting and sill emplacement at 125 Ma. See section 5.5 for a more detailed explanation.

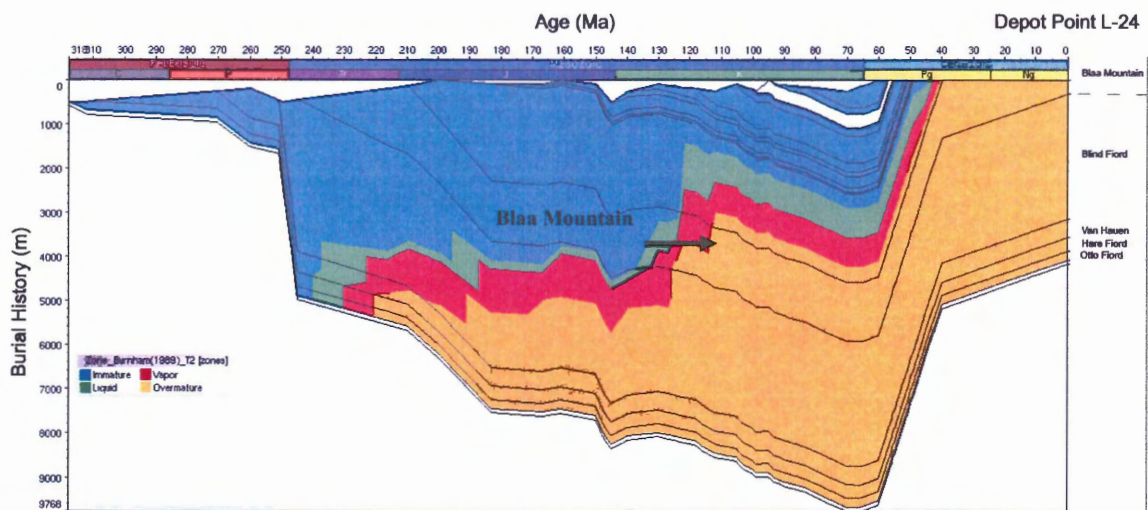


Figure 5.11 b): This model is identical to the original Depot Point L-24 model shown in figure 5.11 a) and discussed earlier in this chapter, except the intrusion of sills has been omitted. In comparison with figure 5.11 a), this variation of the model shows that the Blaa Mountain Formation resides within the oil window for about 5 Ma before entering the gas window. See the text for a more detailed explanation.

Figure 5.11 a) and b) compare maturity zone overlays for the Depot Point L-24 models with sill intrusion and without sill intrusion. Figure 5.11 a) shows the maturity zone plot for the model with sills. There is a sharp jump in the positions of the zones upon rifting and sill intrusion. The Blaa Mountain formation passes quickly through the oil and gas windows as shown by the black arrow. Refer to the text in Section 5.5 for the explanation of the background of this plot. Figure 5.11 b) shows the maturity zone plot for the model without sills. Notice that the Blaa Mountain spends a longer period of time in the oil and gas windows before passing into the over-mature zone. The models with and without sills both produce about 9 million tons of natural gas. The sills do not change the total amount of gas produced, but they do affect the rate at which the Blaa Mountain Formation passes through the various maturity zones. In the Depot Point L-24 simulation where sills are intruded into the lithologic column, gas is rapidly generated. In the model without sill intrusion the Blaa Mountain Formation generates oil, which then cracks to gas over a longer period of time, about 4 Ma.

5.6.2 Varying the Age of Sill Intrusion

Figures 5.12 and 5.13 show temperature overlays from two models which illustrate the effects of varying the age of sill emplacement. These two models have sill emplacement ages of 90 Ma and 110 Ma respectively, and are otherwise identical to one another. Sill emplacement and rifting are associated with one another, but are not coeval processes in these two models as they are in the original model. These models both show the development of two temperature spikes, the first temperature spike represents rifting and the second occurs upon sill intrusion. The rifting temperature spike is rounded with gradual subsidence and the sill intrusion peak is abrupt with a more rapid onset of decay.

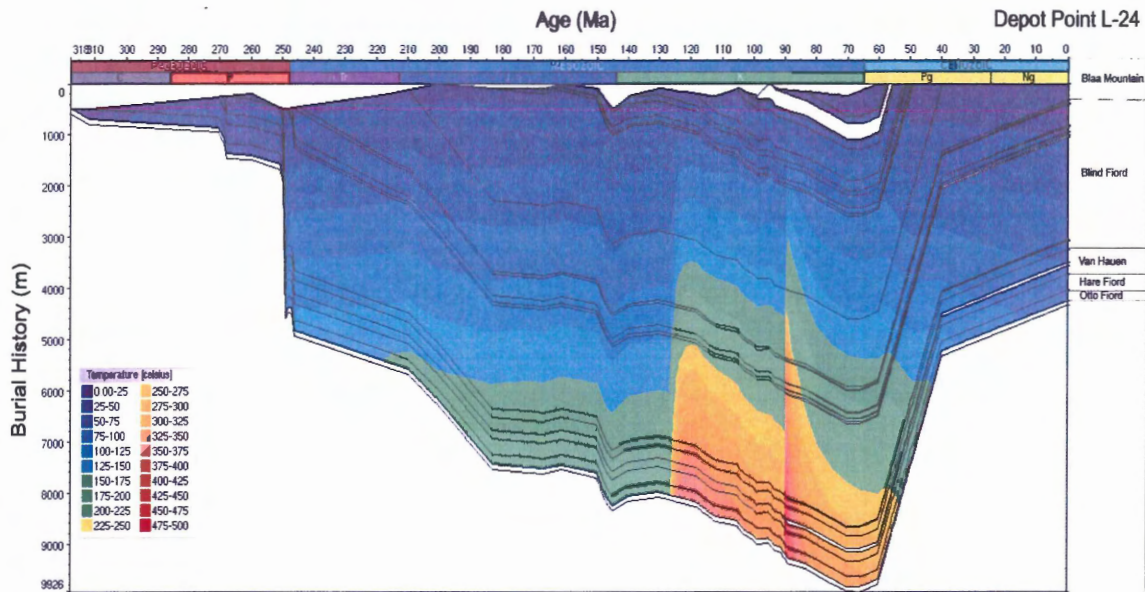


Figure 5.12: In this scenario sill emplacement occurs at 90 Ma. There is a time difference of 35 Ma between the onset of rifting and later sill intrusion. This results in the two separate temperature spikes shown in this figure. The smaller, rounded rifting peak begins at about 125 Ma and the later sill intrusion spike sharply starts at 90 Ma.

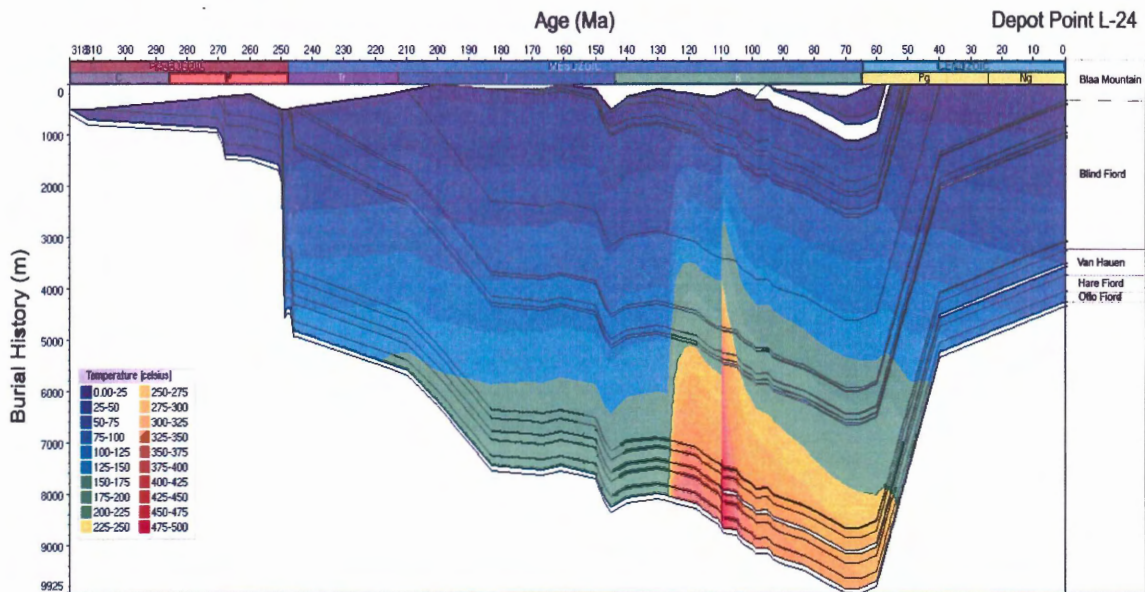


Figure 5.13: This scenario is very similar to that shown in figure 5.12. Rifting begins at 125 Ma and sills are intruded 15 million years later at 110 Ma. There is a shorter time gap between rifting and sill emplacement.

The difference between the models shown in figures 5.12 and 5.13 is the time lapse between rifting and intrusion. Where sills intrude at 90 Ma, a longer time lapse exists between the two temperature spikes than in the model with a sill emplacement at 110 Ma. The longer time lapse allows the effects of rifting to decay for a longer period of time before the sills are intruded.

Varying the age of sill emplacement has an effect on the positions of the maturity zones. When sills are intruded at 90 Ma or 110 Ma, they do not affect hydrocarbon generation. This is because the rifting at 125 Ma caused the Blaa Mountain Formation to generate oil and gas millions of years prior to sill emplacement. When the age of sill emplacement is closer to the age of rifting, there are visible effects in the model results. The Blaa Mountain Formation begins to generate oil at 125 Ma, during rifting. Upon sill intrusion, hydrocarbon generation cracks to natural gas. This is illustrated in the maturity zone plots shown in Figure 5.14.

A comparison of the maturity-zone overlays for three models, the original Depot Point L-24 model, a model variation with sill emplacement at 122 Ma, and a model variation without sill intrusion, clearly illustrates the overall effects of sill emplacement on the hydrocarbon system. These three plots are shown in figure 5.15. The intrusion of sills changes the amount of time that the Blaa Mountain Formation spends in the oil window before cracking it to gas and changes the rate at which the hydrocarbons are generated. The slopes of the black dashed lines on each of the three plots shown in Figure 5.15 represent the rates at which the Blaa Mountain Formation passes through the oil and gas windows. The steeper the slope, the more rapidly the formation passes from the oil window into the gas window. When rifting and sill intrusion both occur at 125 Ma

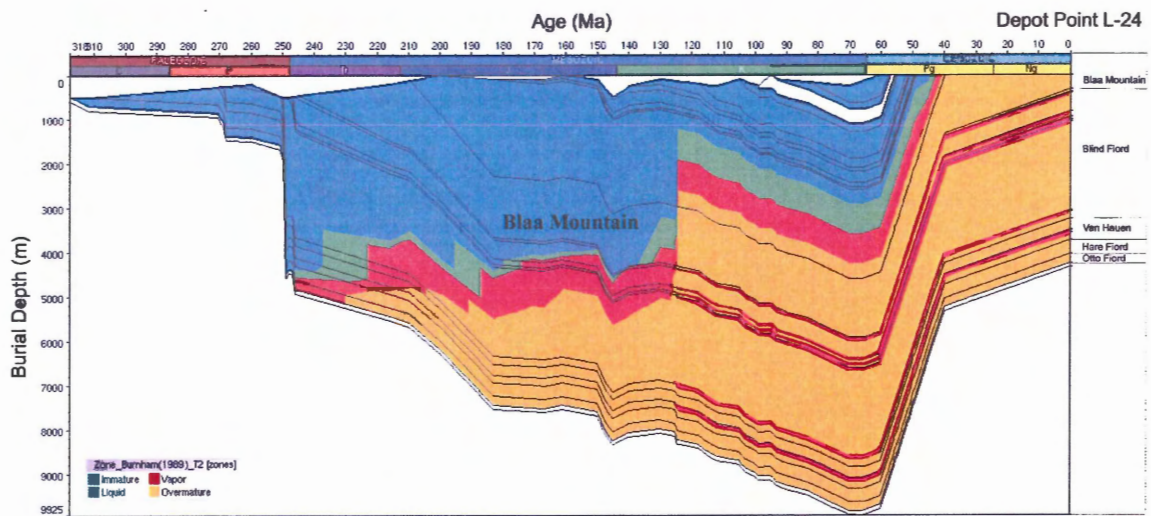


Figure 5.14 a): This image shows the maturity zones for the Depot Point L-24 well. This is the original model, which includes rifting and sill emplacement at 125 Ma. See section 5.5 for a more detailed explanation.

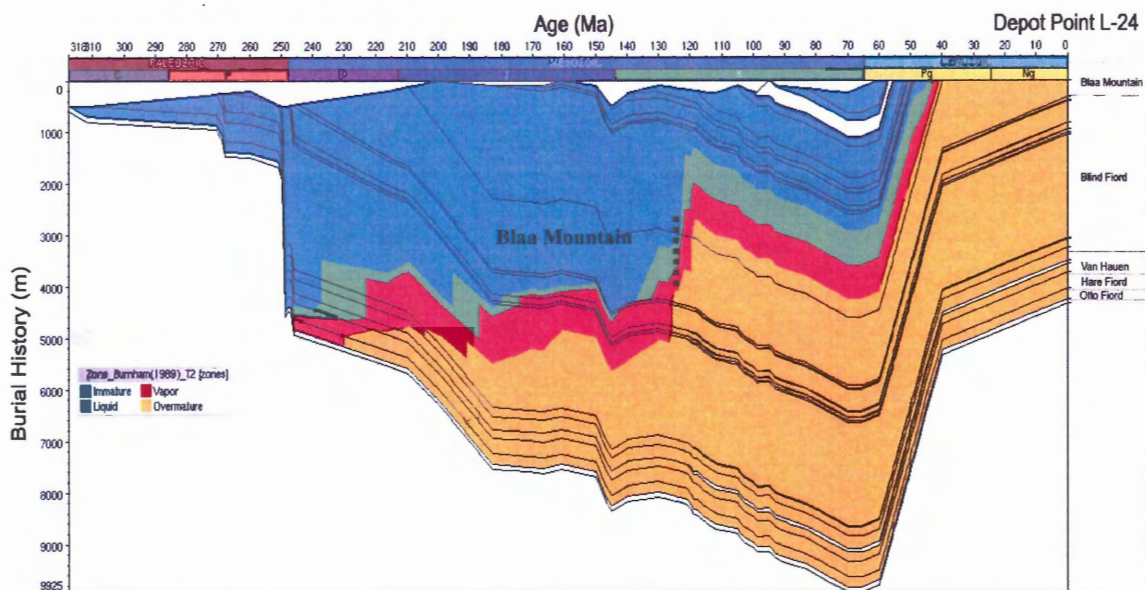


Figure 5.14 b): This model is identical to the original Depot Point L-24 model shown in figure 5.14 a) and discussed earlier in this chapter, except the age of sill emplacement has been changed to 122 Ma. In comparison with figure 5.14 a), this variation of the model shows that the Blaa Mountain Formation resides within the oil window for a short period of time prior to sill emplacement. Intrusion of the sills rapidly initiates gas generation. The black dotted line shows the small jump in the position of the oil and gas windows due to sill emplacement.

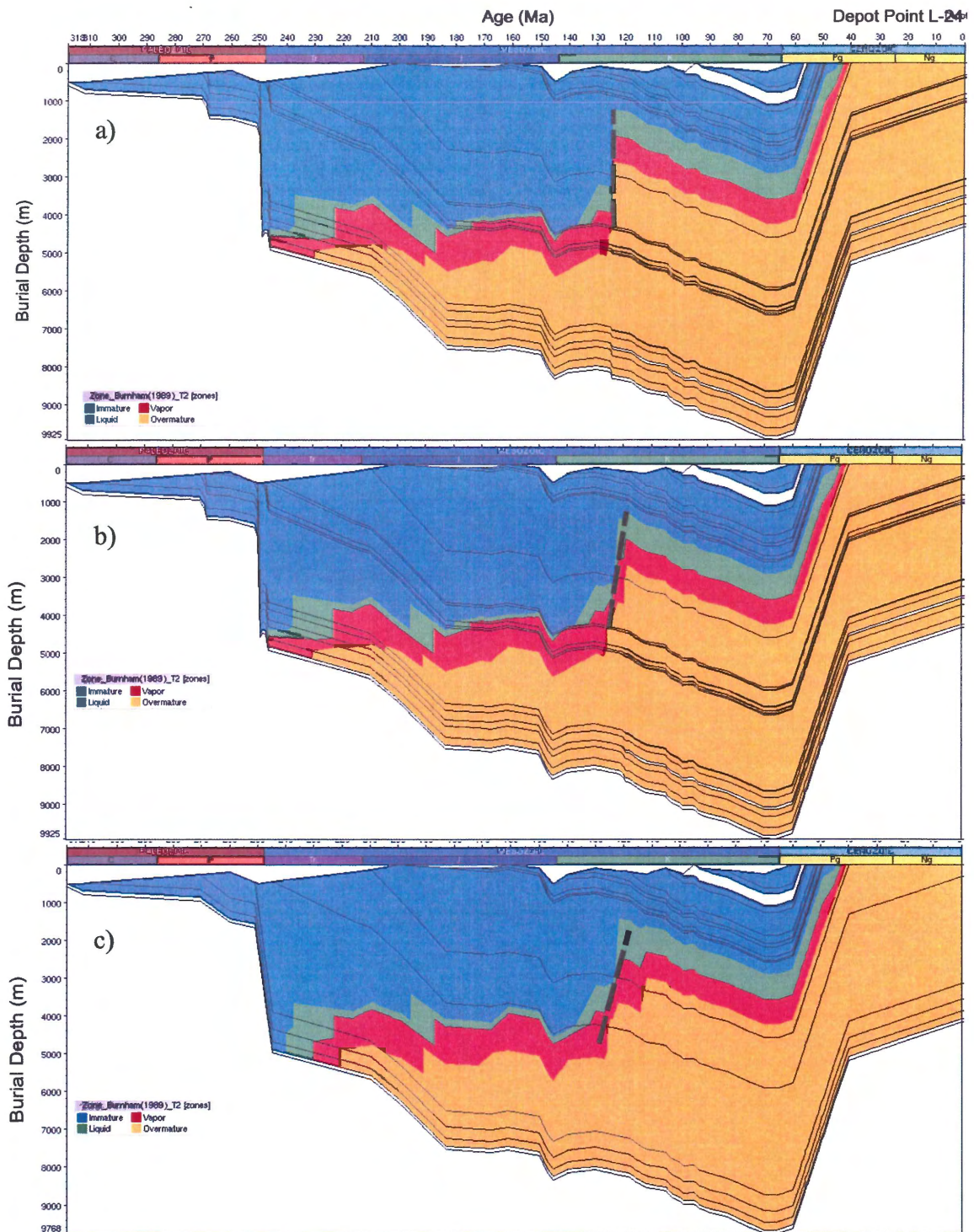


Figure 5.15: A comparison of three models illustrates the effects of sill intrusion; a) rifting and sill intrusion occur at 125 Ma, b) rifting occurs at 125 Ma and sill intrusion follows at 122 Ma, and c) rifting occurs at 125 Ma and sills are omitted. The black dashed line on each of the three plots qualitatively represents the rate at which the Blaa Mountain Formation passes through the oil and gas windows. The steeper the slope of the line, the more rapidly the formation passes from the oil window into the gas window.

(Fig. 5.15 a), hydrocarbon generation involves rapid gas production. When rifting occurs at 125 Ma and the sills intrude at 122 Ma (Fig. 5.15 b), the Blaa Mountain Formation produces oil for three million years and upon sill intrusion, rapidly produces gas.

The abundance of igneous intrusive rocks in the Sverdrup Basin implies that these two scenarios exist in many parts of the basin. This may explain the relative abundance of natural gas within the Sverdrup Basin. When sills are omitted from the model (Figure 5.15 c), oil generation occurs slowly over a period of about 4 Ma initiated by rifting at 125 Ma.

5.6.3 Important Variables Not Considered in this Study

The short sensitivity study completed as part of this thesis explored the effects of omitting the sills from the Depot Point L-24 model and varying the age of sill emplacement. Further investigation of the effects of changing model parameters is outside of the scope of this thesis. However, future work should include a more detailed sensitivity study, which explores the effects of varying the heat flow values and the thicknesses of eroded lithologic units. Both of these parameters influence the thermal history of the Depot Point L-24 lithologic column, thus affecting hydrocarbon generation. Changes in these parameters are expected to have a significant effect on the model results. Changing the position of the source rocks relative to the sills changes the potential for oil and gas production in the Depot Point L-24 well. The close proximity of the Blaa Mountain Formation to sills intruding the underlying Blind Fiord Formation allows the Blaa Mountain Formation to be affected strongly by sill emplacement.

There are several model parameters which are not expected to have a large effect on the thermal history and petroleum generation within the Depot Point L-24 well. The

sediment-water interface temperature and sea level appear to have a minimal influence on the model results.

Summary

The burial history plot created using the PetroMod[®] software shows the evolution of the Depot Point L-24 lithologic column. The temperature overlay reveals the thermal history of the lithologic column. There is a prominent temperature spike at 125 Ma, the time of rifting and sill intrusion. This causes significant heating of the source rocks intersected by the Depot Point L-24 lithologic column. When a maturity zone overlay is applied to the burial history plot, a distinct jump in the position of the oil and gas windows can be correlated with the temperature spike caused by rifting and sill intrusion. Oil and gas generation plots, presented in Appendix C, indicate that the Blaa Mountain Formation undergoes rapid oil and gas generation at 125 Ma, the time of rifting and sill intrusion. Small amounts of oil and gas are generated prior to rifting and sill emplacement in the Hare Fiord and Van Hauen Formations. When interpreting the model results, the relative magnitudes of hydrocarbons produced by each formation should be compared. For example, the Blaa Mountain Formation generated almost ten times more gas than the Hare Fiord and Van Hauen Formations.

The short sensitivity study reveals that the sill emplacement increases the rate of hydrocarbon generation and promotes rapid gas production. All of the modeled scenarios presented in this chapter, the original Depot Point L-24 model, a model without sills, and models with different sill emplacement ages, generate the same amount of oil and gas, however the rates of production vary significantly depending on the time of sill emplacement.

CHAPTER 6: DISCUSSION AND CONCLUSION

6.1 Discussion

6.1.1 Solutions to the Four Scientific Questions

Four questions defining the scientific objectives of this thesis were outlined in Chapter 1. Upon the completion of the numerical modeling, these questions can be answered. The following section is a discussion of the model results to provide solutions to these questions.

1. Key observations on the hydrocarbon and magmatic systems in the Sverdrup Basin: why should they be integrated?

Hydrocarbon generation requires source rocks to be heated so that they can enter the oil or gas windows. In subsiding sedimentary basins, the thermal profile is influenced by the local geothermal gradient, conductivity, and heat flow values. Because of the geothermal gradient, deeper lithologies are heated to higher temperatures than rock units closer to the surface (Hunt, 1996).

Because hydrocarbon generation is dependent on temperature, changes in the thermal conditions within the basin will affect the potential for oil and gas generation and/or under- or over-maturation. Thermal profiles for basins with significant magmatic components are affected by heat introduced by intrusive and extrusive igneous rocks (e.g. Schutter, 2003; Malthe-Sørenssen *et al.*, 2004). Lava flows cool quickly because they are emplaced on the Earth's surface. The heat associated with these flows at the surface has very little to no impact on hydrocarbon systems at depth. Sills have a larger effect because the heat they introduce into the surrounding rocks cannot escape into the atmosphere (Schutter,

2003). The effects of intruding igneous rocks must be considered to produce realistic predictions regarding oil and gas potential in the Sverdrup Basin.

2. ***How and where in the evolution of the Sverdrup Basin does sill emplacement affect the hydrocarbon system?***

In the field, zones of contact metamorphic rocks – the host sedimentary rocks are “baked” - along the edges of intrusive igneous units indicate that sills strongly affect the surrounding strata. Field observations illustrated in Figures 3.7, 3.8, and 3.9 indicate that the width of the contact zones bordering the sills rarely exceed several tens of meters, and represent a local effect. However, the density of sill intrusion in the Mesozoic succession of the Sverdrup Basin (Figure 3.6) suggests that the impact on the thermal profile is a regional effect. The contact metamorphic zones form at very high temperatures, as they are adjacent to the hot, intruding magma. Oil and gas generation occur at much lower temperatures and therefore do not necessarily correlate with visible mineral reactions. Estimates of the volume of magma intruded as sills would contribute to a quantitative assessment of regional effects but are not available. In a one-dimensional model constructed for this study, the intrusion of six sills at 1000°C into the Depot Point L-24 well causes significant changes in the thermal profile. The first important observation is the occurrence of a temperature spike at 125 Ma, related to rifting and sill intrusion; this spike decays over time. The combined temperature spike affects the entire rock column, not just the strata that contact the sills and it significantly heats the Blaa Mountain Formation, a potential source rock, to temperatures between 150 and 300°C.

The change in the geothermal gradient heats the deepest source rocks, the Hare Fiord and Van Hauen Formations, to temperatures well above the oil and gas maturity zones (see Fig. 5.8). Incipient rifting (crustal extension) and sill intrusion occur almost 100 Ma after hydrocarbon generation ceased in the Hare Fiord and Van Hauen Formations, thus rifting and sill emplacement will not affect the hydrocarbons produced by these formations.

The Blaa Mountain Formation, a shallower source rock, suffers its main phase of hydrocarbon generation at 125 Ma, the time of rifting and sill intrusion. Figure 5.8 shows the jump in position of the thermal maturity zones due to rifting and sill intrusion. The sensitivity study described in Chapter 5 shows that the changes in the thermal profile of the Depot Point L-24 well due to rifting alone, initiate oil generation and later gas generation in the Blaa Mountain Formation. The emplacement of sills increases hydrocarbon generation rates in the Blaa Mountain Formation and promotes the generation of gas rather than oil.

By 0 Ma the heat spike has subsided and the geothermal gradient approximates its depth-temperature relationship prior to rifting and sill emplacement. This shows that the thermal effects of rifting and sill emplacement have dissipated and are not longer actively influencing the Depot Point L-24 well.

3. *How do the results for the modeled Depot Point L-24 well differ from scenarios where sills are not introduced or where the age of sill emplacement is different?*

A short sensitivity study, limited to comparison with models without sills and without rifting and varying the age of sill emplacement, is described in section 5.6, and the results summarized here.

The heat spike in the original Depot Point L-24 model represents the combined effects of rifting and sill emplacement; this better explains why the entire lithologic column is heated rather than just the rocks contacting the intrusions. When the sills are omitted from the model, the rifting temperature spike is isolated. The changes in the thermal profile due to rifting initiate slower oil generation in the Blaa Mountain Formation. Gas generation begins in the Blaa Mountain Formation after a time period of about 4 Ma.

Varying the age of sill emplacement separates the thermal effects of rifting from the thermal effects of igneous intrusion. Two temperature spikes are recognized; one corresponding to rifting and the other to sill emplacement. The intrusion of sills causes rapid gas generation in the Blaa Mountain Formation. If the rifting and sill intrusion are coeval, as in the original Depot Point L-24 model, the Blaa Mountain Formation has increased hydrocarbon generation rates. If the sills are introduced shortly after rifting, the Blaa Mountain Formation begins producing oil and at the time of sill intrusion, begins rapid gas generation. Overall, the emplacement of sills increases the hydrocarbon generation rates in the Blaa Mountain Formation, and promotes the production of natural gas rather than oil. The quantity of gas produced by the Blaa Mountain Formation is consistent for all of the Depot Point L-24 model variations, about 9 million tons. The hydrocarbon generation histories differ in each of the model variations. The Blaa Mountain Formation spends different amounts of time in the oil and gas windows in each of the models, but the end results are constant.

The heat flow values and the eroded lithological thicknesses are expected to have a significant influence on the thermal history of the Depot Point L-24 well and should be the subject of a future sensitivity study.

4. *Can one-dimensional modeling quantify the effects of igneous activity on the hydrocarbon system within the Sverdrup Basin?*

The numerical modeling process used in this thesis does not provide a unique quantitative solution to the scientific questions posed at the beginning of the study. Although the model results provide a set of numerical constraints, these numbers reflect the input parameters selected for one-dimensional analysis. A more comprehensive study could use the same approach but would explore the variations caused by changing model input parameters to define appropriate ranges of values. It can be concluded that the application of a one-dimensional model to the Depot Point L-24 well produces some robust qualitative observations on the processes and interactions that occur in volcanic basins and semi-quantitative results that could be refined by making 2- and 3D models.

6.1.2 *Future Work*

The construction of the one-dimensional model allows the user to explore the limitations and knowledge gaps associated with the simulation. The process of constructing the model also allows correlation and comparison between different data sets such as heat flow and time-temperature models from fission-track analysis, and in the future from (U-Th)/He dating (Zentilli, *pers comm.*). Limitations may be due to a lack of reliable data sets. For example, the vitrinite reflectance values used as model input are not well defined and there are no Rock-Eval data available for the Depot Point L-24 well.

These two data sets would improve the model and provide better constrained results, if they are accurately measured and recorded.

The model could be expanded into two- and three-dimensions. Repeating the process used in this thesis for individual well model construction is the first step in producing a 2- or 3D model. Wells along transects can be correlated to 2D seismic profiles and used in the construction of a basin-wide cross-section. Multiple wells can be correlated to 3D seismic surfaces in the construction of a three-dimensional basin simulation. Unlike the approach taken here, these more advanced models would include structural trap analyses as well as hydrocarbon migration pathways. A comprehensive set of 2- and 3D models constructed through the Strand Fiord Project would lead to a quantitative assessment of thermal effects that result from the interaction of magmatic and hydrocarbon systems in the Sverdrup Basin, and provide further insight into the questions left unanswered by the one-dimensional modeling.

6.2 Conclusion

This thesis used numerical modeling techniques to determine the impact of sill emplacement on the hydrocarbon system in the Sverdrup Basin, Canadian Arctic. The model focuses on the Depot Point L-24 well on Axel Heiberg Island, eastern Sverdrup Basin.

Deposition was the dominant process in the Sverdrup Basin from the Carboniferous until the late Cretaceous. In the Cenozoic, basin inversion, exhumation, and erosion became dominant. Extrusive and intrusive igneous activity occurred during the Cretaceous producing thick successions of flood basalts and complex feeder networks of sills and dykes. Outcrops of intrusive units on western Axel Heiberg have visible

contact aureoles. However, not all of the thermal effects of sill intrusion are preserved so visibly in the rock record. The impact on hydrocarbon generation is not as obvious as the zones of contact metamorphism.

Formation names, lithologies, unit thicknesses, depositional and erosional ages, source rock properties, sill characteristics, vitrinite reflectance data, heat flow data, sea level, and other data sets were input into PetroMod[®], the numerical modeling program chosen for this thesis. The one-dimensional model focuses on the burial and thermal histories and the oil and gas generation potential of the formations intersected by the Depot Point L-24 well.

Model results are displayed as a series of plots in Chapter 5. Maximum burial occurs at the onset of the Tertiary and is followed by exhumation and erosion. Rifting and sill intrusion cause temperature spikes in the thermal profile over time; the time gap between rifting and igneous activity determines the amount of overlap and addition of the two heat spikes. The Hare Fiord and Van Hauen Formations produce small quantities of oil and gas prior to sill emplacement. The Blaa Mountain Formation produces more than one hundred times more oil and almost ten times more gas than the Hare Fiord and Van Hauen Formations. The Blaa Mountain Formation produces significant amounts of oil gas at the time of rifting and sill emplacement. Overall, sill intrusion increases the rates of hydrocarbon generation, and promotes the production of natural gas rather than liquid-oil.

The modeling process allows understanding of some of the interactions of the intrusions, and also the identification of knowledge gaps; it explores the reliability of existing data sets. It also shows why this part of the basin appears more gas-prone. Future

work could include refinement of this model by constraining some of the ambiguities such as the vitrinite reflectance data, the present and paleo-heat flow values, and the direct input of fission-track information. There is also potential for the creation of a two- or three-dimensional model of the study area so that hydrocarbon migration and entrapment can be better understood on a basin-wide scale.

References

1. Arne, D. C., Zentilli, M., Grist, A. M., and Collins, M., 1998, Constraints on the timing of thrusting during the Eurekan orogeny, Canadian Arctic Archipelago: an integrated approach to thermal history analysis: *Canadian Journal of Earth Sciences*, v. 35, no.1, p. 30 – 38.
2. Arne, D. C., Grist, A. M., Zentilli, M., Collins, M., Embry, A., and Gentzis, T., 2002, Cooling of the Sverdrup Basin during Tertiary basin inversion: implications for hydrocarbon exploration: *Basin Research*, v. 14, p. 183 – 205.
3. Avison, H. A., 1987, Ar-40/Ar-39 age studies of mafic volcanics from the Sverdrup Basin, Arctic Canada, Bachelor of Science Thesis, Dalhousie University, Halifax, Nova Scotia, 88 p.
4. Balkwill, H. R., 1978, Evolution of Sverdrup Basin, Arctic Canada: *The American Association of Petroleum Geologists Bulletin*, v. 62 no. 6, p. 1004 – 1028.
5. Balkwill, H. R. and Fox, F.G., 1982, Incipient rift zone, western Sverdrup Basin, Arctic Canada, *Memoir - Canadian Society of Petroleum Geologists*, v.8, p.171-187.
6. Balkwill, H. R., Cook, D. G., Detterman, R. L., Embry, A. F., Håkansson, E., Miall, A. D., Poulton, T. P., and Young, F. G., 1983, Arctic North America and Greenland, in M. Moullade and A. E. M. Narin, eds., *The Phanerozoic Geology of the World II; The Mesozoic*, B, Elsevier Science Publishers, Amsterdam, p. 1-31.
7. Buchan, K. L. and Ernst, R. E., submitted, *Giant* dyke swarms and the reconstruction of the Canadian Arctic islands, Greenland, Svalbard, and Franz

- Josef Land, Submitted to Proceedings of the Fifth International Dyke Conference, Rovaniemi, Finland, 23 p.
8. Burnham, A.K. and Sweeney, J.J., 1989, A chemical kinetic model of vitrinite maturation and reflectance, *Geochimica et Cosmochimica Acta*, v. 53, no. 10, p. 2649-2657.
 9. Cameron, B. I., 1989, Petrochemistry and origin of altered Permian basalts in the Sverdrup Basin, Arctic Canada. *Masters Thesis, Dalhousie University, Halifax, Nova Scotia*, 392 p.
 10. Chen, Z., Osadetz, K. G., Embry, A. F., Gao, H., and Hannigan, P. K., 2000, Petroleum potential in western Sverdrup Basin, Canadian Arctic Archipelago, *Bulletin of Canadian Petroleum Geology*, v. 48, no. 4, p. 323 – 338.
 11. Chen, Z., Osadetz, K. G., Embry, A. F., and Hannigan, P. K., 2002, Hydrocarbon favourability mapping using fuzzy integration: western Sverdrup Basin, Canada, *Bulletin of Canadian Petroleum Geology*, v. 50, no. 4, p. 492 – 506.
 12. Coffin, M. F., and Eldholm, O., 1994, Large igneous provinces: crustal structure, dimensions, and external consequences, *Reviews in Geophysics*, v. 32 p. 1 – 36.
 13. Davies, G. R. and Nassichuk, W. W., 1991, Carboniferous and Permian History of the Sverdrup Basin, Arctic Islands, in H. P. Trettin, ed., *Geology of the Innuitian Orogen and Arctic Platform of Canada and Greenland*, Geological Survey of Canada, *Geology of Canada no. 3*, p. 344 – 368.
 14. Embry, A. F., 1991, Mesozoic History of the Arctic Islands, in H. P. Trettin, ed., *Geology of the Innuitian Orogen and Arctic Platform of Canada and Greenland*, Geological Survey of Canada, *Geology of Canada no. 3*, p. 369 – 436.

15. Embry, A. F. and Osadetz, K. G., 1988, Stratigraphy and tectonic significance of Cretaceous volcanism in the Queen Elizabeth Islands, Canadian Arctic Archipelago, *Canadian Journal of Earth Sciences*, v. 25 p. 1209 – 1219.
16. Gentzis, T. and Goodarzi, F., 1991, Thermal maturity and hydrocarbon potential of the sedimentary succession from the Hecla field in Sverdrup Basin, Arctic Canada, *International Journal of Coal Geology*, v. 19, p. 483 – 517.
17. Gentzis, T. and Goodarzi, F., 1993a, Thermal Maturity and Source-Rock Potential of the Sedimentary Succession from the Drake Field, Sverdrup Basin, Arctic Canada, *Journal of Petroleum Geology*, v. 16, no. 1, p. 33 – 54.
18. Gentzis, T. and Goodarzi, F., 1993b, Maturity studies and source-rock potential in the southern Sverdrup Basin, Arctic Canada, *International Journal of Coal Geology*, v. 24, p. 141 – 177.
19. Gradstein, F. M. and Ogg, J., 1996, A Phanerozoic time scale, *Episodes*, v.19, no. 1-2, p. 3-5.
20. Greenwood, D. R. and Basinger, J. F., 1994, The paleoecology of high-latitude Eocene swamp forests from Axel Heiberg Island, Canadian High Arctic, *Review of Palaeobotany and Palynology*, v. 81, no. 1, p. 83 – 97.
21. Grist, A. M. and Zentilli, M., 2005, The thermal history of the Nares Strait, Kane Basin, and Smith Sound region in Canada and Greenland: constraints from apatite fission-track and (U-Th-Sm)/He dating, *Canadian Journal of Earth Science*, v. 42, p. 1547-1569.
22. Harrison, J. C., 2005, Geological history of the Arctic, in M. Nuttall, ed., *Encyclopedia of the Arctic*, Routledge, New York, p. 711 – 722.

23. Hunt, J. M., 1996, *Petroleum Geochemistry and Geology*, W. H. Freeman, New York 743 p.
24. Jollimore, W., 1986, *Analyses of dyke swarms within the Sverdrup Basin, Queen Elizabeth Islands*. Bachelor of Science Thesis, Dalhousie University, Halifax, Nova Scotia. 54 p.
25. Jones, F. W., Majorowicz, J. A., and Embry, A. F., 1989, A heat flow profile across the Sverdrup Basin, Canadian Arctic Islands, *Geophysics*, v. 54, no. 2, p. 170 – 180.
26. Jones, F. W., Majorowicz, J. A., Embry, A. F., and Jesspo, A. M., 1990, Geothermal gradients and terrestrial heat flow along a south-north profile in the Sverdrup Basin, Canadian Arctic Archipelago, *Geophysics*, v. 55, no. 8, p. 1105 – 1107.
27. Kuagai, H., Sweda, T., Hayashi, K., Kojima, S., Basinger, J. F., Shibuya, M., and Fukao, Y., 1995, Growth-ring analysis of early Tertiary conifer woods from the Canadian High Arctic and its paleoclimatic interpretation, *Palaeogeography, Palaeoclimatology, Palaeoecology*, v. 116, no. 3-4, p. 247 – 262.
28. Lyon, S. A., 2005, *Geoscience applications of geographic information systems for the Strand Fiord area, west Axel Heiberg Island, Nunavut*, Bachelor of Science Thesis, Dalhousie University, Halifax, Nova Scotia. 92 p.
29. MacRae, R. A., 1996, *Late Albian palynology and sequence stratigraphy, central Sverdrup Basin, Axel Heiberg Island, N.W.T.*, Ph.D. Thesis, University of Calgary, Calgary, Alberta, 442 p.

30. MacRae, R. A, Hills, R. V., and McIntyre, D. J., 1996, The paleoecological significance of new species of *Limbicysta* (Acritarcha) from the upper Albian of the Canadian Arctic Islands, *Canadian Journal of Earth Sciences*, v. 33, no. 11, p. 1475 – 1486.
31. MacRae, R. A. and Hills, L., 2006, Biostratigraphic constraints on the Cretaceous Strand Fiord Formation flood basalts, central Sverdrup Basin, Canadian Arctic Islands. The Atlantic Geoscience Society (AGS) 32nd Colloquium and Annual Meeting, February 3-4 Wolfville, Nova Scotia.
32. Majorowicz, J. A. and Embry, A. F., 1998, Present heat flow and paleo-geothermal regime in the Canadian Arctic margin: analysis of industrial thermal data and coalification gradients, *Tectonophysics*, v. 291, p. 141 – 159.
33. Malthe-Sørenssen, A., Planke, S., Svensen, H., and Jamtveit, B., 2004, Formation of saucer-shaped sills, in C. Breitkreuz and N. Petford, eds., *Physical Geology of High-Level Magmatic Systems*, Geological Society, London, Special Publications, v. 234, p. 215 – 227.
34. Muecke, G. K., Williamson, M-C., and MacRae, R. A., 1991, Recognition and significance of invasive flows in the Strand Fiord volcanics, Axel Heiberg island, Canadian Arctic Archipelago. Geological Association of Canada/Mineralogical Association of Canada Joint Annual Meeting 16: A109.
35. Musset, A. E. and Khan, M. A., 2000, *Looking Into the Earth; An Introduction to Geological Geophysics*, Cambridge University Press, United States, 470 p.

36. Ricketts, B., Osadetz, K. G., and Embry, A. F., 1985, Volcanic style in the Strand Fiord Formation (Upper Cretaceous), Axel Heiberg Island, Canadian Arctic Archipelago, *Polar Research*, v. 3, no. 1, p. 107 – 122.
37. Schutter, S. R., 2003, Hydrocarbon occurrence and exploration in and around igneous rocks, in N. Petford and K.J.W. McCaffrey, eds., *Hydrocarbons in Crystalline Rocks*, Geological Society, London, Special Publications 214, p. 7 – 33.
38. Svensen, H. and Planke, S., eds., 2003, *Petroleum Implications of Sill Intrusion; Intrusive Volcanic Complexes in the Karoo Basin*, Appendix B, Volcanic Basin Petroleum Research and TGS-NOPEC, Oslo, 178 p.
39. Svensen, H., Planke, S., Malthé-Sørenssen, A., Jamtveit, B., Myklebust, R., Eldem, T. R., and Rey, S. S., 2004, Release of methane from a volcanic basin as a mechanism for initial Eocene global warming, *Nature*, v. 429, p. 542 – 545.
40. Sweeney, J. F., 1977, Subsidence of the Sverdrup Basin, Canadian Arctic Islands, *Bulletin of the Geological Society of America*, v. 88, p. 41 – 48.
41. Tarduno, J. A., 1998, The high Arctic large igneous province, Third International Conference on Arctic Margins (ICAM III), Celle, Germany, Fed. Inst. Geosci. Nat Res. Abstract.
42. Tarduno, J. A., Brinkman, D. B., Renne, P. R., Cottrell, R. D., Scher, H., and Castillo, P., 1998, Evidence for Extreme Climatic Warmth from Late Cretaceous Arctic Vertebrates, *Science*, v. 282, p. 2241 – 2244.
43. Thorsteinsson, R., 1971a, Geology, Middle Fiord, District of Franklin, Geological Survey of Canada, 'A' Series Map, 1299A, 1:250,000, 1 sheet.

44. Thorsteinsson, R., 1971b, Geology, Strand Fiord, District of Franklin, Geological Survey of Canada, 'A' Series Map, 1301A, 1:250,000, 1 sheet.
45. Thorsteinsson, R., 1971c, Geology, Eureka Sound North, District of Franklin, Geological Survey of Canada, 'A' Series Map, 1302A, 1:250,000, 1 sheet.
46. Tozer, E. T., 1960, Summary account of Mesozoic and Tertiary stratigraphy, Canadian Arctic Archipelago, Geological Survey of Canada, Paper 60-5, 7 p.
47. Trettin, H. P., 1989, The Arctic Islands, in A. W. Bally and A. R. Palmer, eds., The Geology of North America- An Overview, Vol. A, The Geological Society of America, p. 349 – 370.
48. Turcotte, D. L. and Schubert, G., 2002, Geodynamics, 2nd ed., Cambridge University Press, Cambridge, United Kingdom, p. 153 – 160.
49. Villeneuve, M., and M- C. Williamson, in press, $^{40}\text{Ar}/^{39}\text{Ar}$ dating of mafic magmatism from the Sverdrup Basin Magmatic Province, Proceedings of the Fourth International Conference on Arctic Margins, Dartmouth, Nova Scotia, Canada, Sept. 30-Oct. 3, 2003 12p.
50. Vogt, P. R., Jung, W- Y., Jakobsson, M, Mayer, L., and Williamson, M- C., 2006, The Alpha-Mendeleev Magmatic Province, Arctic Ocean: A new synthesis, The Atlantic Geoscience Society (AGS) 32nd Colloquium and Annual Meeting, Program with Abstracts: 72-73.
51. Waples, D. W., 1998, Basin modeling: how well have we done?, in S. J. Duppenbecker and J. E. Iliffe, eds., Basin Modelling: Practice and Progress, Geological Society, London Special Publications 141, p. 1 – 14.

52. Williamson, M- C., 1988, The Cretaceous igneous province of the Sverdrup Basin, Canadian Arctic: Field relations and petrochemical studies, Ph.D. Thesis, Dalhousie University, Halifax, Nova Scotia, 417 p.
53. Williamson, M- C., 1998, The mantle source of flood basalts from the Sverdrup Basin Magmatic Province, Canadian Arctic, International Volcanological Congress IAVCEI '98, Cape Town, South Africa: 70.
54. Williamson, M- C., 2003, Field notes, Expedition to Axel Heiberg and Ellesmere Islands.
55. Williamson, M- C., 2005/2006, Personal communication regarding the Sverdrup Basin Magmatic Province and its characteristics and petrology.
56. Williamson, M- C. and MacRae, A., 2001, Mineralization potential in Volcanic Rocks of the Strand Fiord Formation and Associated Intrusions, Axel Heiberg Island, Nunavut, Canada, Natural Resources Canada Project in Development, Geological Survey of Canada (Atlantic)
57. Williamson, M- C., Zentilli, M., Dostal, J., and MacRae, R. A., 2005, Critical effects of the chronology and mode of emplacement of flood basalts on the thermal history of the Sverdrup Basin, Arctic Islands, Nunavut, 31st Atlantic Geoscience Society Colloquium and Annual General Meeting, Program with Abstracts: 45.
58. Winter J. D., 2001, An Introduction to Igneous and Metamorphic Petrology, Prentice-Hall Inc., New Jersey, 697 p.

59. Zentilli, M., 2005-2006, Personal communication regarding the application of fission-track analyses to the Sverdrup Basin and the timing of the Eurekan orogeny.
60. Zentilli, M., Williamson, M-C., Budkewitsch, P., Pollard, W., Hamilton, C., Mosher, A., Lyon, S. A., Grist, A. M., Kettanah, Y., Jensen, A. B. O., and Schwerdtner, W. M., 2005, Evaporite diapirs in Axel Heiberg Island, Nunavut: gauging their past and present growth rate and their geothermal energy potential, *Atlantic Geology*, v. 41, p. 86.

APPENDIX A:**Hand Sample Descriptions: Axel Heiberg Volcanic and Intrusive Igneous Rocks**

AX03-14

Dark grey- black in colour, aphanitic, aphyric, amygdaloidal (1-2% quartz filled amygdaloes), massive, cut by thin quartz filled veins (average 1mm diameter).

AX03-19

Dark grey in colour, fine grained, phyrical, seriate porphyritic, phenocryst detail cannot be well observed (require thin section), phenocrysts are plagioclase, massive.

AX03-20

Grey in colour, medium grained, aphyric, massive.

AX03-24

Grey- dark grey in colour, medium grained, aphyric but inequigranular, plagioclase distribution is not homogenous, overall sample is massive.

AX03-27

Grey in colour, very fine grained with a few large grains, generally aphyric, 3% elongated larger plagioclase or microlitic plagioclase with no preferred orientation, dark brown- black titanomagnetites 0.5-1mm diameter also visible.

AX03-30

Dark grey in colour, fine grained, aphyric, visible plagioclase grains, massive.

AX03-37

Dark grey in colour, phyrical, hiatal porphyritic, aphanitic groundmass, fine grained phenocrysts, 10-15% plagioclase phenocrysts, phenocrysts do not show preferred orientation, some thin quartz veins (<1mm diameter), massive.

AX03-39

Dark grey in colour, aphyric, fine- medium grained, euhedral to subhedral plagioclase, titanomagnetites, homogeneous, massive.

AX03-41

Dark grey in colour, equigranular, aphanitic- fine grained, subhedral- euhedral plagioclase and mafic minerals are visible (<1mm in diameter), homogeneous, massive, some small fractures (not filled).

AX03-45

Dark grey in colour, aphyric, inequigranular, 25% plagioclase and mafic fine- medium grained mineral, homogeneous, massive.

AX03-46

Dark grey in colour, inequigranular, 30% fine- medium grained plagioclase grains (largest plagioclase up to 5mm in diameter), homogeneous, massive.

AX03-48

Grey in colour, aphyric, inequigranular, fine- medium grained, largest crystals are rectangular plagioclase (some have a darker core and light rim), homogeneous, massive.

AX03-50

Grey- dark grey in colour, phyrlic, seriate porphyritic, fine-grained, microlites visible with a hand lens, massive.

AX03-51

Light grey in colour, aphyric, inequigranular, fine- medium grained, visible plagioclase and mafic mineral, crystals appear intergrown, homogeneous.

AX03-52

Grey in colour, inequigranular, fine- medium grained, largest crystals up to 4mm in diameter, some fractures and cracks (not filled), massive.

AX03-54

Grey in colour, weathered surface, aphyric, medium grained, visible alteration which is not homogeneous throughout the sample, variation in plagioclase colour and shape, interstitial pyrite?

AX03-69

Grey- dark grey in colour, fine grained, dark colour minerals, some reflective minerals (sulphides?), small cracks and fractures (not filled), massive.

AX03-71

Dark grey in colour, >90% aphanitic, few large black/dark grains (up to 3mm diameter, rounded to straight grain boundaries, generally equant, some have depletion halo), few large plagioclase grains, massive.

AX03-73

Grey- dark grey in colour, fine to medium grained, inequigranular grained, visible minerals include plagioclase and mafic mineral, massive.

AX03-74

Dark grey in colour, inequigranular, fine- medium grained, plagioclase and mafic mineral visible, cloudy/fuzzy grain boundaries (shows extensive intergrowth), massive.

Alteration Index:
 (Classification scheme based on Williamson, 1988 and Williamson, pers. Comm.):

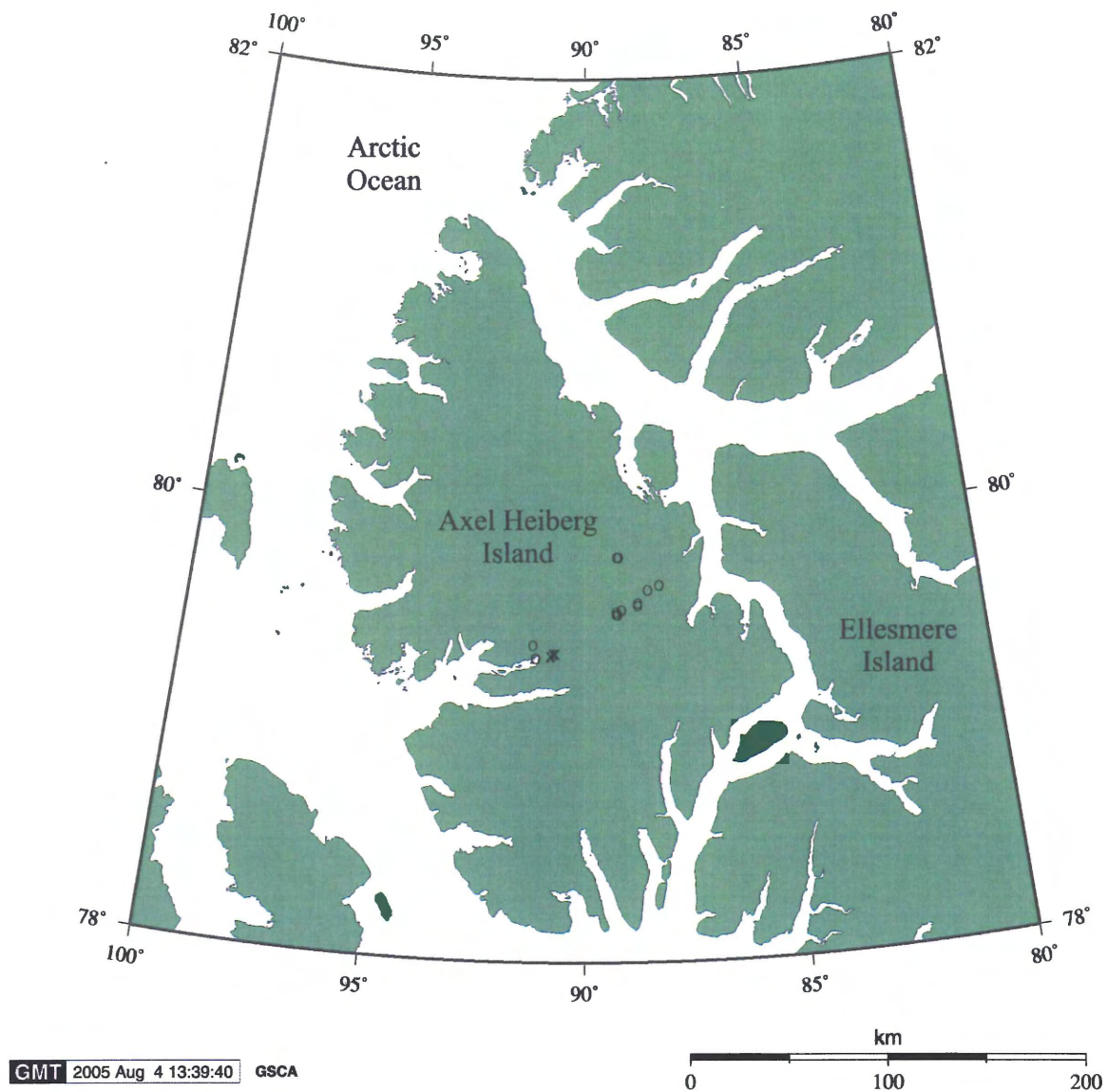
Alteration Index	1	2	3	4
Olivine	Partially or completely altered	Completely altered/ pseudomorphed	Completely altered/ pseudomorphed	Completely altered/ pseudomorphed
Feldspar	Minor or no alteration	Minor or no alteration	Altered to clays	Completely altered/ pseudomorphed
Clinopyroxene	Minor or no alteration	Advanced alteration	Minor to no alteration	Completely altered/ pseudomorphed
Clays	Present only interstitially	Present	Present	Present
Textures	Preserved	Preserved	Preserved	Partially to completely destroyed

Sample Coordinates

Sample No.	Latitude	Longitude
AX03-14	79° 50.3'	89° 15.8'
AX03-19	?	?
AX03-20	79° 50.6'	89° 17.8'
AX03-24	79° 41.1'	88° 32.6'
AX03-27	79° 42.3'	88° 24.8'
AX03-30	79° 42.3'	88° 24.8'
AX03-37	79° 37.6'	88° 46.7'
AX03-39	79° 37.6'	88° 46.7'
AX03-41	79° 37.8'	88° 46.8'
AX03-45	79° 37.27'	88° 47.57'
AX03-46	79° 37.27'	88° 47.57'
AX03-48	79° 34.57'	89° 17.57'
AX03-50	79° 34.6'	89° 20.0'
AX03-51	79° 35.1'	89° 19.6'
AX03-52	79° 36.0'	89° 12.1'
AX03-54	79° 36.0'	89° 12.1'
AX03-69	79° 26.14'	91° 24.11'
AX03-71	79° 22.7'	91° 20.0'
AX03-73	79° 22.65'	91° 19.4'
AX03-74	?	?

Wolf Intrusion

Sample No.	Latitude	Longitude
AX03-13	?	?
AX03-17	79° 50.5'	89° 17.7'
AX03-22	79° 41.6'	88° 31.6'
AX03-60	79° 24.2'	90° 52.4'
AX03-63	79° 24.054'	90° 50.266'
AX03-66	79° 23.772'	90° 54.292'
AX03-67	79° 23.3'	90° 57.3'
AX03-68	79° 23.3'	90° 57.3'

Sample Location Map:

This location map shows the samples that have been described petrographically. The Wolf Intrusion samples are marked with an 'x' and the central Axel Heiberg sills are marked with an 'o'.

Petrographic Descriptions: Intrusive Rocks from Axel Heiberg Island.

Sample Number	Primary Mineralogy				Secondary Minerals	Textures	Alteration Index	Hand Sample
	Olivine	Plagioclase	Clinopyroxene	Other				
AX03-14	none	30%, laths, tabular, subhedral, 0.4mm	5%, anhedral, alteration, opaque inclusions, 0.1-0.4mm	15%, equant-skeletal opaques, 0.1-0.2mm; <1% biotite	brown clays between minerals	Very fine grained, holocrystalline, aphyric, inequigranular	2	√
AX03-19	5%, anhedral, ≤0.4mm	40%, laths, tabular, 0.1-0.8mm	25-30%, round-anhedral, 0.1-0.6mm	15%, equant-skeletal opaques, 0.1-0.3mm	iddingsite after olivine, very little clay	fine grained, inequigranular, seriate porphyritic, glomeroporphyritic, holocrystalline, subophitic relationship of plag and cpx	1	√
AX03-20	none	25%, tabular, altered cores, avg. 2mm	30-35%, fractures, anhedral, irregular, ≤1mm	5%, equant opaques, 0.5-1mm; <1% biotite with alteration to chlorite; acicular apatite	abundant clays and alteration minerals, amphibole	fine to medium grained, equigranular, holocrystalline, cannot see primary textures	4	√
AX03-24	none	50%, tabular, avg. 2mm	25%, anhedral, <1-2mm	5%, equant-irregular opaques, avg. 1mm; <1% biotite with alteration to chlorite		fine to medium grained, holocrystalline, inequigranular	2	√
AX03-27	none	20%, completely altered, avg. 0.3mm	15%, anhedral, major alteration, 0.1mm	7%, equant opaques, <0.1mm; <1% biotite with alteration to chlorite		very fine grained, holocrystalline, mostly equigranular, some larger altered plagioclase grains, cannot determine primary textures	4	√

Sample Number	Primary Mineralogy				Secondary Minerals	Textures	Alteration Index	Hand Sample
	Olivine	Plagioclase	Clinopyroxene	Other				
AX03-30	none	30%, subhedral, tabular, $\leq 0.3\text{mm}$	completely altered	10%, small equant and large irregular opaques, $< 0.1\text{mm}$	chlorite	very fine grained, holocrystalline, highly altered	4	√
AX03-37	2%, phenocryst phase, round, alteration rims, 0.5mm	12%, subhedral, phyrical, zoning, microlites in gm, avg. 1mm	5%, phenocryst phase, subhedral-anhedral, avg. 0.5mm	3%, small, equant opaques	some interstitial clays	hiatal porphyritic, fine grained phenocrysts, aphanitic groundmass, 15% phenocrysts, glomeroporphyritic subophitic cpx and plag	1	√
AX03-39	none	40%, tabular, lath, $\leq 2\text{mm}$	20%, round-anhedral, $\leq 2\text{mm}$	3%, skeletal-irregular opaques, $< 0.1\text{mm}$	clays after glass, some interstitial chlorite	fine to medium grained, hypocrySTALLINE, mostly equigranular, some subophitic texture with cpx and plag, devitrified glass?	1	√
AX03-41	none	40%, euhedral-subhedral, completely altered, avg. 1mm	10%, subhedral-anhedral, $\leq 1.5\text{mm}$	10%, skeletal-equant opaques, avg. 0.1mm	chlorite, alteration of plagioclase	fine grained, equigranular, holocrystalline?	3	√
AX03-45	4%, anhedral, $\leq 0.5\text{mm}$	40%, anhedral-subhedral, $\leq 2.5\text{mm}$	30%, rounded-irregular, anhedral, alteration rims, $0.5 - 1\text{mm}$	5%, equant-blocky, anhedral-subhedral opaques, very fine to 1mm ; 1% biotite with alteration to chlorite	clays after glass, chlorite after biotite	medium grained, hypocrySTALLINE, inequigranular, aphyric, subophitic texture with plag and cpx	1	√

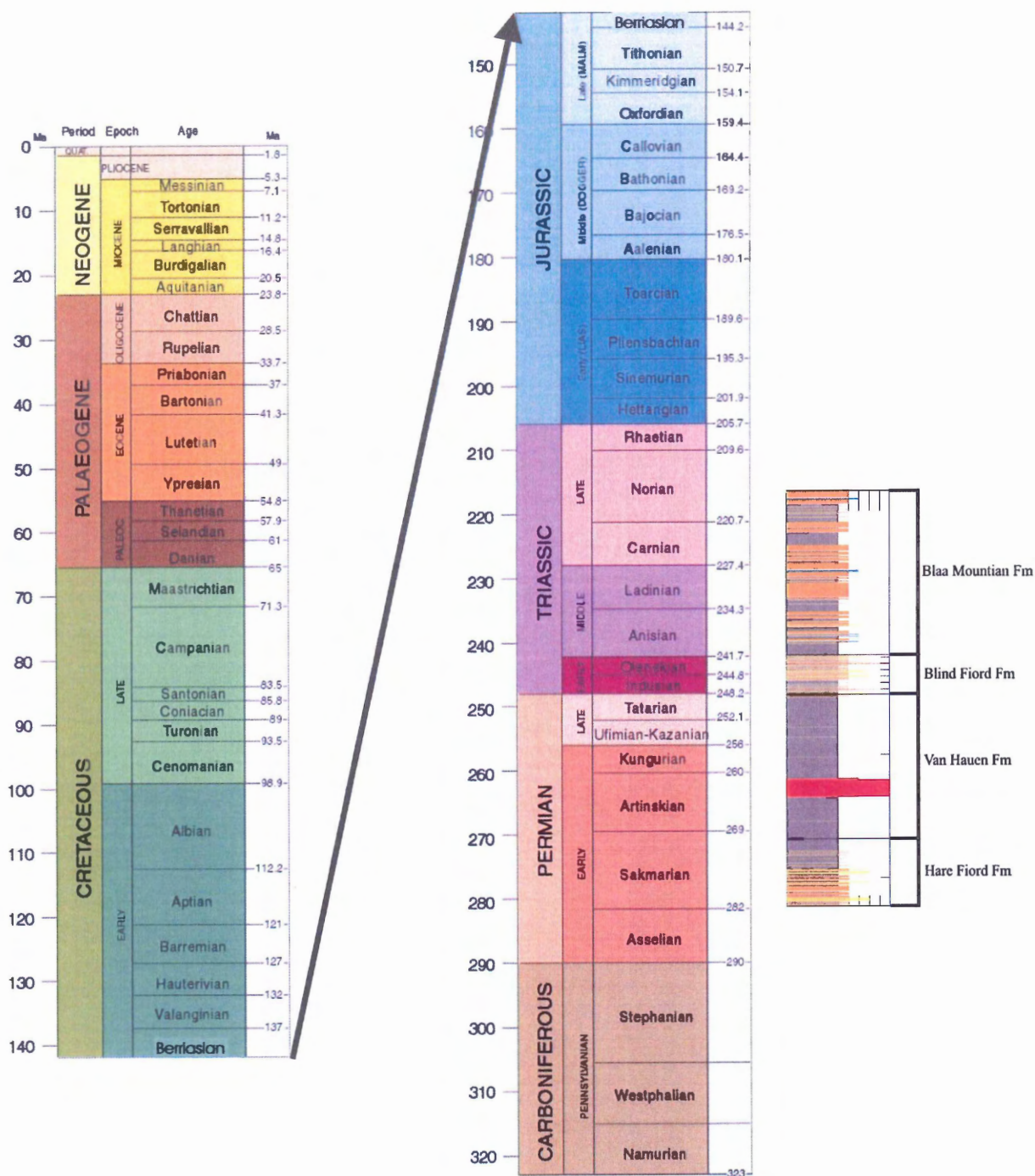
Sample Number	Primary Mineralogy				Secondary Minerals	Textures	Alteration Index	Hand Sample
	Olivine	Plagioclase	Clinopyroxene	Other				
AX03-46	<2%, fragmented, anhedral, alteration rims, ≤0.5mm	35-40%, tabular, subhedral-anhedral, ≤2.5mm	30%, irregular, ≤1.5mm	3%, skeletal-equant, irregular opaques, very fine to 0.5mm	interstitial clays, chlorite, amphibole, sericite after plagioclase (1%)	fine to medium grained, hypocrytalline, inequigranular, aphyric, subophitic texture with cpx and plag	2	√
AX03-48	none	25-30%, laths, tabular, ≤2.5mm	20%, rounded-irregular, cracked/fractured, anhedral, ≤1mm	10%, equant, anhedral-subhedral opaques, very fine to 0.5mm; <1% biotite with alteration to chlorite; zircon; acicular apatite	fibrous amphibole, chlorite	fine to medium grained, inequigranular, aphyric, hypocrytalline, primary subophitic texture with cpx and plag	3	√
AX03-50	<1%, fragments, anhedral, alteration rims, very fine	30%, laths, tabular, irregular grain boundaries, ≤2mm	10%, round, avg. 0.3mm	15%, skeletal-equant, anhedral opaques, very fine; 1% titanite	chlorite, interstitial clays	seriate porphyritic, phenocrysts: fine to medium grained, groundmass: very fine grained, hypocrytalline, fuzzy grain boundaries, inequigranular,	1	√
AX03-51	none	30%, completely altered, ≤1mm	20%, rounded, irregular-anhedral, ≤0.5mm	5-7%, skeletal-equant, anhedral-subhedral opaques, very fine to 0.5mm	(5% total) chlorite, fibrous amphibole, carbonate (1%)	fine to medium grained, aphyric, inequigranular, subophitic primary texture with cpx and plag, holocrystalline	3	√
AX03-52	<1%, anhedral, <0.5mm	35-40%, laths, anhedral-equant, ≤1.5mm	25-35%, round-irregular, ≤0.5mm	7%, skeletal-equant, anhedral-subhedral opaques, avg. 0.1-0.2mm; <1% biotite altered to chlorite		fine to medium grained, holocrystalline, subophitic texture with cpx and plagioclase, aphyric, inequigranular	1	√

Sample Number	Primary Mineralogy				Secondary Minerals	Textures	Alteration Index	Hand Sample
	Olivine	Plagioclase	Clinopyroxene	Other				
AX03-54	none	30%, completely altered, $\leq 3\text{mm}$	30%, irregular, $\leq 1\text{mm}$	7%, equant-irregular, anhedral-subhedral opaques, very fine	chlorite, clays	medium grained, major alteration, primary textures cannot be determined	4	√
AX03-69	none	40-45%, laths, tabular-irregular, $\leq 1.5\text{mm}$	25-30%, completely altered, $\leq 1\text{mm}$	5%, equant-irregular, anhedral, very fine; <1% acicular apatite	interstitial clays, green mineral	fine grained, inequigranular, aphyric, hypocrySTALLINE	2	√
AX03-71	none	40-45%, laths, tabular, subhedral, 0.1-0.2mm	25%, sparse equant grains, subhedral, $\leq 0.3\text{mm}$	10%, equant opaques, very fine; <1% small rectangular colourless grain within the green mineral	5% devitrified glass, 1% green mineral/chlorite	very fine grained, hypocrySTALLINE, inequigranular, amygdale present	1	√
AX03-73	none	50%, laths, tabular, subhedral-anhedral, $\leq 1.5\text{mm}$	20%, subhedral-anhedral, $\leq 1\text{mm}$	4%, equant opaques, very fine; <1% titanite	interstitial brown and green clays	fine to medium grained, subophitic texture with cpx and plag, hypocrySTALLINE, inequigranular, aphyric	1	√
AX03-74	1%, equant, round, alteration rims, very fine	35-40%, laths, anhedral-subhedral, $\leq 2.5\text{mm}$	30%, equant, round, avg. 1mm	5%, equant-skeletal, irregular opaques, very fine-0.5mm	3% interstitial brown and green clays	fine to medium grained, hypocrySTALLINE, sharp grain boundaries, inequigranular, ophitic texture with cpx and plag	1	√

Sample Number	Primary Mineralogy				Secondary Minerals	Textures	Alteration Index	Hand Sample
	Olivine	Plagioclase	Clinopyroxene	Other				
AX03-13	none	40%, microlites, tabular-quant phenocryst phase, avg. 0.5-1mm	10%, phenocrysts are equant-rounded, ≤0.5mm	25%, equant-skeletal opaques, very fine; <1% titanite	interstitial clays	phyric, very fine groundmass, glomeroporphyritic, supophitic (plag and cpx), fine grained phenocrysts	1	
AX03-17	none	35%, microlites, tabular phenocryst phase, avg. 0.5-1mm	20%, phenocrysts are equant-rounded, ≤0.5mm	10%, equant-skeletal, anhedral-subhedral opaques, very fine; <1% biotite, apatite needles	interstitial clays, alteration product of olivine, chlorite	seriate porphyritic, glomeroporphyritic, subophitic texture (some)	1	
AX03-22	none	25%, zoning, subhedral-equant, ≤1.5mm	15%, round, ≤1mm	15%, equant-skeletal, anhedral-subhedral opaques, very fine; <1% biotite with chloritic alteration; apatite needles	chlorite, interstitial clays, some clays within mineral grains	inequigranular, textures gone, subophitic, glomeroporphyritic, carbonate vein (very thin)	4	
AX03-60	<2%, anhedral, alteration rims, ≤0.8	30%, laths, tabular, subhedral-anhedral, ≤2mm	20%, equant-irregular, anhedral, ≤2mm	10%, equant-skeletal, anhedral-subhedral opaques, very fine to 1.5mm; <1% hexagonal apatite	iddingsite, chlorite	hypocrystalline, medium grained, inequigranular, ophitic, sharp grain boundaries	1	
AX03-63	none	30%, microlites, laths, subhedral, ≤1mm	20%, rounded-irregular, anhedral, avg. 0.2-0.5mm	10%, skeletal opaques, avg. 0.5mm; <1% biotite	interstitial clays	fine grained, inequigranular, hypocrystalline, subophitic	1	

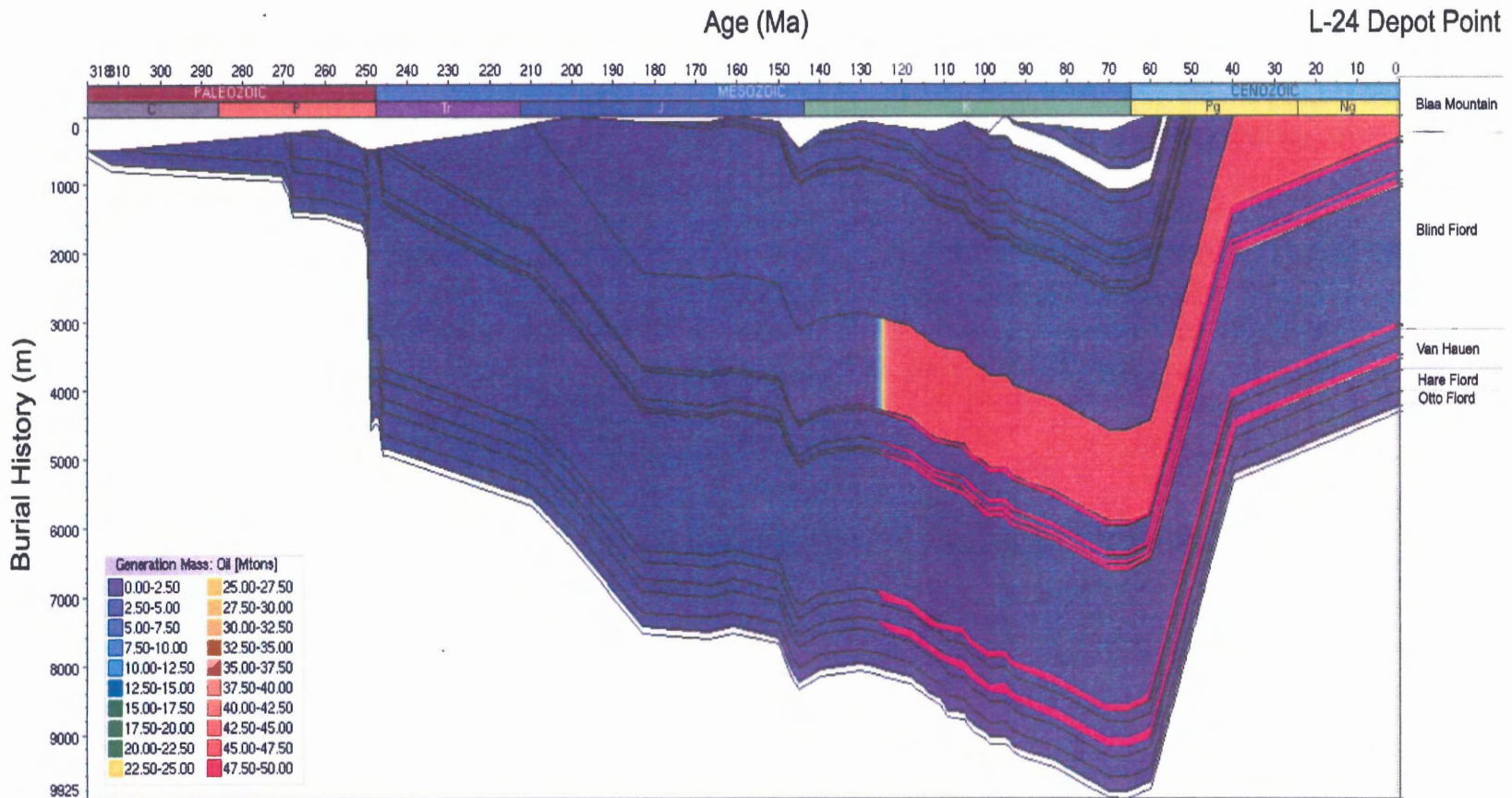
Sample Number	Primary Mineralogy				Secondary Minerals	Textures	Alteration Index	Hand Sample
	Olivine	Plagioclase	Clinopyroxene	Other				
AX03-66	7%, round, alteration rims, 0.25-1mm	30-35%, laths, tabular, subhedral, ≤2mm	25%, rounded, anhedral-subhedral, avg. 0.5-1mm	7%, irregular, interstitial opaques, avg. 1-2mm; <1% apatite needles	very few clays, chlorite	holocrystalline, subophitic-ophitic, medium grained, sharp grain boundaries, inequigranular	1	
AX03-67	7%, round, ≤1mm	30%, laths, tabular, subhedral, ≤2mm	20%, round-elongate, anhedral, avg. 0.5-1mm	5%, equant-skeletal opaques, very fine-2mm; <1% apatite needles	sericite, very few clays	medium grained, inequigranular, holocrystalline, subophitic-ophitic	1	
AX03-68	5%, round-irregular, 0.5mm	35%, tabular/lath shaped, subhedral, zoning, ≤1.5mm	20%, equant, anhedral-subhedral, avg. 0.5-1mm	5%, irregular-equant, anhedral, some interstitial opaques, avg. 0.5mm; <1% biotite	very few clays, chlorite	fine to medium grained, holocrystalline, inequigranular, subophitic	1	

APPENDIX B: GEOLOGICAL TIME SCALE

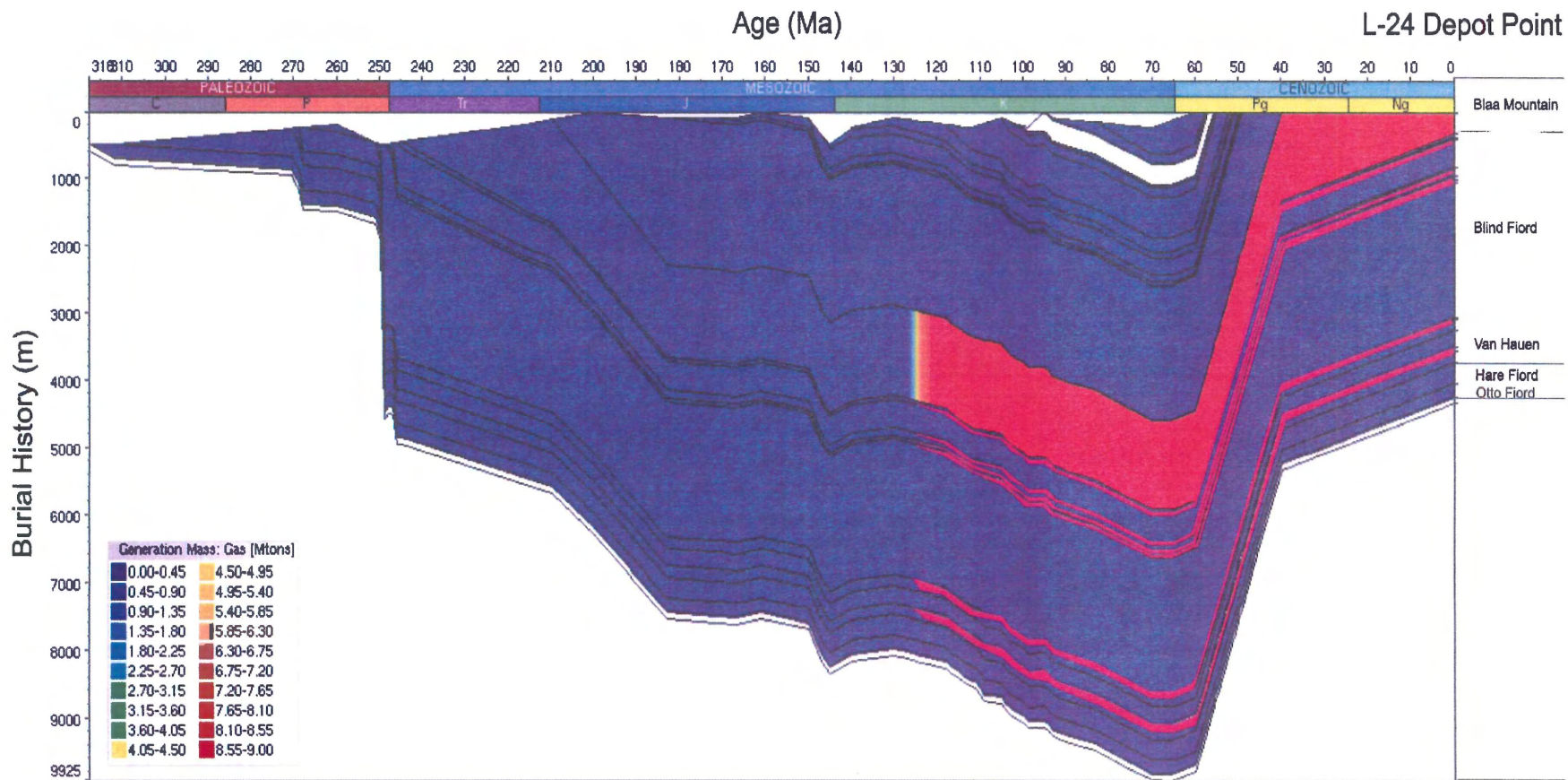


Time scale from: Gradstein and Ogg 1996, Episodes, v18 nos.1&2

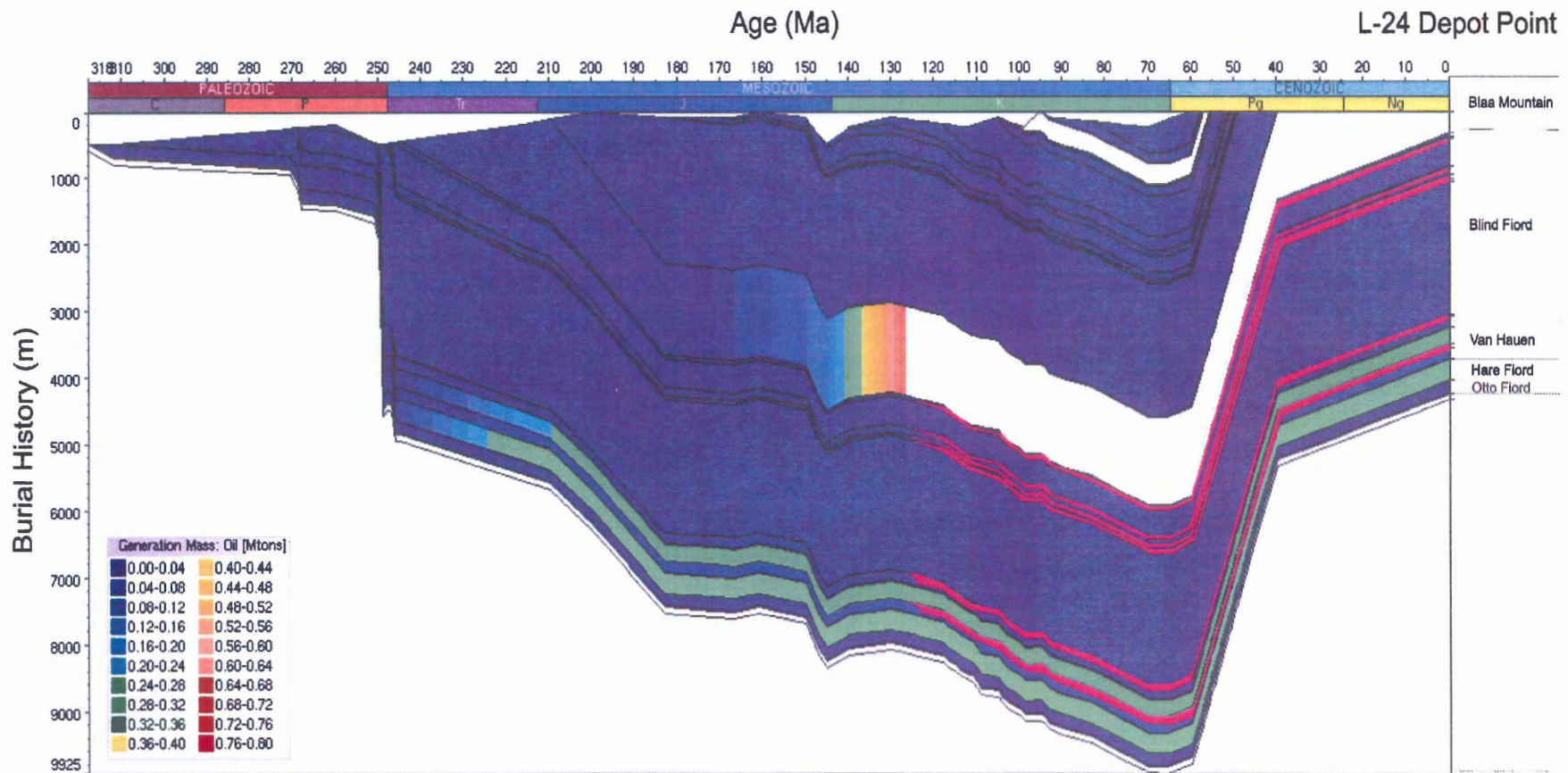
This image shows the time scale used in model construction. The Depot Point L-24 litholog is aligned with the corresponding formational ages. Note: The litholog is not to scale.



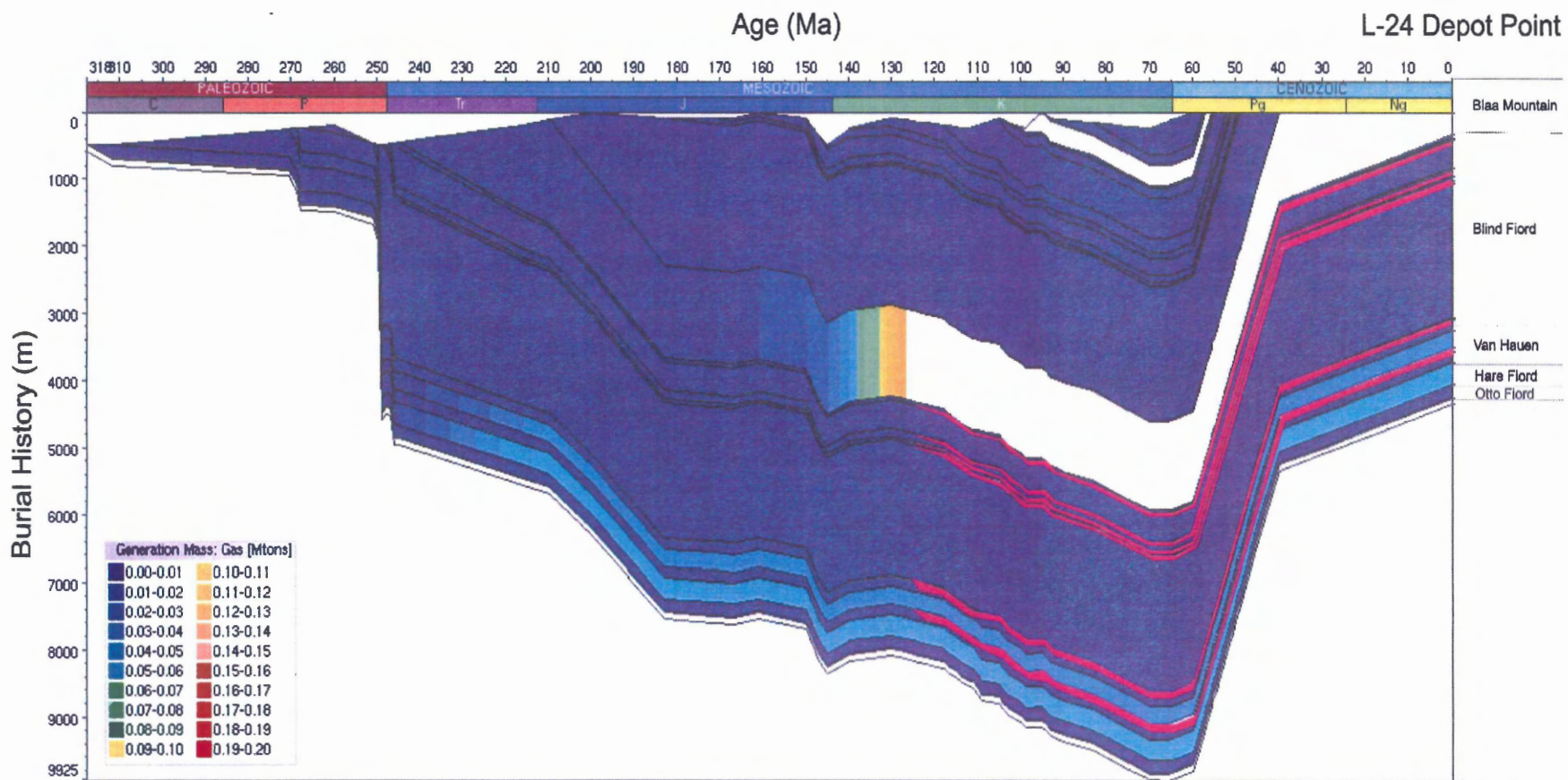
This plot shows that the Blaa Mountain Formation produces approximately 40 million tons of oil due to the heat introduced by rifting and sill emplacement. Generation begins at about 126 Ma, as the heat flow is gradually increasing just prior to rifting. The most significant generation occurs at 125 Ma, the time of rifting and sill emplacement. The constant colour after 125 Ma indicates that the total amount of oil produced by the Blaa Mountain Formation does not change after this time. The sills are traced in magenta on this plot.



This plot shows that the Blaa Mountain Formation produces approximately 9 million tons of gas due to the heat introduced by rifting and sill emplacement. Generation begins at about 126 Ma, as the heat flow is gradually increasing just prior to rifting. The most significant generation occurs between 125-122 Ma, at and after the time of rifting and sill emplacement. The constant colour after 122 Ma indicates that the total amount of gas produced by the Blaa Mountain Formation does not change after this time. The sills are traced in magenta on this plot.



This plot shows that the Hare Fiord and Van Hauen Formations generate small quantities of oil prior to rifting and sill emplacement. Each formation produces about 0.3 million tons of oil. The Hare Fiord Formation generates between 245-220 Ma and the Van Hauen Formation generates between 240-210 Ma. This plot also shows that the Blaa Mountain Formation generated small amounts of oil, less than 1 million tons, between 165-125 Ma, prior to rifting and sill emplacement. This corresponds to the period of time where the Blaa Mountain Formation was residing at temperatures between 75-100°C (see Figure 5.5). The sills are traced in magenta on this plot.



This plot shows that the Hare Fiord and Van Hauen Formations generate small quantities of gas prior to rifting and sill emplacement. Each formation produces about 0.6 million tons of gas. The Hare Fiord Formation generates between 245-220 Ma (coeval with oil generation) and the Van Hauen Formation generates between 240-210 Ma (coeval with oil generation). This plot also shows that the Blaa Mountain Formation generated small amounts of gas, less than 0.2 million tons, between 165-125 Ma, prior to rifting and sill emplacement. This corresponds to the period of time where the Blaa Mountain Formation was residing at temperatures between 75-100°C (see Figure 5.5). The sills are traced in magenta on this plot.